FEDERAL UNIVERSITY OF ITAJUBÁ
ITAJUBÁ
ELECTRICAL ENGINEERING POSTGRADUATE PROGRAM

DOCTORAL THESIS

UNIFIED CENTRALIZED/DECENTRALIZED VOLTAGE AND FREQUENCY CONTROL STRUCTURE FOR MICROGRIDS

PAULO THIAGO DE GODOY

ITAJUBÁ
2024

Paulo Thiago de Godoy

Unified Centralized/Decentralized Voltage and Frequency Control Structure for Microgrids

Doctoral Thesis presented to the Electrical Engineering Postgraduate Program as part of the requirements for obtaining the Doctor's degree in Sciences in Electrical Engineering.

Advisor: Antonio Carlos Zambroni de Souza
Advisor: Adriano Batista de Almeida

Itajubá
2024

Unified Centralized/Decentralized Voltage and Frequency Control Structure for Microgrids

Paulo Thiago de Godoy

This Doctoral Thesis was presented to the Electrical Engineering Doctoral Program and approved by the Examination Board:
Public defense date: 09/05/2024.

Prof. Dr. **Antonio Carlos Zambroni de Souza** - (Advisor)
Federal University of Itajubá - UNIFEI

Prof. Dr. **Adriano Batista de Almeida** - (Advisor)
Western Paraná State University - UNIOESTE

Prof. Dr. **Eliane Valença Nascimento de Lorenci**
Federal University of Itajubá - UNIFEI

Prof. Dr. **Benedito Donizeti Bonatto**
Federal University of Itajubá - UNIFEI

Prof. Dr. **Ahda Pionkoski Grilo Pavani**
Federal University of ABC - UFABC

Prof. Dr. **Rui Jovita Godinho Corrêa da Silva**
Itaipu - ITAIPU

Abstract

The centralized secondary control strategies for microgrids (MG) are widely used due to their ease of control and coordination with distributed resources. However, the reliability of these strategies is extensively influenced by the communication system. To address the reliability issues associated with centralized control, this work proposes a novel Unified Secondary Control Structure (USCS). The USCS ensures regulation of the MG's voltage and frequency even during communication or control failures. During normal operation, the USCS operates solely using the centralized control strategy, ensuring coordination with distributed resources. In case of communication system or centralized control failure, the USCS switches to the decentralized control strategy as a backup, ensuring voltage and frequency regulation. To facilitate the USCS voltage regulation, a novel decentralized voltage regulation strategy is proposed. This voltage control strategy is based on state estimation and equivalent systems. The proposed USCS and decentralized voltage strategy are implemented and tested on a benchmark MG based on the CIGRE residential European grid in Matlab/Simulink. The results demonstrate that the decentralized voltage strategy can effectively regulate MG voltage, and the USCS ensures voltage and frequency regulation even during failures, with a smooth transition between control modes even during communication delays. Additionally, a hardware-in-the-loop environment is employed to test the proposed USCS, where the centralized control is built in a real-time digital controller, and the MG system, converter controls, and decentralized controls are implemented in the Real Time Digital Simulator (RTDS) simulation environment. The results show that the proposed control structure can guarantee regulation even during failures and restore regular operation after failure. While the results are satisfactory, further development of a new gain-adjust strategy is necessary for the strategies operating in the USCS.

Keywords: Microgrids, Secondary Control, Centralized Control, Decentralized Control, USCS.

Acknowledgments

First of all, I would like to thank my advisors Prof. Dr. Antonio Carlos Zambroni de Souza and Prof. Dr. Adriano Batista de Almeida for the opportunity, for the trust, and especially for the guidance that made the development of the work possible.

To my research colleagues and professors for providing me with knowledge and experiences that helped me not only in developing my work, but in my personal and professional growth.

And finally, all the family, friends and colleagues who supported me during these years.

Summary

List of Figures

List of Tables

List of Symbols

t	Time
f	Frequency
P	Active power
V	Voltage
Q	Reactive power
ω	Angular frequency
ω^*	Droop angular frequency reference
m	Droop frequency coefficient
P^*	Active power reference for the droop control
V^*	Voltage reference for the droop control
n	Droop voltage coefficient
Q^*	Reactive power reference for the droop control
$\Delta\omega_{sec}$	Secondary frequency control action
ΔV_{sec}	Secondary voltage control action
i	Index for a DG
$\Delta\omega_{s_C}$	Centralized secondary frequency control action
ΔV_{s_C}	Centralized secondary voltage control action
CmC	MGCC operating state variable send for a DCU
CmT	DCU operating mode command variable sent by MGCC
$(\Delta\omega_{s_D})$	Decentralized secondary frequency control action
(ΔV_{s_D})	Decentralized secondary voltage control action
CmD_i	DCU operating state variable send for the MGCC
CmK_i	DCU operating mode variable send for the MGCC
CC_f	Centralized secondary control strategy for frequency regulation
CC_V	Centralized secondary control strategy for voltage regulation
$()\prime$	Variable received from other component
IH_f	CSC mode initialization variable for frequency
IH_V	CSC mode initialization variable for voltage
$State$	State operation of a communication channel
X	Time reference for the tracking process interruption

$\delta T(t)$	Time variation that the MGCC does not fail
Z	Smallest derivative value of frequency and voltage for the tracking process interruption
$Fail$	Variable that indicates the state of failure of the MGCC
$PCCS$	Variable that indicates the operation state of the MG
Rst	Auxiliary variable that indicates if the the MGCC is in tracking mode
ETR_f	Frequency derivative
ETR_V	Voltage derivative
t_f	Time when the information CmT received changes its state to 1)
V_{EQ}	Voltage in the equivalent bus
L_{EQ}	Total load of the MG
Z_{EQ}	Equivalent impedance
I	DG current
VV	Control portion that is responsible for the voltage regulation
VQ	control portion that is responsible for the power sharing
V_{s0}	Voltage reference for the proposed decentralized voltage control
Q_{EQ}	Estimated reactive power in the equivalent system
k_1	Control gain for the voltage regulation portion
k_2	Control gain for the reactive power sharing portion
ϕ	Tangent of the power factor
T_{2_i}	Low-pass filter time constant for the decentralized frequency strategy
α_i	Proportional gain for the decentralized frequency strategy
Kp_ω	Proportional gain for the centralized frequency strategy
Ki_ω	Integrative gain for the centralized frequency strategy
ω_{PCC}	Frequency measured in the PCC
Ω_{s0}	Frequency reference for the centralized strategy
Kp_V	Proportional gain for the centralized voltage strategy
Ki_V	Integrative gain for the centralized voltage strategy
V_{PCC}	Voltage measured in the PCC
V_{s0}	Voltage reference for the centralized strategy
HB	heartbeat variable
V_{DC}	Inverter DC link voltage
$S_1(t)$	Switching function of switch S1
$S_4(t)$	Switching function of switch S4

$i_t(t)$	Output current of the inverter switching process
$V_t(t)$	Voltage before the inverter filter
$V_s(t)$	Voltage after the inverter filter
h	Harmonic order of the Fourier series
ω_s	Angular frequency of the Fourier series
T_s	Period of the Fourier series
a_h	Fourier constant for cosine portion
b_h	Fourier constant for sine portion
W	Oscillatory variable
$\overline{W}$	Moving average of the variable W
$\overline{d}$	Ratio between the time switch S1 is conducting and the switching time
M	Modulating signal
Y	Quantity
$()_{abc}$	Represents a three-phase quantity
$()_{dq0}$	Represents a dq0 quantity
T	Transformation matrix
θ	Transform angular reference
PIC	PI controller for the inverter current control
Kc_p	Proportional gain for the inverter current control
Kc_i	Integrative gain for the inverter current control
$Iref$	Control reference for the inverter current control
$Pref$	Control reference for the inverter active power control
$Qref$	Control reference for the inverter reactive power control
PIV	PI controller for the inverter voltage control
Kv_p	Proportional gain for the inverter voltage control
Kv_i	Integrative gain for the inverter voltage control
S	Inverter apparent power
θ_p	Power factor angle
X_{filt}	Inverter filter reactance
Q_{max_C}	Maximum current reactive power limit
Q_{max_V}	Maximum DC voltage reactive power limit

List of Acronyms and Abbreviations

MG	Microgrid
USCS	Unified Secondary Control Structure
CIGRE	Council on Large Electric Systems
RTDS	Real Time Digital Simulator
DG	Distributed Generation
UCDFCS	Unified Centralized/Decentralized Frequency Control Structure
PCC	Point of Common Coupling
HIL	Hardware-in-the-Loop
RTS	Real Time Simulations
RTAC-SEL	Real-Time Automation Controller from the Schweitzer Engineering Laboratories
BESS	Battery Energy Storage Systems
DCU	Decentralized Control Unit
DSC	Decentralized Secondary Control
CSC	Centralized Secondary Control
PV	Photovoltaic Systems
PLL	Phase Lock Loop

Chapter 1

Introduction

1.1 Initial considerations

With the advancement of new technologies in power systems, the concept of conventional power systems is evolving. One such technology is Distributed Generation (DG). Due to the recent cost benefits of DG technologies, their deployment within power systems has increased. However, the increasing deployment of DG in low and medium voltage systems introduces new operational and control challenges in distribution systems. These challenges include changes in power flow direction, high levels of intermittent generation, and difficulties in voltage control, among others.

To ensure the successful integration of DG into the distribution system, new control and operation strategies specifically tailored for this purpose are required. In this context, Microgrids (MGs) emerge as one of the possible solutions. MGs can facilitate the integration of DG into the main grid. An MG can be considered a small-scale power system that operates in two different modes: islanded mode, where it operates independently, and connected mode, where it is synchronized with the main power grid [1, 2, 3].

In connected mode, the voltage and frequency references are imposed by the main grid, and the MG can import or export power from the main grid. Failures may drive the MG to islanded mode, where the dispatchable DGs of the MG must maintain the load balance. Thus, in islanded mode, the MG must generate its own power and control its voltage and frequency references [1, 2, 3].

For an MG to operate in connected or islanded mode, several control and operation requirements are necessary, such as maintaining its own stability, regulating frequency and voltage, sharing active and reactive power between sources, economic dispatch, and synchronization, among others. These requirements necessitate different control actions and occur at different times, making a hierarchical control structure the most suitable for MG control.

The hierarchical control structure consists of primary, secondary, and tertiary control levels. Primary control ensures the stable operation of DGs and power sharing among them. Secondary control adjusts the MG frequency and voltages, acting over the primary control by

setting new frequency and voltage references. At the tertiary level, MG autonomy is achieved [4, 5]. The objectives of secondary and tertiary control sometimes overlap in the literature. According to [6], secondary control aims to find the optimal dispatch of available DG units. However, reference [4] considers that secondary control is responsible for compensating frequency and voltage deviations, while optimal management and power flow control are performed in tertiary control. The definition presented in [4] is adopted in this thesis.

Secondary control can be performed using many different strategies, which can be classified as centralized, distributed, and decentralized [7, 8, 9, 10]. In centralized strategies, the control is performed by the Microgrid Central Controller (MGCC), where variables collected from DGs and critical loads are monitored through a communication link [4, 5, 11, 12]. Centralized strategies are well-suited for small-scale MGs or for MGs where the owners of DGs and loads have common goals [13, 11].

Centralized strategies offer rapid and efficient control of the microgrid due to the centralized access to information within the MGCC. However, dependence on centralized communication increases vulnerability to failures, as any local failure in the communication system or in the MGCC can compromise frequency and voltage regulation. Thus, one of the disadvantages of centralized control is its low reliability due to the centralization of the process [13].

Decentralized and distributed approaches have been proposed in the literature to address the reliability challenges associated with centralized strategies. These methods are well-suited for MGs where the owners of DGs and loads have different goals or for large-scale MGs, where centralized control requires a massive database and fast computational processing [11, 14, 8, 9]. In the literature, decentralized and distributed control are sometimes defined as the same. However, for this work, the definitions presented in [15, 8] are followed.

Decentralized strategies are characterized by control being performed only based on local measurements, presenting high reliability due to dismissing the communication network. However, these strategies cannot guarantee optimal performance due to the lack of information about the whole system. Consequently, without communication, coordination between controllers is not achieved in decentralized control structures [16, 14, 8, 9].

In distributed strategies, control is performed by multiple computational units (i.e., distributed control units) that can exchange information through a sparse communication network. These strategies use a small database and fast processing in each distributed control unit and can be as efficient as centralized strategies. However, the performance of these strategies still depends on the communication network [16, 14].

Regarding centralized control and its reliability drawbacks, this thesis proposes a novel unified structure for secondary control, incorporating both centralized and decentralized elements. This structure ensures that voltage and frequency regulation of the MG can be achieved even during communication or control failures. The principle of the proposed control is to employ decentralized strategies as a backup for the centralized ones. Thus, during normal op-

eration, the benefits of centralized control are maintained, and the reliability of decentralized control is guaranteed during communication and control failures. Additionally, a novel decentralized secondary voltage control strategy is proposed, based on the MG equivalent system observed by the DG.

In the proposed Unified Secondary Control Structure (USCS), a decentralized control unit (DCU) is integrated between the DGs and the MGCC. During normal operation, termed as centralized mode, the MGCC regulates the frequency and voltage. However, in the event of a failure where the MGCC loses communication, the DCUs detect this and initiate frequency and voltage regulation using a decentralized strategy, transitioning to decentralized mode. In the proposed USCS, both centralized and decentralized secondary control strategies operate concurrently, enabling the utilization of the strengths of both approaches.

1.2 Motivation and objectives

As a result of primary control actions, voltage and frequency may deviate from their nominal values. Without adequate regulation of voltage and frequency, these variables can drop to lower levels, potentially leading to load shedding, equipment shutdown, and activation of protection mechanisms. Therefore, secondary control plays a crucial role in regulating both frequency and voltage [5, 4].

Centralized secondary control strategies are commonly employed in MGs because they offer easy access to information, decision-making, and simple control configuration [12]. However, as mentioned earlier, centralized strategies performed in the MGCC can lead to reliability issues due to their centralization. To address these reliability issues, decentralized and distributed strategies are proposed. Distributed strategies maintain communication links between individual controllers, while decentralized strategies lack communication between controllers, leading to coordination issues. Despite this, distributed strategies exhibit better reliability than centralized ones, thanks to sparse communication and each DG having its own controller. Moreover, decentralized strategies offer even greater reliability compared to both centralized and distributed strategies, as they do not rely on communication between controllers [17].

To enhance reliability in centralized control, the Unified Centralized/Decentralized Frequency Control Structure (UCDFCS) is proposed in [18]. This structure incorporates a decentralized control strategy as a backup for the centralized strategy, ensuring that even during communication or control failures, the frequency of the MG can be regulated.

The UCDFCS combines the characteristics of both centralized and decentralized control strategies, ensuring coordinated operation during normal conditions and frequency regulation even during failures. Additionally, through an initialization system, the UCDFCS ensures a smooth transition between control operation modes (normal or fault operation mode), main-

taining system stability during the transition.

Despite the advantages of UCDFCS, some disadvantages are observed [18]:

- The UCDFCS is limited to frequency control only, with only the primary control operation acting for voltage control. Under and over-voltage problems can arise if only the primary control is operating;
- The smooth transition between operating modes is guaranteed only when the communication channel has little or no communication delay. However, due to the nature of communication systems, delays are almost inevitable;
- The author in [18] developed the framework based only on the PI strategy with fixed gains for centralized control. However, this control structure is able to support other centralized and decentralized control strategies.

Considering the drawbacks of the UCDFCS, this study proposes a new Unified Secondary Control Structure (USCS), which not only addresses frequency control as in [18], but also integrates voltage control. The secondary voltage control structure will be based on the UCDFCS framework. However, unlike [18], the proposed structure allows for the implementation of different control strategies in centralized control, facilitated by the tracking process. Additionally, a new decentralized voltage control strategy is proposed, aiming to regulate the voltage at the MG Point of Common Coupling (PCC).

Modifications to the initialization structure are proposed to ensure that the transition between controls is immune to communication delays. Consequently, when the system returns to normal operation after a failure, communication delays will not affect the transition of control topology.

The USCS is evaluated using the adapted low-voltage distribution network CIGRE benchmark MG proposed in [19], employing simulations in Matlab/Simulink and Real-Time Digital Simulator (RTDS) with the Hardware-in-the-Loop (HIL) environment. For Real-Time Simulations (RTS), the centralized control is implemented in the Real-Time Automation Controller from Schweitzer Engineering Laboratories (RTAC-SEL). Additionally, the MODBUS communication protocol is utilized as the communication structure due to its ease of implementation in the RTDS environment and its widespread use in MGs and power systems [20].

1.2.1 Objectives

The general objective of this thesis is to propose a new unified control structure. Which employs a decentralized control strategy as a backup of centralized control strategy, in order to maintain frequency and voltage regulation even during communication or control failures.

The following specific objectives can be listed:

- Conduct a literature review on secondary control, frequency, and voltage control in MGs;
- Implement the MG proposed in [19] in the Matlab/Simulink and RSCAD software for transient regime simulations;
- Implement the proposed control strategy in the Matlab/Simulink software and built the centralized control in the RTAC-SEL;
- Simulate and investigate the operation of the proposed strategy in the implemented MG.

1.2.2 Contributions

The contributions of this thesis are listed below:

- Present a USCS for voltage and frequency regulation, wherein the influence of the communication delay is reduced when the USCS changes its operation mode. Additionally, it proposes a tracking process that enables the use of non-PID based centralized strategies;
- Present a novel equivalent system-based decentralized secondary strategy for voltage regulation and reactive power-sharing;
- Evaluation of the proposed strategy and control thought simulations and RTS for different scenarios of control and communication contingencies.

1.3 Document Structure

The structure of this thesis is divided into six sections. Section 2 introduces the concepts and techniques related to hierarchical control of MGs, along with a literature review on secondary control techniques and strategies. In Section 3, the proposed USCS is detailed, covering its operation during normal, partial failure, and total failure modes. Additionally, the proposed decentralized secondary voltage control is discussed.

The results obtained through Matlab/Simulink are presented in Section 4. This section showcases the MG structure and controls utilized to evaluate the proposed USCS. Three cases are presented in this section: the first case demonstrates the operation of the proposed Secondary Voltage Strategy, the second case illustrates the operation of the USCS under total and partial failure conditions with and without communication delays, and the last case compares the performance of the USCS with that of the USFCS.

Section 5 focuses on the HIL results of the proposed control. This section highlights two cases: the first case examines total failure scenarios, while the second case analyzes partial failure scenarios. Finally, Section 6 presents the conclusions and final discussions regarding the proposed USCS and the decentralized voltage control.

1.4 Publications

Bellow is presented the publications related to the topic carried out during the doctorate degree.

1.4.1 First author

DE GODOY, PAULO T.; DE ALMEIDA, ADRIANO B.; DE SOUZA, A.C. ZAMBRONI; MARUJO, DIOGO; SOUZA, JONAS V.. Unified centralized/decentralized voltage and frequency control structure for microgrids. Sustainable Energy Grids & Networks, v. 38, p. 101366, 2024.

DE GODOY, PAULO T.; DE ALMEIDA, ADRIANO B.; DE SOUZA, ANTONIO CARLOS ZAMBRONI; VENKATESH, BALA; DOS SANTOS, FELIPE CRESTANI; DE SOUZA, JONAS VILLELA. Analysis and Implementation of the Unified Centralized/Decentralized Frequency Control Structure in Hardware in the Loop Environment with RTDS. In: 2022 IEEE Power & Energy Society General Meeting (PESGM), 2022, Denver. 2022 IEEE Power & Energy Society General Meeting (PESGM), 2022. p. 1.

DE GODOY, PAULO T.; DE ALMEIDA, ADRIANO B.; ZAMBRONI DE SOUZA, ANTONIO CARLOS; VENKATESH, BALA. Global Power flow for Microgrids. In: 2021 IEEE Power & Energy Society General Meeting (PESGM), 2021, Washington. 2021 IEEE Power & Energy Society General Meeting (PESGM), 2021. p. 1.

GODOY, PAULO THIAGO; ALMEIDA, ADRIANO BATISTA; MARUJO, DIOGO. Unified centralised/decentralised frequency control structure for microgrids. IET RENEWABLE POWER GENERATION (ONLINE), v. 1, p. 1-14, 2021.

1.4.2 Coauthor

FELISBERTO, KIM DIEFREI REMBOSKI; DE GODOY, PAULO THIAGO; MARUJO, DIOGO; DE ALMEIDA, ADRIANO BATISTA; DE BARROS ISCUISSATI, RODRIGO. Trends in Microgrid Droop Control and the Power Sharing Problem. Journal Of Control Automation And Electrical Systems, v. 1, p. 1, 2022.

BENDER, S. G.; ALMEIDA, A. B.; GODOY, P. T.; OLIVO, D.. Avaliação do Desempenho Dinâmico de Técnicas de Phase-Locked Loop Aplicadas a Microrredes. In: XIX ERIAC - Encontro Regional Ibero-Americano do CIGRE-ERIAC, 2023, Foz do Iguaçu. XIX ERIAC - Encontro Regional Ibero-Americano do CIGRE-ERIAC, 2023.

OLIVO, D.; ALMEIDA, A. B.; GODOY, P. T.; BENDER, S. G.. Contribuição das estratégias de PWM na prestação de serviços ancilares em microrredes. In: XIX ERIAC - Encontro Regional Ibero-Americano do CIGRE-ERIAC, 2023, Foz do Iguaçu. XIX ERIAC - Encontro Regional Ibero-Americano do CIGRE-ERIAC, 2023.

MOTA, GUILHERME L. G. S.; DE GODOY, PAULO T.; DE ALMEIDA, ADRIANO B.. Decentralized Underfrequency Load Shedding Based on the Droop Characteristic for Microgrids. In: 2021 IEEE Madrid PowerTech, 2021, Madrid. 2021 IEEE Madrid PowerTech, 2021. p. 1.

IORIS, DARLAN; DE ALMEIDA, ADRIANO BATISTA; DE GODOY, PAULO THIAGO. A Microgrid Islanding Performance Study Considering Time Delay in Island Detection. In: 2020 IEEE PES Transmission & Distribution Conference and Exhibition Latin America (T&D LA), 2020, Montevideo. 2020 IEEE PES Transmission & Distribution Conference and Exhibition - Latin America (T&D LA), 2020. p. 1.

K. D. R. Felisberto; A. B. Almeida; GODOY, P. T.. Avaliação de técnicas de controle primário aplicadas em microrredes. In: VIII Simpósio Brasileiro de Sistemas Elétricos - SBSE 2020, 2020, Santo André. VIII Simpósio Brasileiro de Sistemas Elétricos, 2020.

IORIS, DARLAN; DE GODOY, PAULO THIAGO; FELISBERTO, KIM DIEFREI REMBOSKI; POLONI, PATRÍCIA; DE ALMEIDA, ADRIANO BATISTA ; MARUJO, DIOGO . A power electronic converter-based microgrid model for simulation studies. Energy Systems, v. 1, p. 1, 2021.

Chapter 2

Secondary Control in Microgrids

2.1 Initial considerations

In Chapter 1, the importance of studying control strategies applied to MGs was emphasized, as it is crucial to maintain frequency and voltage regulation through secondary control to prevent these variables from exceeding their operating limits.

This chapter explores the concepts and techniques related to control applied to MGs, with a particular emphasis on secondary control techniques and strategies. Initially, the chapter introduces the structure and concepts pertaining to MGs and hierarchical control. Subsequently, it delves into the secondary control, the primary focus of this thesis, and discusses the main techniques of centralized and decentralized control, while highlighting the drawbacks of centralized control.

2.2 Hierarchical Control and Microgrid Structure

An MG can consist of different generation sources, loads, Battery Energy Storage Systems (BESS) and control and monitoring devices [1, 2]. Fig. 2.1 presents a basic structure of an MG.

One of the main operating features of an MG is the ability to operate connected or isolated from the main network. In connected mode, the MG is linked to the main grid, with power flowing between the two systems through the PCC. In this configuration, the MG must regulate the power flow at the PCC to optimize energy sales or minimize operating costs. Additionally, the MG can provide ancillary services to the main grid, such as reactive power or voltage control [1, 2].

In islanded operation mode, the MG operates independently without any electrical connection to the main network. In this mode, the MG is responsible for maintaining its active and reactive power balance and also generates its own voltage and frequency references. To operate in island mode, the MG requires a BESSs or a dispatchable generation sources, which are

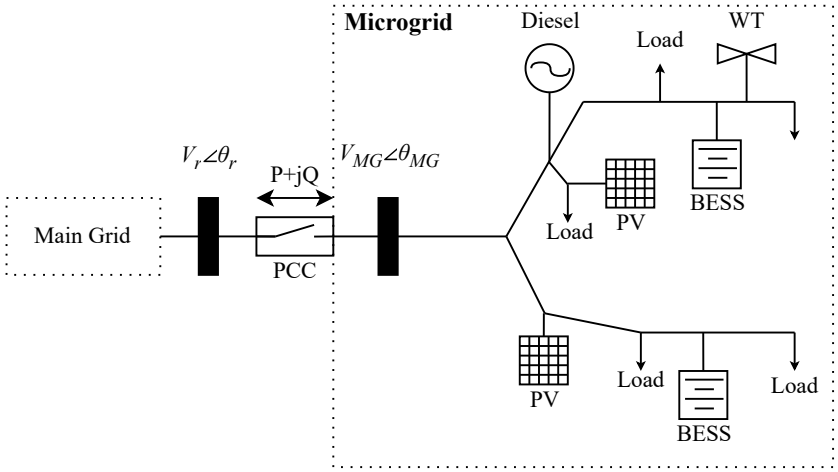

Figure 2.1: Example of MG structure.
Source: Adapted from [3]

capable of dispatching energy as needed to maintain the MG's power balance. Furthermore, if the MG has multiple dispatchable sources, it is essential to share power among these generation sources [1, 2].

In an islanded MG, voltage and frequency regulation are crucial for maintaining the quality of electric energy. Moreover, during islanded operation, the MG must possess the capability to synchronize with the main grid, optimize the dispatch of generation sources, and recover the system after a failure — a process known as black start [4, 5, 12].

The diverse activities involved in operating MGs require different times and control actions, making a hierarchical control structure more suitable for MG applications [4, 5]. Typically, hierarchical control in MGs consists of three layers: primary, secondary, and tertiary control, as illustrated in Fig. 2.2. Each layer serves a distinct function and operates with different performance times [4, 5].

2.2.1 Primary Control

The primary control strategies are inspired in the conventional droop control, used in synchronous generators of large power systems [21, 1]. The droop control strategies employed in MGs can be described using the graphics of Fig. 2.3.

Primary control dispatches DGs to regulate frequency and voltage, where the references for these variables are determined by the droop controls of frequency (Fig. 2.3(a)) and voltage (Fig. 2.3(b)), respectively. In response to changes in demand or generation, dispatchable DGs adjust their generation to compensate for power balance deviations (ΔP and ΔQ). The droop controllers of each DG receive the generation deviation and, consequently, adjust the frequency ($\Delta\omega$) and voltage (ΔV) control actions of each source [21, 1, 2]. The droop controls for frequency and voltage, shown in Fig. 2.3, are described by the following equations:

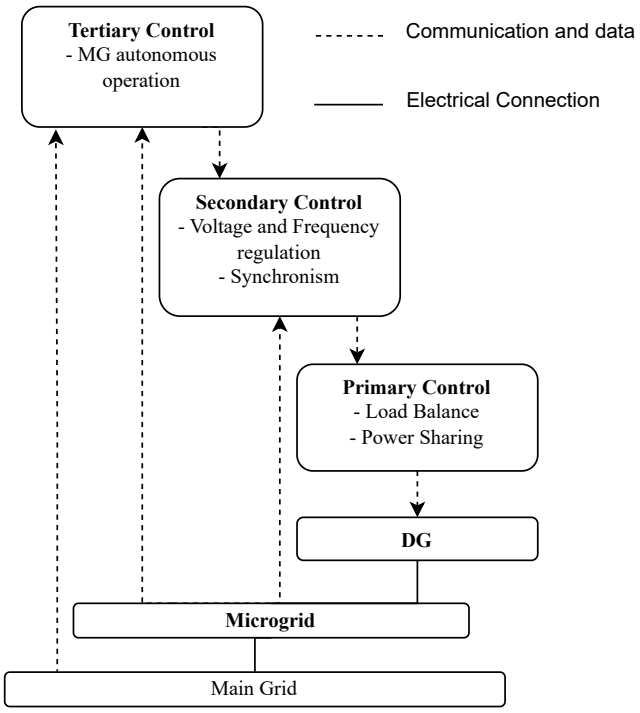

Figure 2.2: Hierarchical Control Structure for MGs.

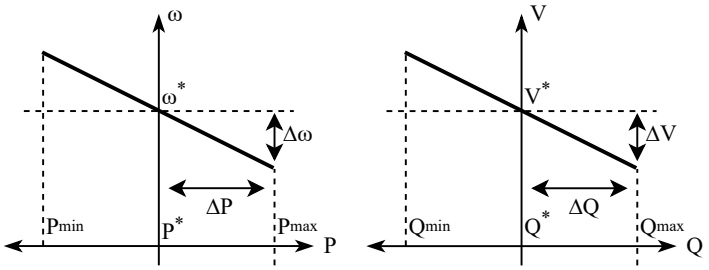

Figure 2.3: Droop control in MGs. (a) f/P. (b) V/Q.
Source: Adapted from [4]

$$\omega = \omega^* - m \cdot (P - P^*) \tag{2.1}$$

$$V = V^* - n \cdot (Q - Q^*) \tag{2.2}$$

where ω is the new frequency generated by the droop controller, ω^* is the reference frequency of the droop controller, m is the coefficient of droop for frequency, P is the active power generated by the DG, P^* is the reference active power for the DG, V is the new voltage generated by the controller droop, V^* is the reference voltage of the droop controller, n is the voltage droop coefficient, Q is the reactive power generated by DG and Q^* is the reference reactive power for DG.

Several droop control techniques have been evaluated for application in MGs, including:

- Resistive droop: In this technique, the voltage variation is proportional to the variation in active power, while the voltage variation is proportional to the opposite of the variation in reactive power [22, 23];
- Rotational matrix: This technique involves passing the variations of active and reactive power through a rotational matrix to generate reflected active and reactive power. The variations in frequency and voltage are then generated considering the reflected active and reactive power [24, 25];
- Virtual impedance: One of the most explored techniques in the literature, where a virtual impedance is implemented to control voltage and frequency variations [26].

2.2.2 Secondary Control

Given the presence of frequency and voltage deviations resulting from primary control actions, secondary control aims to regulate the frequency and voltage of the MG to their nominal values [4, 5, 27].

The secondary control adjusts the frequency (ω^*) and voltage (V^*) references in the droop controllers of each DG using the control actions $\Delta\omega_{sec}$ and ΔV_{sec} [4, 5, 27]. The interaction between secondary and primary control can be illustrated in Fig. 2.4, where the activation of primary control leads to frequency and voltage values deviating from their nominal values. The secondary control then modifies the frequency (ω^*) and voltage (V^*) references, altering the position of the droop curve of each generator to restore the frequency and voltage to their nominal values [27].

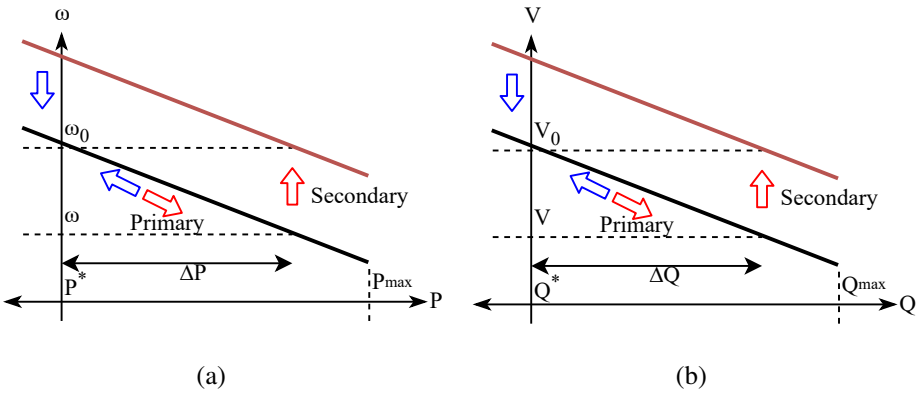

Figure 2.4: Secondary control actions over the primary control. (a) f/P. (b) V/Q. Source: Adapted from [27]

Several secondary control techniques have been developed, broadly classified into three categories [12, 8]:

- Centralized: Control is conducted through a single control entity known as MGCC. Information and communication are centralized;
- Decentralized: Control is executed by multiple control entities, with each controller utilizing only local information for decision-making, without communication with other controllers;
- Distributed: Control is managed by multiple control entities, with each controller utilizing local information and information from some of its neighbors to make decisions. The communication structure is sparse, without the need for controllers to communicate with all other controllers.

The choice of strategy depends on the characteristics of the MG, the requirements for reliability, accuracy, response time, and other desired specifications for the control.

The Figs. 2.5 and 2.6 illustrate the frequency, voltage, active and reactive power of a hypothetical MG. This hypothetical MG comprises a BESS DG connected to a load. The converter data are provided in [19], and the load is represented by a resistor and inductance in parallel. Although droop control is not necessary in the hypothetical MG due to having only one converter, the objective is to illustrate the dynamics of secondary and primary control. Two cases are presented: the first case depicts the MG without regulation, while the second case shows the MG with regulation. The hypothetical MG is assumed to be islanded, and the secondary control is activated at 0.5 s. At 2.2 s, the MG load increases.

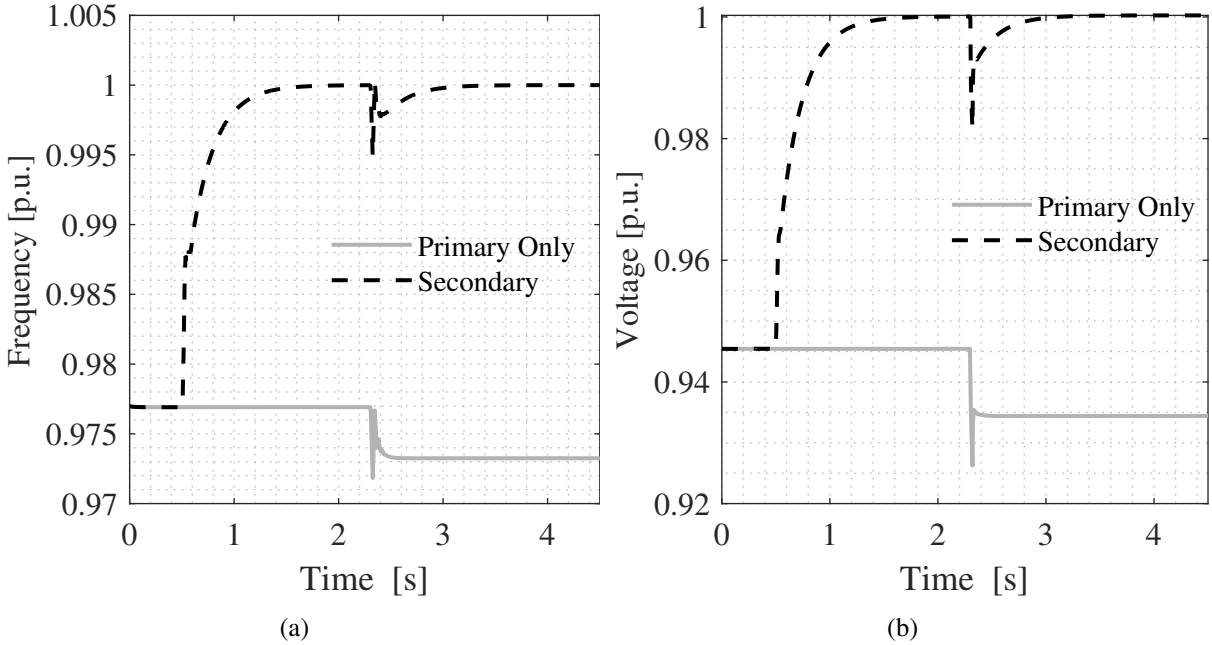

Figure 2.5: Secondary Control Dynamics. (a) Frequency. (b) Voltage.

Through Figs. 2.5 and 2.6 it is possible to observe the performance of the primary control. Because, with the increase of the load at 2.2 s, the active and reactive power generated by the MG sources increase, however, the frequency and the voltage in the PAC decrease significantly.

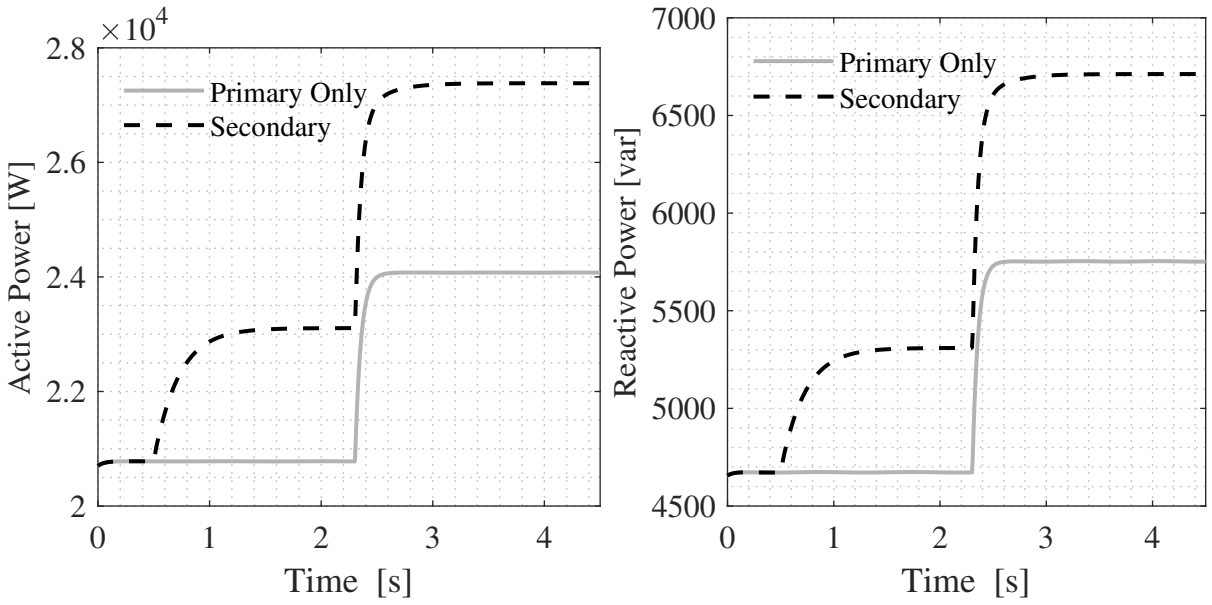

Figure 2.6: Hypothetical MG dynamic. (a) Active Power. (b) Reactive Power.

Without the operation of the secondary control, the voltage and frequency in an MG can reach values lower than those allowed, which can even cause the MG to shut down. Only with the action of the secondary control voltage and frequency are regulated to safe values.

It is also possible to observe that with the action of the secondary control, the power generated by the system increased. This is due to the dependence of the load on voltage and frequency.

2.2.3 Tertiary Control

The tertiary control involves the optimal energy management problem in MGs, aiming to optimize the operation of each DER available in the system. Fig. 2.7 shows, schematically, the energy management problem in an MG [28, 17]. It is a problem of considerable complexity [13, 6, 28].

In grid-connected mode, the tertiary control seeks to combine the available DERs to meet the variable demand of consumers with the minimum possible cost and respecting the restrictions of the system, taking advantage of local intermittent renewable sources and the possibility of power exchange with the main grid [28, 6].

In the islanded mode, the tertiary control must guarantee the MG autonomy, so that the output power of the DERs must meet the total load demand of the MG. It is sometimes necessary to undergo a load-shedding process to match generation and demand. The main objective in this mode is to maintain the MG's operation as long as possible, supplying the most important loads. Additionally, operation cost optimization and minimizing losses can be considered [28, 6].

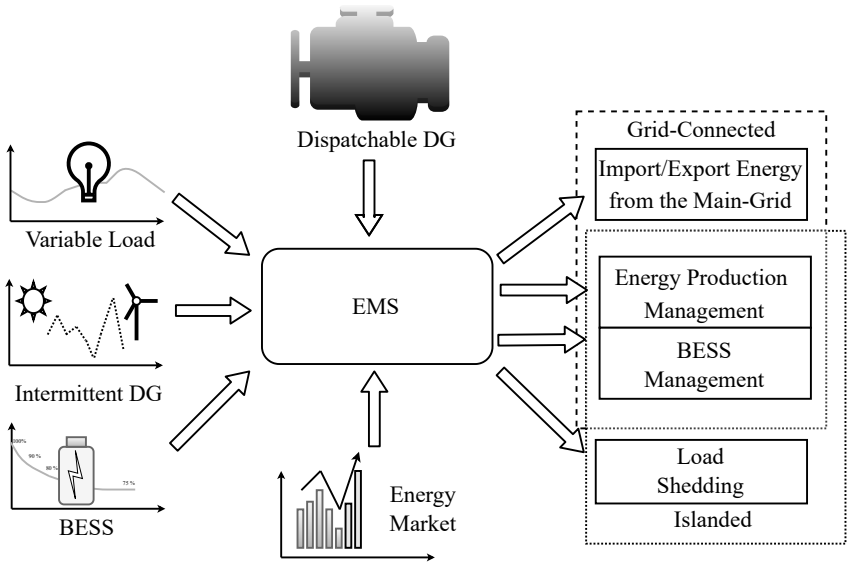

Figure 2.7: Tertiary Control Structure for MGs.
Source: Adapted from [17].

2.3 Secondary Control Strategies

Several pieces of research have been proposed to improve secondary frequency control. References [29, 30, 31] propose local measurement-based decentralized secondary control strategies. Reference [29] proposes a lossy integral for frequency restoration. Thus, the proposed strategy presents a frequency deviation in the steady state. A proportional control with a low-pass filter for frequency regulation is proposed in [30]. Again, a frequency deviation in the steady state is observed. Reference [32] presents a fully decentralized leaky integral controller for frequency regulation derived from a classic lag element.

The equivalence between secondary control and the Washout Filter-Based power-sharing strategy for frequency and voltage regulation is presented in [31]. Reference [33] proposes a linear model-based state estimator, considering a cost function to the voltage regulation. Cooperative control of frequency and voltage by using a Luenberger observer is proposed in [34]. A decentralized sliding mode estimator with a frequency and voltage cooperative control is proposed in [35].

In [36] is proposed a secondary frequency control based on the proportional control with a low-pass filter. Wherein the main objective is to ensure power-sharing during clock drifting. To achieve the objective, the active power is considered in the secondary control, where the generated active power is compared to the maximum active power, and the difference is added to the secondary control action.

The clock drift occurs due to the digital processors, each having its own clock, thus the time signal of the processor differs from the time signals of the other processors due to the clock drifts. The effects of the clock drift in the droop-based primary control are investigated in reference [37], where it is nearly negligible. However, for secondary controls, the effects of

the clock drift can depend on the control strategy. Employing local integral controllers as the secondary control tends to lead the system to an unstable equilibrium point [38], on the other side, distributed strategies tend to be less affected by clock drift if the controls are properly tuned [39, 40, 41, 42]. However, for decentralized strategies, the clock drift tends to lead to active power-sharing errors [43].

In the distributed control strategies, most research involves the concept of a multiagent system [10]. Reference [44] employs a PI controller in each distributed control unit, using an average value of frequency and voltage. A Distributed Averaging PI control to regulate the frequency and voltage is employed in [45]. Reference [8] proposes an optimal distributed control for frequency and voltage regulation. A finite-time controller provides frequency regulation and active power-sharing.

Reference [46] proposed a consensus-based for frequency control and a distributed finite-time for voltage control. Both strategies have the objective of regulation and power sharing. The transmission interval and message dropouts in the consensus-based secondary control are investigated in reference [47]. The effects of communication failure that provoke network partitions for the distributed consensus secondary control are presented in reference [48]. During the partitioned operation, various sub-MGs are formed, thus the power sharing is lost and the MG tends to maintain its stability.

A distributed frequency regulation control is proposed in [49]. It is important to note that the authors proposed a novel strategy where the distributed frequency regulation control acts as both primary and secondary control, however, when a communication failure occurs, the system changes to the droop control. For the distributed strategy, the sum of the active power of the neighbors is employed in a proportional control. This strategy was a similar concept of the proposed strategy presented in these, however, a centralized strategy is employed and additionally, a decentralized secondary voltage control is employed.

Reference [50] proposes a centralized/distributed structure, where the frequency and voltage regulation, power-sharing, and optimal power dispatch are considered as control objectives. The frequency regulation and the power-sharing are carried out by a consensus-distributed strategy, in which the primary and secondary control are considered in this one control strategy. The optimal power dispatch and the voltage regulation are carried out by a central controller, where a PI controller is employed for voltage regulation, and a non-linear optimization problem is employed for the optimal power dispatch.

A distributed reactive and active power sharing and frequency and voltage regulation strategy is proposed in [51]. In this strategy, the author proposed two decoupled controls, where the frequency and voltage regulation are determined by the combination of both controls. One control is responsible for the voltage regulation, and the other is for the power-sharing. For both controls, the power and voltage of the other converters must be known.

In [52] a non-linear distributed control strategy is proposed, this control can work as

both primary and secondary control. To achieve its objective of control robustness for system changes, a Sliding Mode Control is proposed. The controls employ the concept of graph theory, where the average value of the active and reactive power is calculated through the average values of its neighbors.

Concerning the secondary consensus control strategies, the authors in [53] proposed a method for tuning the control gains. The method proposed in [53] is based on the factorial design of experiments using screening and fractional factorial designs. The design of experiments is a method that tends to optimize the experimental procedure, through varying the factor levels for each experiment. Additionally, the experimental conditions were ordered to obtain accurate information, in order to reduce the number of experiments. In other words, the method can ensure optimal settings for the control tuning with a minimal number of experiments.

Additionally, event-triggered-based strategies are being adopted in the distributed strategies [54, 55, 56]. A Lyapunov-based method with a cooperative event-trigger controller for centralized and decentralized control strategies is proposed in [54]. Reference [55] proposes a consensus algorithm with event-triggered where the frequency regulation and the economic dispatch are achieved. A distributed event-trigger-based control is proposed in [56]. The pinning-based protocol is used for frequency and voltage regulation, and a consensus-based optimal power-sharing control protocol is considered for economic dispatch.

In [57], a decentralized approach with a time-dependent protocol is proposed for frequency regulation. Where a Switched Control Scheme is employed, the control switches between two configurations: the filtered proportional controller and the integral controller. Thus, in this strategy, the control can ensure that a better performance is achieved in a steady state. Additionally, in references [58, 59] an extension of the strategy presented in [57] is proposed, where the reduction of the frequency regulation in steady state is achieved. The control proposed employs a dynamic droop control gain during the time-dependent protocol.

Multi-MG (MMG) secondary control strategies are proposed in the literature [60, 61]. In [60], the Grey Wolf optimization algorithm is employed to adjust the PID controller gains for the MMG secondary control. Furthermore, a secondary fuzzy PD controller in cascade with a PI-PD controller for MMG is proposed in [61]. Additionally, the control gains are adjusted through the JAYA heuristic algorithm.

Regarding the centralized strategies, references [62, 63, 64, 65, 66] proposes a fuzzy system to automatically tune the PI gains of the secondary control to improve the stability and the performance. An artificial neural network is employed in [64] to provide an online modification of the control parameters. The membership functions are obtained in the [65] by the particle swarm optimization algorithm. In [66], the frequency regulation in a system with high penetration of wind generation is considered. With regard to the communication influences in the secondary control, reference [67] analyzes the influence of the communication delay in the PI control.

In [68], the influence of communication multi-delay on the stability frequency regulation with the PI controller is analyzed. Finally, a predictive model controller to avoid communication delays in the frequency regulation is proposed in [69].

Concerning the reliability of the centralized strategies, reference [18] proposes a UCDFCS, where the frequency of the MG can still be regulated even during control and communication failures. In the UCDFCS, the decentralized strategy is employed as a backup for the centralized strategy. However, the UCDFCS considers only the frequency regulation, and the centralized strategy must be a PI control strategy. Additionally, the UCDFCS are influenced by communication delays when the control changes from one strategy to another.

Chapter 3

Proposed Controls

3.1 Initial considerations

In this Chapter, the proposed USCS and the decentralized voltage control are presented. The novel USCS is designed to address the shortcomings of the UCDFCS and enhance the reliability of secondary control. Additionally, the new decentralized voltage control is proposed to operate within the USCS framework, ensuring voltage regulation and facilitating reactive power sharing.

Chapters 1 and 2 presented the operation of the hierarchical control and the secondary control, and their importance to the MG operation. In the secondary control, the frequency and voltage regulation are the main objectives, different strategies are employed in order to achieves these objective - i.e. the centralized, distributed and decentralized strategies. The centralized strategy is one of most simple and widely employed strategy in MGs systems. However, this strategy suffers from reliability problems.

To guarantee the centralized secondary control frequency regulation reliability, the UCDFCS is proposed in [18]. Since a decentralized control strategy operates as a backup for the centralized strategy. The UCDFCS also has an initialization strategy, which ensures a smooth transition between control strategies, maintaining stability in the system.

However, some issues can be observed in UCDFCS: it was designed only for PI-based centralized control, and although the system supports several decentralized control strategies, only one strategy was presented. The proposed initialization strategy is affected by the communication delay between the DCU and the MGCC, so non-smooth transitions can be observed. And, as shown, the UCDFCS will operate only for frequency, with voltage regulation being disregarded.

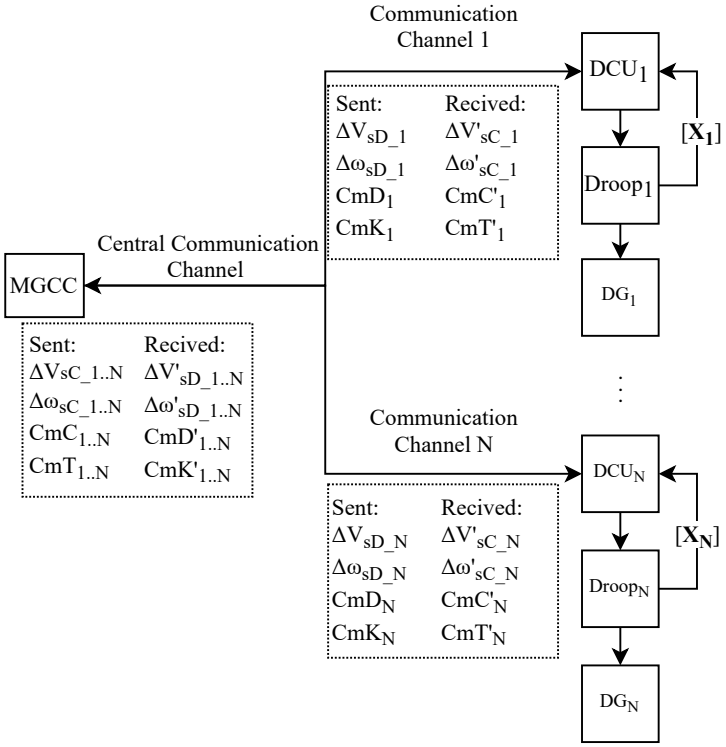

Figure 3.1: Proposed structure of the secondary control.

3.2 Proposed unified Secondary Control

As mentioned previously, the proposed USCS is based on the UCDFCS [18]. The structure of the proposed USCS is presented in Fig. 3.1, where the DCUs are employed between the MGCC and the DGs that participate in the secondary control. As presented in [18], the messages sent by a controller are denoted without an apostrophe, and the messages received by a controller are denoted with an apostrophe.

A Decentralized Control Unit (DCU) is employed between the DGs and the MGCC. When in normal operation, i.e., without failures, the MGCC regulates the frequency and the voltage. This mode is nominated as a centralized mode. When a failure occurs, the DCUs identify that the MGCC cannot communicate and thus begin to regulate the frequency and voltage through a decentralized strategy, changing to a decentralized mode. In the proposed USCS, both centralized and decentralized secondary control strategies operate simultaneously, which makes it possible to take advantage of the potential of each strategy. Thus, the decentralized strategies are employed as a backup for the centralized ones. Some modifications are proposed to reduce the communication delay's influence when the USCS changes its operation mode.

Observe in Fig. 3.1 that the DGs that participate in the secondary control are denoted with the index i, where the source with the lowest index has the highest hierarchy. The attribution of the index to DG can be carried out based on power data, reliability, generation cost, or other desired characteristics. For this work, the DGs index are selected arbitrary.

The MGCC and the DCUs exchange information through the communication channel,

thus the MGCC is able to know the states of all the DCUs, and each DCU is able to know the state of the MGCC. The MGCC sends a message to each DCU, containing the following variables: the frequency ($\Delta\omega_{s_{C_i}}$) and voltage ($\Delta V s_{C_i}$) control actions generated for each DG; a signal indicating the operation of the MGCC and the communication channel (CmC_i); and the mode in which each DCU must operate (CmT_i).

The DCU also sends a message to the MGCC, containing the following variables: the frequency ($\Delta\omega_{s_{D_i}}$) and voltage ($\Delta V_{s_{D_i}}$) control actions received/generated for each DG; a signal indicating the operation state of the DCU (CmD_i); and the operating mode in which DCU is (CmK_i).

The proposed USCS presents three operational conditions:

- Normal operation: the DCUs and the MGCC have no communication or control failures, thus the DCUs and the MGCC can communicate;
- Total failure: all the DCUs cannot communicate with the MGCC. Then, all DCUs change to Decentralized Secondary Control (DSC) mode;
- Partial failure: one or more DCUs cannot communicate with the MGCC. Hence, only the DCUs that present failure change to DSC mode.

The normal operation refers to the operation without failures, thus the centralized strategies can operate without any issues. The failure conditions can be classified as total or partial For each failure the control will take different actions.

3.2.1 Normal Operation

In normal operation, the MGCC will regulate the frequency and the voltage by setting the control actions $\Delta V_{s_{C_i}}$ for voltage and $\Delta\omega_{s_{C_i}}$ for frequency, and sending them to each DCU through the communication channel. The MGCC generates the control actions through the centralized control strategy, where CC_f and CC_V are the centralized secondary frequency and voltage strategies. Along with the control actions, the MGCC sends more information to the DCUs, the $CmC = 1$ to indicate whether the MGCC is operational and the $CmT = 0$ to inform the DCU to operate in DSC mode.

Each DCU receives the message from the MGCC, and if the variable CmT indicates it to operate in Centralized Secondary Control (CSC) mode ($CmT = 1$), the DCU will send the received control action to its respective DG. The control actions sent to the droop controller of a DG is denoted by $\Delta\omega_{s_D}$ for frequency and by ΔV_{s_D} for voltage. Thus, for regular operation, the control actions of the secondary control sent to a DG denoted with index i will be $[\Delta\omega_{s_{D_i}}, \Delta V_{s_{D_i}}] = [\Delta\omega'_{s_{CC_{f_i}}}, \Delta V'_{s_{CC_{V_i}}}]$. Each DCU, after receiving the messages from the MGCC, sends a new message to the MGCC reporting the control actions sent to the droop

controller, the variable $CmD_i = 1$ indicating that the DCU is operational, and the variable $CmK_i = 0$ indicating that the DCU is operating in DSC mode.

To illustrate this control mode, the Fig. 3.2 presents the messages sent and received for each component. Note that the control actions message sent by the DCUs to the MGCC presents the control actions received from the MGCC added with the initialization variables (IH_f and IH_V), theses variables are employed when the control changes its operation mode (DSC to CSC and CSC to DSC), ensuring that the control actions do not change abruptly.

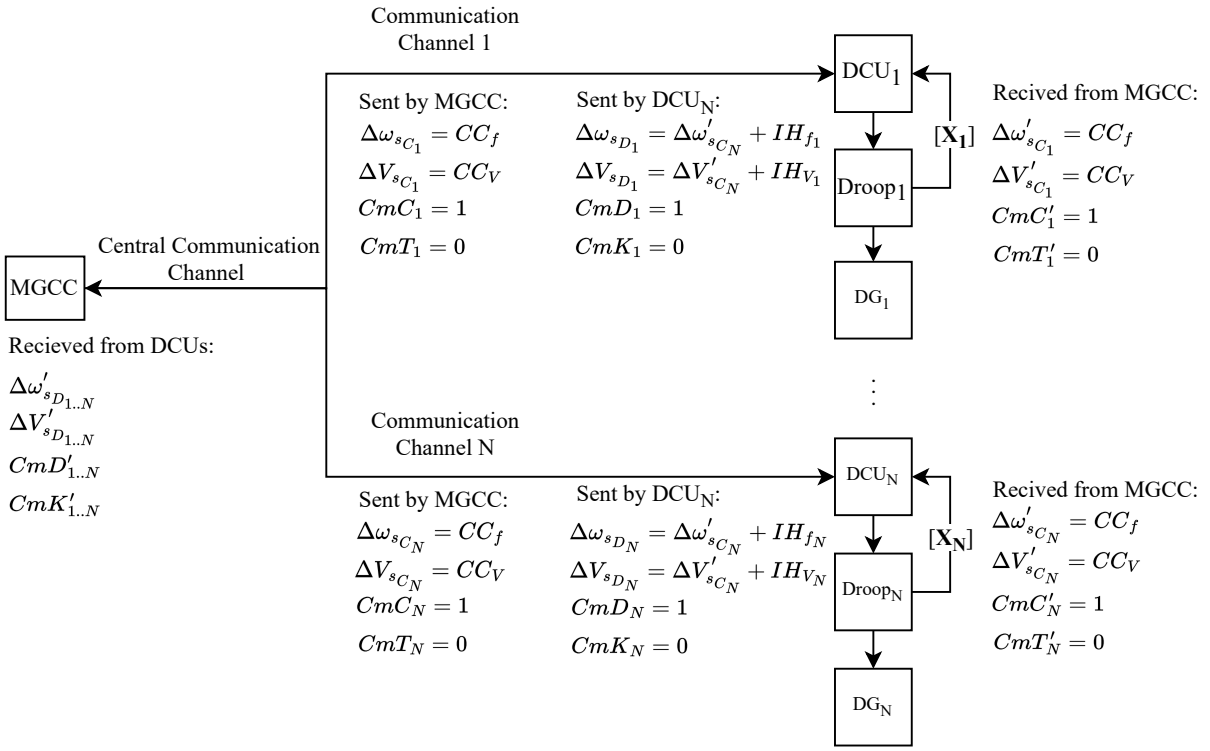

Figure 3.2: Messages during the normal operation.

3.2.2 Partial Failure

A partial failure is determined when some DCUs cannot communicate with the centralized controller. Some causes of this failure is the communication cable breakage or the communication interface of the DCUs fails. If a partial failure occurs, the DCUs affected by the failure will no longer communicate with the MGCC; thus, these DCUs change to DSC mode. In DSC mode, the DCUs assume the frequency and the voltage regulation using only local information. When the DCUs change to DSC mode, the control actions generated by the decentralized strategies must be initialized with the last control actions sent by the MGCC, thus avoiding the abrupt variation of the control actions - this initialization occurs in the decentralized strategy, where the first value generated by the decentralized strategies must present the same values of the last increment sent by the MGCC. Fig. 3.3 shows this state of operation when the communication

channel of the DCU 1 presents the failure.

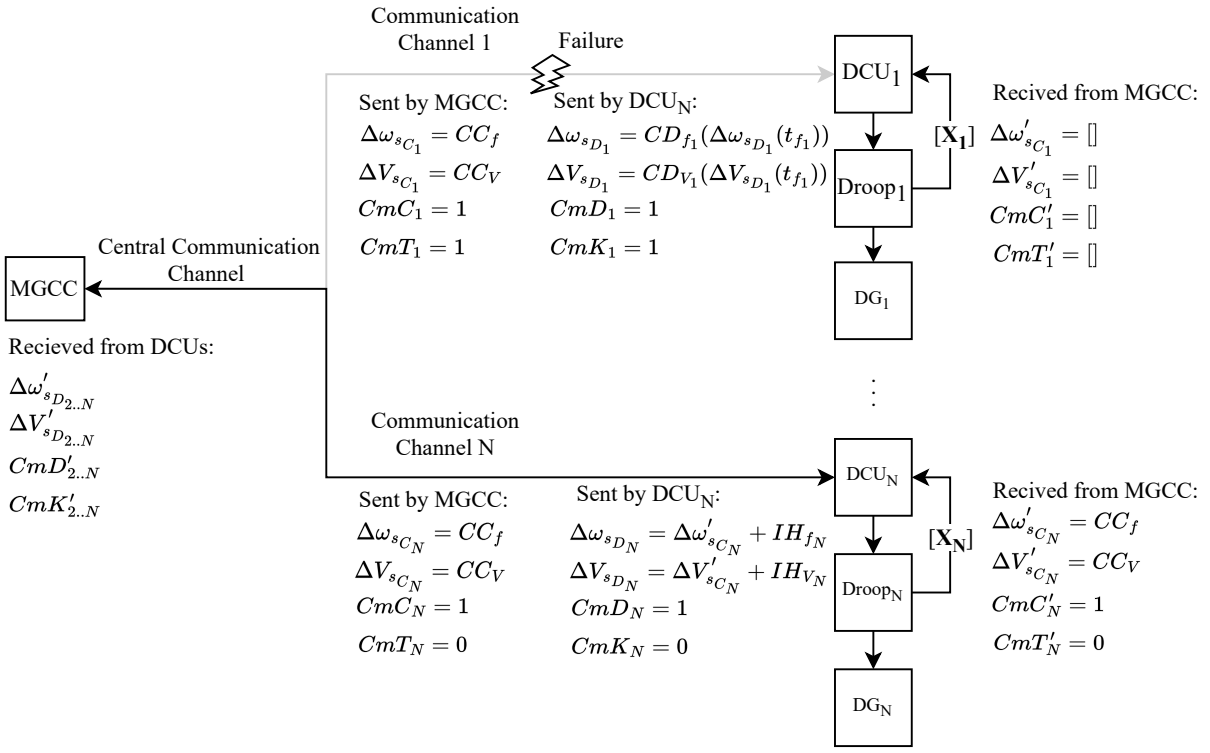

Figure 3.3: Messages during the partial failure.

It is possible to observe in Fig. 3.3 that both the DCU 1 and the MGCC cannot receive messages from each other. The variables sent to each control are only set, however, due to the failure the message is not received. Note too, that the other DCUs still operate in the CSC mode.

If the DCU communication channel returns ($State_i = 1, i \in N$), the MGCC and the DCU can exchange information again, thus the DCU sends a message to the MGCC with its current operation mode ($CmD = 1$ and $CmK = 1$) and the control actions generated by the DSC strategies ($\Delta\omega_{s_{D_i}}$ and $\Delta V_{s_{D_i}}$). At first, the MGCC will inform the DCU to continue operating in DSC mode for a while, this state is presented in Fig. 3.4; then, the MGCC will send the message to the DCUs to operate in CSC mode. Observe that in this process, only the DCU with failure maintains its operation in DSC mode, the other DCUs still operate in CSC mode. Additionally, this process is very short, it only lasts until the DSC changes its mode to CSC.

Once the DCU receives the message from the MGCC, it will first calculate an initialization variable for both control actions (IH_f and IH_V) and then switch to CSC mode. The initialization variable is calculated by the difference between the last control actions generated by the DCU and the first control actions received from the MGCC when changing to CSC mode. Thus, by applying this process, the voltage and frequency control actions sent by the MGCC and observed by the DCU will equal the last control actions generated by this DCU when it was operating in DSC mode. Note that, different from [18], the initialization variable is calculated in DCU and not in the MGCC. This procedure in the DCU ensures that communication delays do not affect the control actions when changing to CSC mode. Because, if calculated in the

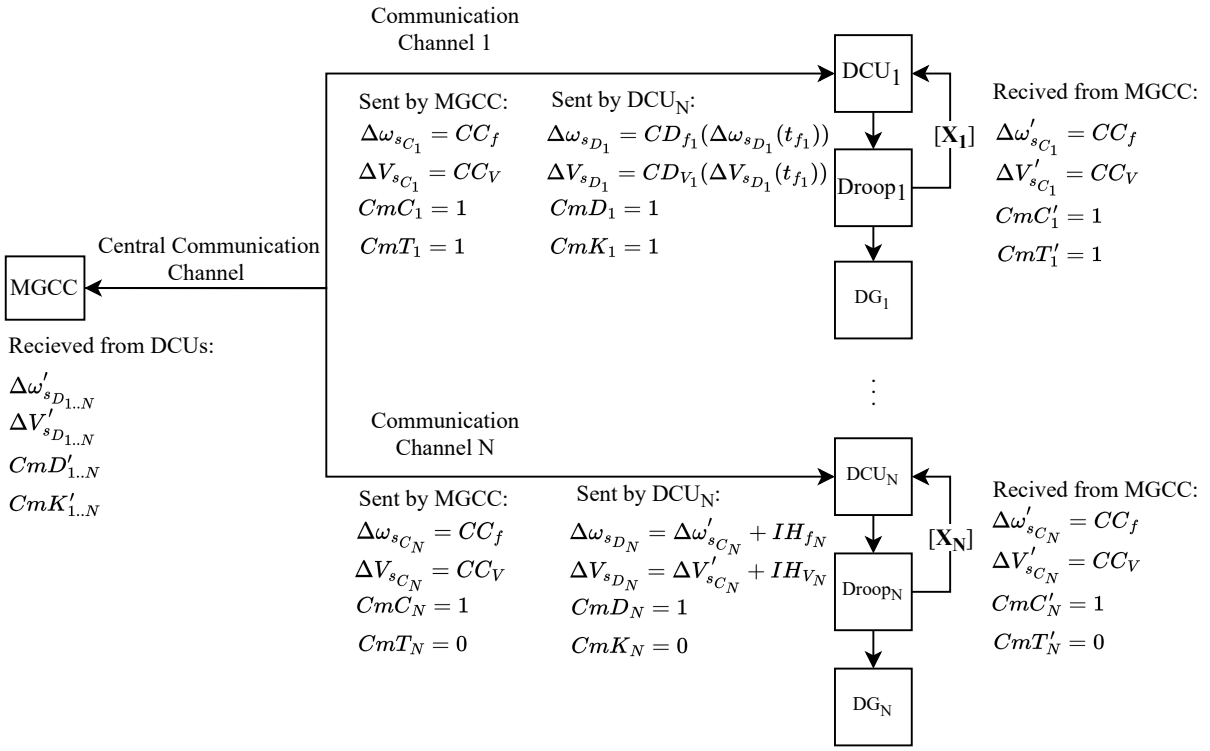

Figure 3.4: Messages after the partial failure ends.

MGGC, when the DCU receives the command to change the operation mode with the new control actions, due to the communication delay, a difference between the CSC and DSC control actions can occur. Thus, when this process ends, the system returns to operating in the normal mode.

3.2.3 Total Failure

A total failure is determined when all the DCUs cannot communicate with the centralized controller. Some causes of this failure is the failure of the central communication switch, the communication interface of the MGCC fails, or the MGCC turns off. If a total failure occurs, all DCUs will change to DSC mode, and, as in partial failure, the DCUs use the last control actions sent by the MGCC to initialize the decentralized strategy - the same procedure for the partial failure is employed. The state of total failure is presented in Fig. 3.5, note that MGCC does not send or receive any messages, however, the DCUs still change their states to ensure the DSC operation mode.

When the failure ends, the MGCC and the DCUs can exchange information again. The MGCC sends a message containing the variables $CmC = 1$, $CmT = 1$, and the control actions to all DCUs that have their communication channels operating. The variable $CmT = 1$ warns the DCU to maintain its operation in DSC mode. Thus, each DCU maintains the DSC mode and sends a message to the MGCC containing the variables $CmD = 1$, $CmK = 1$, and the value

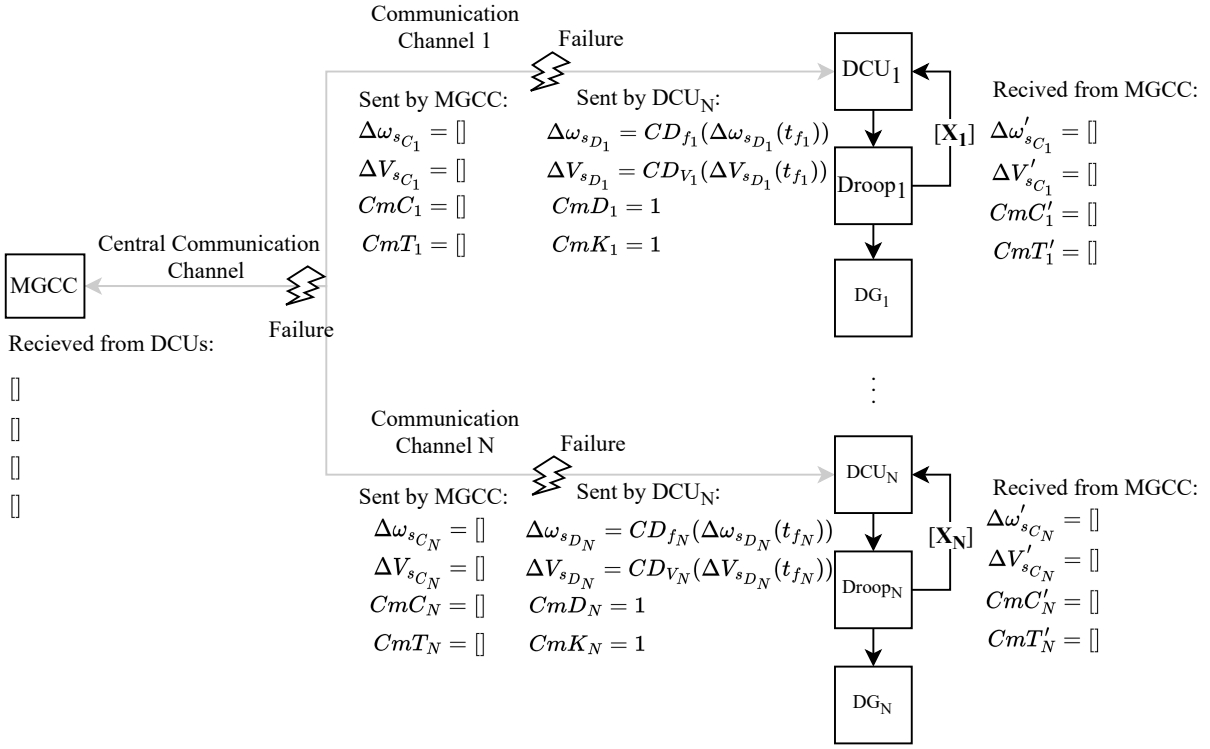

Figure 3.5: Messages during the total failure.

of the control actions generated by the DSC strategy. The state when the DCUs are operating in DSC mode and the MGCC resumes operation is presented in Fig. 3.6, where the MGCC sends the same messages to all DCUs. Note that the increments generated by the centralized strategies are sent to the DCUs, but these values are not applied.

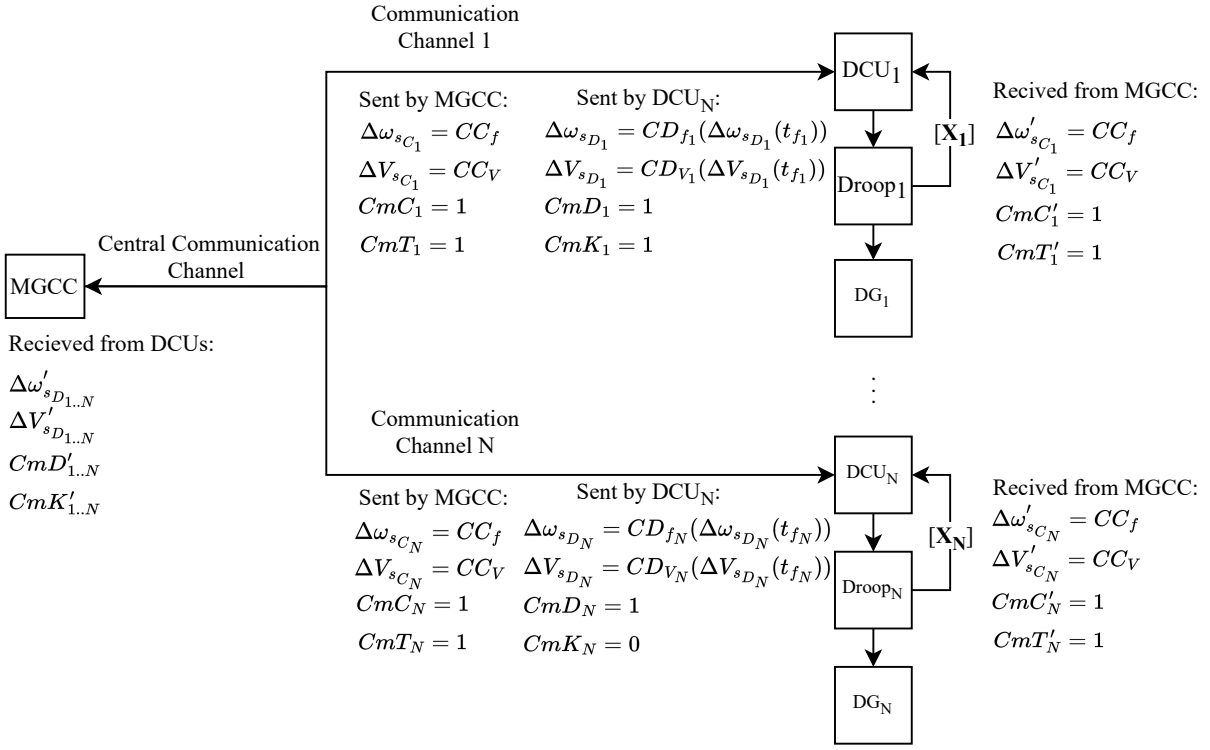

Figure 3.6: Messages during the tracking process.

The MGCC, when receiving the messages from the DCUs, can know which communication channels are operating ($CmD'_i = 1$). After that, the MGCC will arbitrarily select a DCU (denoted by index k) to start the tracking process. The tracking process is carried out to ensure that the first control actions sent to the DCUs are near the control actions generated by the selected DCU when operating in the DSC mode.

Unlike [18], where the tracking process is coupled with the PI controller, the proposed tracking process does not include a coupled control mesh in the centralized controller. Thus, to apply the proposed USCS with various types of centralized strategies, the proposed tracking process only changes the initialization value of the centralized control strategy when two conditions are maintained: during a period of X time ($X \in \Re^+$) the system does not suffer any communication or control failure; and the voltage and frequency derivative must be less than a value Z ($Z \in \Re^+$). These two conditions ensure that the system is not oscillatory and has stable communication and control.

In order to highlight the tracking process, lets consider the voltage graphs presented in Fig. 3.7. Before the failure ends, represented by (1) in Fig. 3.7, the DCUs operates in DSC mode, and the MGCC and DCUs cannot receives data from each other. When the failures end, in time (1), the MGCC start the tracking process, that are composed of two steps: system and communication verification; and commanding the control mode change.

In the system and communication verification step, the MGCC check if the communication is stable and the system does not present oscillations. The first verification is achieved through the waiting time X, and the second is through the voltage and frequency derivative. As presented in Fig. 3.7, if the the waiting time verification is achieved (1), but the voltage or frequency derivative are still with high values (2), the MGCC does not start the second step.

If the both conditions is achieved, represented in time (3) of Fig 3.7, the MGCC start the commanding the control step, the MGCC sends the message containing the values of the control actions and the command $CmT = 0$ to the DCUs change to CSC mode. As in the partial failure, when the DCUs receive the message from the MGCC, they calculate an initialization variable for both control actions (IH_f and IH_V) and then switch to CSC mode. As mentioned, with this tracking process, any centralized secondary control strategy can be implemented in the MGCC.

3.2.4 MGCC Control Scheme

The proposed MGCC control scheme can be summarized in the diagram of Fig. 3.8. Wherein, the control actions for normal operation, partial failure, and total failure are highlighted. Additionally, note that the total failure presents three paths: one refers to the failure of MGCC, and the other refers to communication failures.

For the MGCC it is possible to represent its control actions mathematically. The control

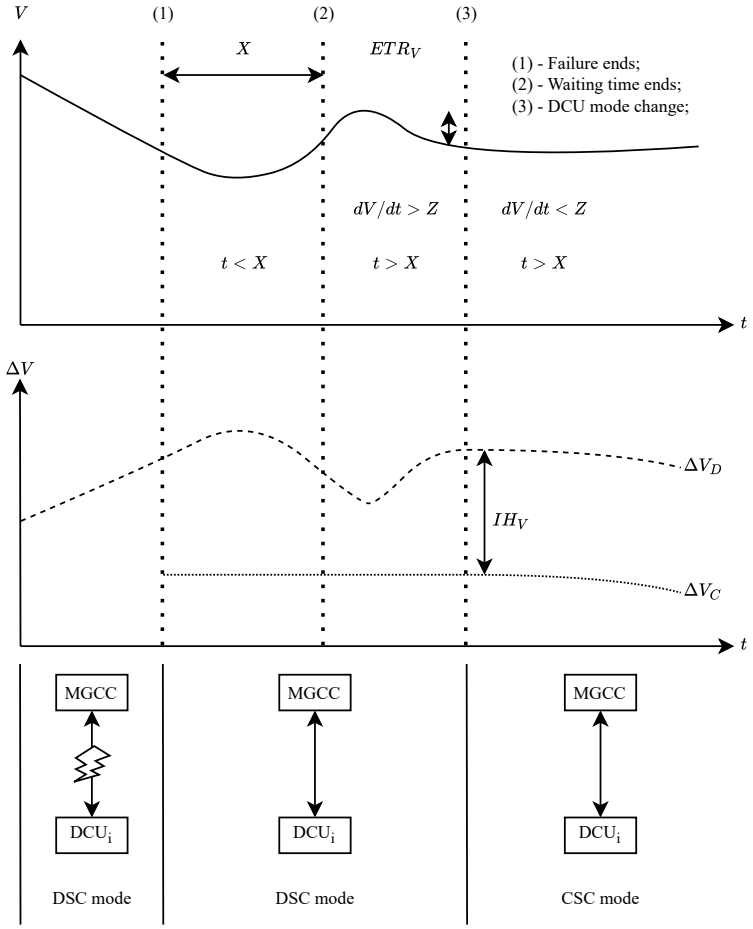

Figure 3.7: Tracking process in the proposed USCS.

action generated by the centralized control strategy in the MGCC is sent to a certain DCU – denoted with index i – only when all the following conditions are met: the MR is in islanded mode ($PCCS = 0$); the MGCC is not in failure ($Fail = 0$); the DCU in question is not in failure mode ($CmD'_i = 0$); and, it is not operating in DSC mode ($CmK'_i = 1$). Mathematically, it is possible to represent the frequency and voltage control actions through the following equations:

$$\Delta\omega_{s_{C_i}}(t) = \begin{cases} 0 & \text{if} \quad \begin{array}{r} Fail = 1 \,||\, PCCS = 1 \,|| \\ CmK'_i = 1 \,||\, CmD'_1 = 0 \,|| \\ Rst = 1 \end{array} \\ CC_f & \text{if} \quad \begin{array}{r} Fail = 0 \;\; \& \;\; PCCS = 0 \;\; \& \\ CmK'_i = 0 \;\; \& \;\; CmD'_i = 1 \\ \& \;\; Rst = 0 \end{array} \end{cases} \tag{3.1}$$

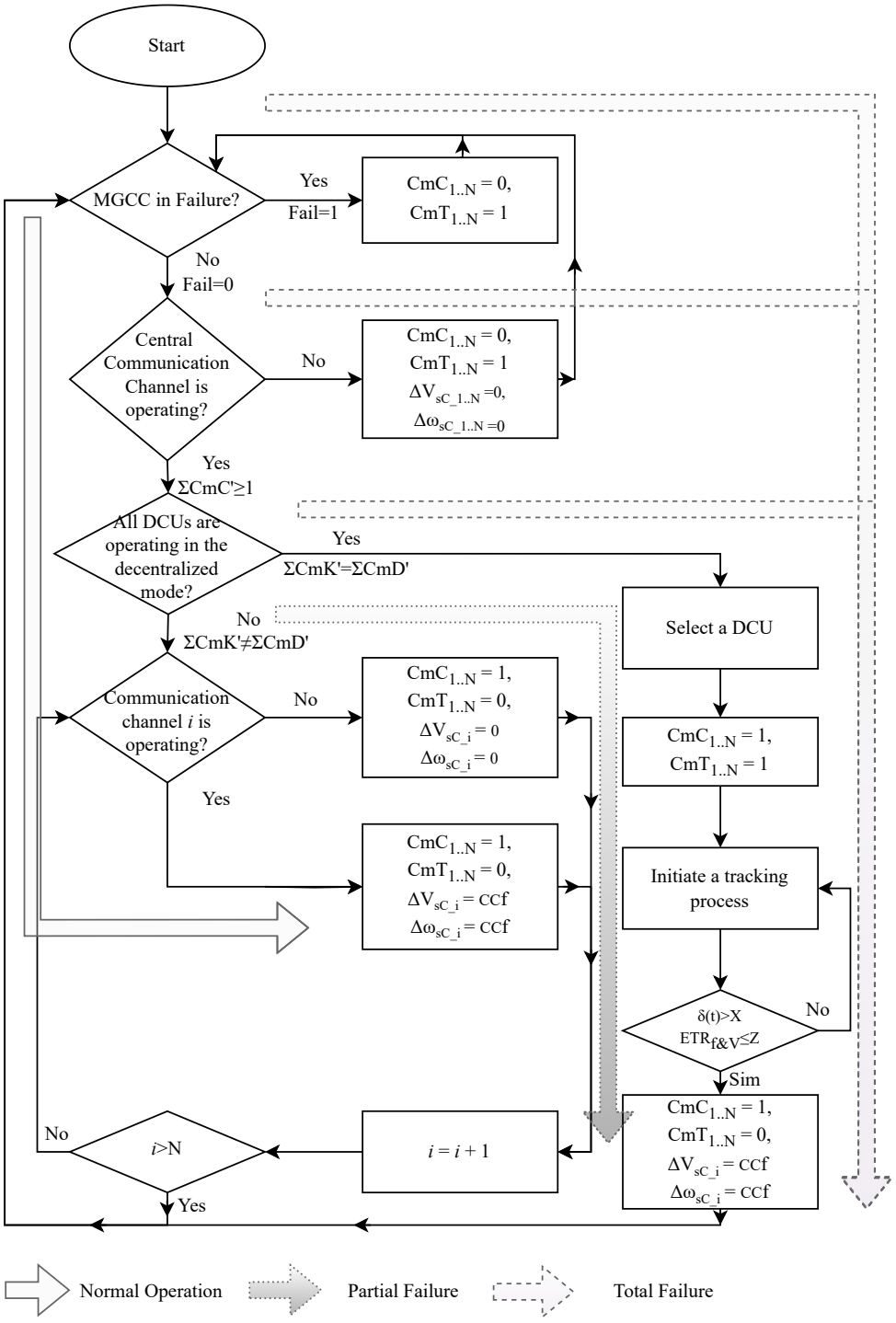

Figure 3.8: Proposed secondary control - MGCC.

$$\Delta V_{s_{C_i}}(t) = \begin{cases} 0 & \text{if} \quad \begin{array}{r} Fail = 1 \,||\, PCCS = 1 \,|| \\ CmK'_i = 1 \,||\, CmD'_1 = 0 \,|| \\ Rst = 1 \end{array} \\ CC_V & \text{if} \quad \begin{array}{r} Fail = 0 \;\; \& \;\; PCCS = 0 \;\; \& \\ CmK'_i = 0 \;\; \& \;\; CmD'_i = 1 \\ \& \;\; Rst = 0 \end{array} \end{cases} \tag{3.2}$$

In equations (3.1) and (3.2), $Fail$ indicates the MGCC failure condition, $PCCS$ indicates the MG operation mode, CmD' and CmK' is the information received by the MGCC from each DCU, CC_f and CC_V are the mathematical representations of the centralized frequency and voltage control strategies, and Rst is an auxiliary variable that indicates if the MGCC is in tracking mode, as represented in the equation (3.3).

$$Rst(t) = \begin{cases} 0 \quad \text{if} & \begin{array}{r} Fail = 1 \,||\, PCCS = 1 \,|| \\ ((\delta T(t) \leq X \;\;\&\;\; ETR_f \leq Z \;\;\&\;\; ETR_V \leq Z)|| \\ \sum_{i=1}^{N} CmD'_i \neq \sum_{i=1}^{N} CmK'_i) \;\;\&\;\; PCCS = 0) \end{array} \\ 1 \quad \text{if} & \begin{array}{r} Fail = 0 \;\;\&\;\; PCCS = 0 \;\;\& \\ \sum_{i=1}^{N} CmD'_i = \sum_{i=1}^{N} CmK'_i \neq 0 \\ \&\;\; ETR_f > Z \;\;\&\;\; ETR_V > Z \;\;\&\;\; \delta T(t) > X \end{array} \end{cases} \tag{3.3}$$

where X is the time reference for the tracking process interruption, $\delta T(t)$ is the time variation that the MGCC does not fail, Z is the smallest derivative value of frequency and voltage for the tracking process interruption, and ETR_f and ETR_V are defined by:

$$ETR_f(t) = |\frac{df}{dt}| \tag{3.4}$$

$$ETR_V(t) = |\frac{dV}{dt}| \tag{3.5}$$

The tracking process starts only if the MGCC does not present faulty ($Fail = 0$) and all DCUs, which have the communication channel transmitting and does not present faulty ($CmD'_i = 1$), are operating in DSC mode ($CmK'_i = 1$). This process only ends when the frequency and voltage derivatives are less than Z, and no failures occur in X seconds of time.

When in normal operation, the MGCC sends the information $CmT_i = 0$ for all the DCUs to operate in CSC mode. The information $CmT_i = 1$, for DCUs operating in DSC mode, is only sent when in the tracking process. Mathematically, is possible to define $CmT_i(t)$ as follows:

$$CmT_i(t) = \begin{cases} 0 \quad \text{if} & Fail = 1 \,||\, PCCS = 1 \,||\, Rst = 0 \,||\, CmD'_i = 0 \\ 1 \quad \text{if} & \begin{array}{r} Fail = 0 \;\;\&\;\; PCCS = 0 \;\;\&\;\; CmD'_i = 1 \;\;\& \\ (Rst = 1 \,||\, (Rst = 0 \;\;\&\;\; CmK'_i = 1 \;\;\&\;\; IH_i = 0)) \end{array} \end{cases} \tag{3.6}$$

During its entire operation, the MGCC sends the information $CmC_i = 1$ to all DCUs, regardless of whether the communication channel is operating or not. However, if the MGCC fails, the information sent by it becomes null, that is:

$$CmC_i(t) = \begin{cases} 0 & \text{if} \quad Fail = 1 \\ 1 & \text{if} \quad Fail = 0 \end{cases} \tag{3.7}$$

3.2.5 DCUs Control Scheme

Similarly to the MGCC, the proposed DCUs control scheme can be summarized in the diagram of Fig. 3.9. Note that, in the diagram, the normal operation mode, the failure operation mode, and the returning to CSC mode are highlighted. Different from the MGCC control scheme, the actions for partial failure and total failure are the same.

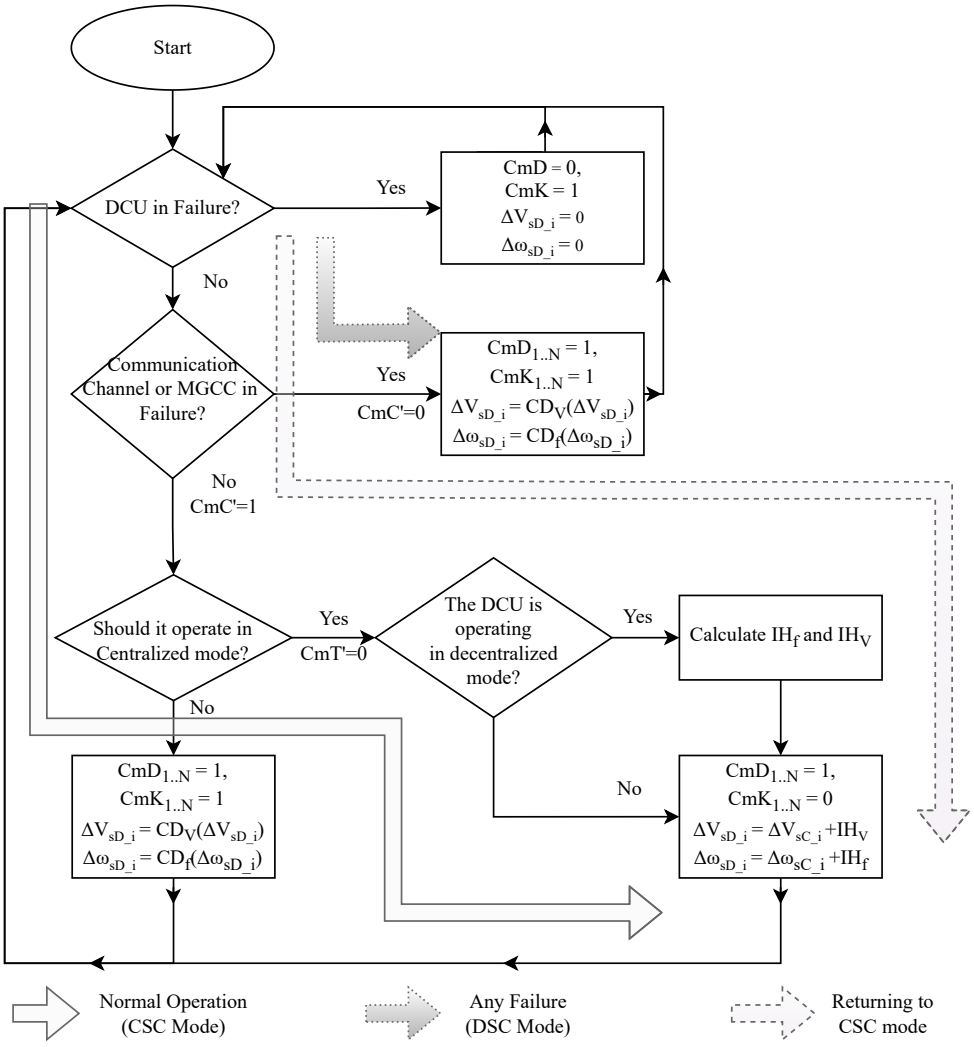

Figure 3.9: Proposed secondary control - DCU.

In CSC mode, the control actions of the DCUs are equal to the control actions received from the MGCC plus the initialization variables. In case of a failure, the last control action values sent by the MGCC to the DCUs, before the failure, are used as initialization variables for the DSC strategy. It is possible to represent the control actions generated by a DCU through

the following equations:

$$\Delta\omega_{s_{D_i}} = \begin{cases} 0 & \text{if} \quad PCCS = 1 \\ \Delta\omega'_{s_{C_i}} + IH_{f_i} & \text{if} \quad \begin{array}{c} PCCS = 0 \ \ \& \ \ CmC'_i = 1 \\ \& \ \ CmT'_i = 0 \end{array} \\ CD_{f_i}(\Delta\omega_{s_{D_i}}(t_{f_i})) & \text{if} \quad \begin{array}{c} PCCS = 0 \ \ \& \\ (CmC'_i = 0 \,||\, CmT'_i = 1) \end{array} \end{cases} \tag{3.8}$$

$$\Delta V_{s_{D_i}} = \begin{cases} 0 & \text{if} \quad PCCS = 1 \\ \Delta V'_{s_{C_i}} + IH_{V_i} & \text{if} \quad \begin{array}{c} PCCS = 0 \ \ \& \ \ CmC'_i = 1 \\ \& \ \ CmT'_i = 0 \end{array} \\ CD_{V_i}(\Delta V_{s_{D_i}}(t_{f_i})) & \text{if} \quad \begin{array}{c} PCCS = 0 \ \ \& \\ (CmC'_i = 0 \,||\, CmT'_i = 1) \end{array} \end{cases} \tag{3.9}$$

where CmC'_i and CmT'_i are the information sent by the MGCC and received by each DCU, $\Delta\omega'_{s_{C_i}}$ and $\Delta V'_{s_{C_i}}$ are the control actions sent by MGCC to each DCU, t_{f_i} is the time when the information CmT'_i changes its state to 1, CD_{V_i} and CD_{ω_i} are the functions of the DSC strategies implemented in DCUs, IH_f and IH_V are the CSC mode initialization variables for frequency and voltage:

$$IH_{f_i}(t) = \begin{cases} 0 & \text{se} \quad PCCS = 1 \ \ \& \ \ CmK_i = 1 \\ \Delta\omega_{s_{D_i}}(t_{e_i}) - \omega'_{s_{C_i}}(t_{e_i}) & \text{se} \quad CmC'_i = 1 \ \ \& \ \ CmT'_i = 0 \end{cases} \tag{3.10}$$

$$IH_{V_i}(t) = \begin{cases} 0 & \text{se} \quad PCCS = 1 \ \ \& \ \ CmK_i = 1 \\ \Delta V_{s_{D_i}}(t_{e_i}) - V'_{s_{C_i}}(t_{e_i}) & \text{se} \quad CmC'_i = 1 \ \ \& \ \ CmT'_i = 0 \end{cases} \tag{3.11}$$

where t_e is the time that the DCU receives the signal from the MGCC to switch to CSC mode.

The initialization variable receives a null value when the MG is connected ($PCCS = 1$) or the DCU is operating in DSC mode. Otherwise, the initialization variables are calculated through the difference between the control actions of the respective DCU and the control actions of the MGCC, being changed in value only when the respective DCU changes from DSC to CSC mode.

The variable $CmD_i = 1$ is sent regardless of the operation mode. This variable will only receive the value null if the DCU is in a failure state. The Equation (3.12) presents the states for the variable CmD_i.

$$CmD_i(t) = \begin{cases} 0 & \text{se} \quad Fail_i = 1 \\ 1 & \text{se} \quad Fail_i = 0 \end{cases} \tag{3.12}$$

During the CSC mode, the DCUs send the information $CmK_i = 0$ to the MGCC. In the DSC mode, the DCUs send the information $CmK_i = 1$. These actions are represented by the following equation:

$$CmK_i(t) = \begin{cases} 0 \quad \text{se} & PCCS = 1 \,||\, (CmC'_i = 1 \;\; \& \\ & \quad PCCS = 0 \;\; \& \;\; CmT'_i = 0) \\ 1 \quad \text{se} & PCCS = 0 \;\; \& \;\; (CmC'_i = 0 \\ & \qquad ||\, CmT'_i = 1) \end{cases} \tag{3.13}$$

3.3 Proposed Decentralized Voltage Secondary Control

The decentralized control strategies proposed in the literature for voltage regulation often involve very complex functions or state estimation systems [33, 34, 35], which can make it difficult to employ these strategies to an MG with the USCS. Thus, in order to overcome these disadvantages, a new decentralized voltage control strategy is proposed.

The novel decentralized secondary voltage control is based on equivalent system representation and local measurement, wherein the voltage regulation in the PCC and the reactive power sharing are the main objectives of this control.

To understand the concept of the proposed control, let's consider the MG presented in Fig. 3.10. Note that this MG presents four buses, four loads, and three DGs. The buses are connected through three cables - Z12, Z23, and Z24 - and any bus can be considered the PCC. Any DG sees the system where it is connected as an equivalent generator, as shown in Fig. 3.11.

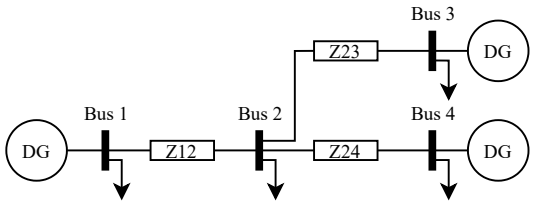

Figure 3.10: MG for voltage control.

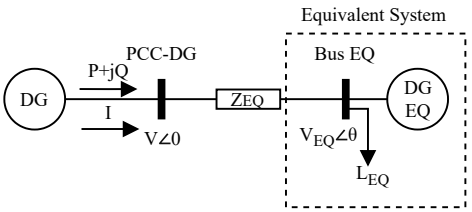

Figure 3.11: Equivalent system observed by a DG.

In Fig. 3.11, V_{EQ} represents the voltage in the equivalent bus, L_{EQ} is the total load of the MG, Z_{EQ} is an equivalent impedance, P and Q are the active and reactive power, I are the DG

current.

Let's consider that the MG operates with a conventional droop control (P vs ω) with a decentralized secondary frequency control. Thus, due to the droop control, active power sharing is achieved in the steady state. If the power factor of the MG is known, it is possible for each DG to dispatch the reactive power according to its active power generated. Hence, based on the affirmation above, the following control law is proposed:

$$\Delta V_{sec} = -\int (VV + VQ)dt \tag{3.14}$$

$$VV = (V_i - V_{s0} + I_i \cdot Z_{EQ}) \cdot k_1 \tag{3.15}$$

$$VQ = (m_i \cdot Q_i - Q_{EQ_i}) \cdot k_2 \tag{3.16}$$

$$Q_{EQ} = \phi \cdot m_i \cdot P_i \tag{3.17}$$

where VV is the control portion that is responsible for the voltage regulation, VQ is the control portion that is responsible for the reactive power sharing, V_i is the local voltage for the i^{th} DG, V_{s0} is the voltage reference, I_i is the current of the i^{th} DG, k_1 is control gain for the voltage regulation portion, Q_i is the reactive power of the i^{th} DG, Q_{EQ_i} is the estimated reactive power in the equivalent system in the perspective of the i^{th} DG, k_2 is the control gain for the reactive power sharing regulation portion, ϕ is the tangent of the power factor, m_i is the voltage droop coefficient of the i^{th} DG, P_i is the active power of the i^{th} DG.

The strategy only requires local voltage, current, and active and reactive power measures. As the active power sharing is guaranteed through the primary control strategy, the proposed strategy estimates the amount of reactive power that must be generated through the generated active power. Thus, knowing the power factor of the system generation, the strategy is able to guarantee the sharing of reactive power.

As the strategy only needs to know the power factor of the total generation of the system, the topology changes may affect the strategy. As presented in [70] for the primary control, in decentralized strategies MG topology and load changes can affect the reactive power chairing. This behavior occurs due to the voltage being a local variable. Thus, if the system changes the voltage in each bus of MG differently, it causes different decentralized control actions. This phenomenon can occur for the decentralized secondary voltage strategies too. Thus, the loss or entry of new generators is considered only as a load change for the control. In addition, knowing the entire network topology or the number of generators in the system is not necessary.

The proposed strategy is proposed to operate with the USCS, therefore, it is only a temporary solution for voltage regulation. Thus, the system power factor is not estimated, but informed by the MGCC during the CSC operation, and in case of failures, the proposed strategy would use the last power factor value received.

If the power factor of the MG changes during the DSC operation mode, the reactive power

sharing of the DGs will present deviations. However, these deviations will not present high values, due to all DGs present the same ϕ gain. Thus, it is important to the ϕ gain being adjusted with the same value for all DGs, if not, deviations in the reactive power will be presented.

The strategy is parameterized through three variables: k_1, k_2 and Z_{EQ}. The Z_{EQ} variable is responsible impedance of the remote bus control and allows controlling the voltage close to the PCC, if inserting the Thévenin impedance value between the DG bus and the PCC bus. The variables k_1 and k_2 are responsible for voltage regulating and reactive power sharing, respectively. If $k_1 > k_2$, the control will tend to keep the MG voltages closer to the reference value (V_{s0}), otherwise, if $k_1 < k_2$, the control will tend to prioritize reactive power sharing.

Chapter 4

Simulation Results

4.1 Initial considerations

In Chapter 3 the proposed decentralized secondary voltage control and the novel USCS are presented. In order to test the proposed controls an MG is modeled in the Matlab/Simulink environment. The MG models and converters control are presented in [19].

Thus, in this Chapter, the MG test and the simulation results are presented. The simulation considers three cases, the first shows the results for the secondary decentralized voltage control; the second case presents the results for the USCS where the total and partial failures are simulated; and the last, presents the comparison between the proposed USCS and the UCDFCS.

4.2 Microgrid Structure

The MG structure employed in this work is based on the MG proposed in [19]. The implemented MG is presented in Fig. 4.1, where two Photovoltaic Systems (PV) and two BESSs are present. The MG data can be found in Table 4.1, and other parameters and control descriptions and gains can be found in [19].

The MG is simulated in Matlab/Simulink software using the **simpower system** library. Therefore, the simulations consider the electromagnetic transient regime. The Matlab/Simulink is a widely used tool to test MG control strategies [71], additionally, past works [72, 73, 74, 70, 19, 17] employed the Matlab/Simulink to test MG's control and operation strategies.

For the MG implementation, the impedance model was used for the cables and loads. The converters are represented through the average value model, therefore, the high-frequency dynamics are not represented. As presented in [72, 75] the average values model does not influence the dynamics converters controls, when operating in an MG. The dynamics of the primary sources and the DC/DC converters of the DGs are not represented, so an ideal source is adopted to compose the DC bus of the sources.

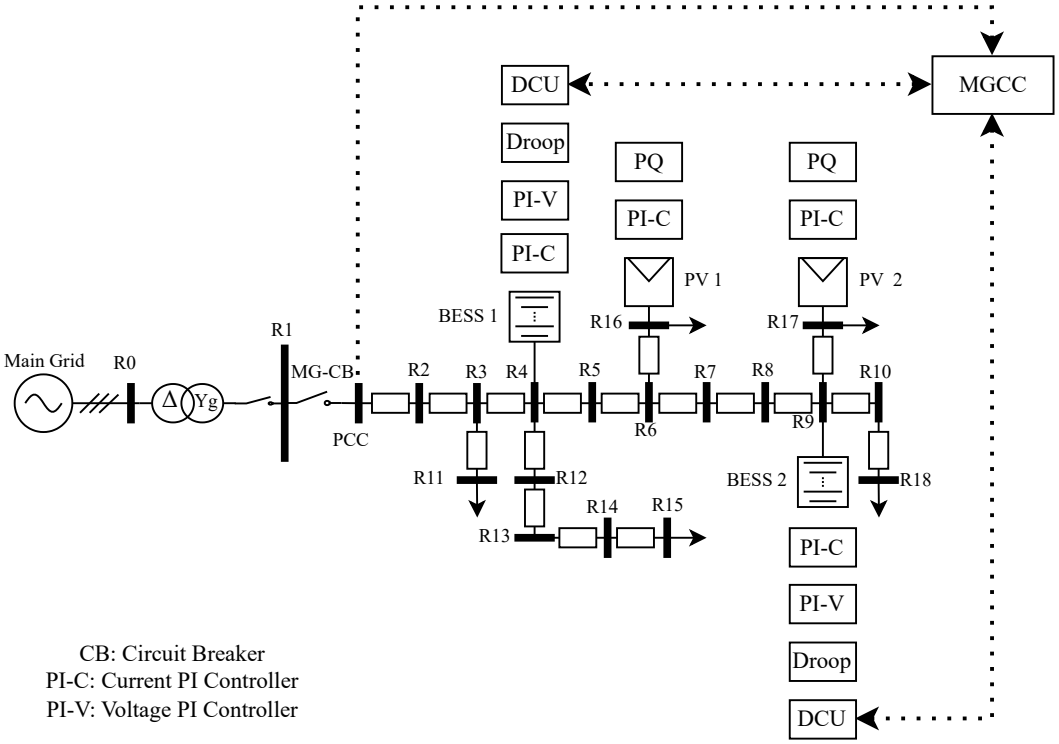

Figure 4.1: MG CIGRE, [19].

Table 4.1: MG Data [19].

Element	Parameters
Main Grid	20 kV; 100 kVA; X/R = 1
Transformer	20/0.38 kV; 100 kVA; $X_t = 6\%$
Inverter of BESS 1 ($i = 1$)	45 kVA
Inverter of BESS 2 ($i = 2$)	45 kVA
Inverter of PV 1	20 kVA
Inverter of PV 2	20 kVA
Load R11 ($j = 1$)	14,25 kW e 4,68 kvar
Load R15 ($j = 2$)	49,40 kW e 16,24 kvar
Load R16 ($j = 3$)	52,25 kW e 17,17 kvar
Load R17 ($j = 4$)	33,25 kW e 10,93 kvar
Load R18 ($j = 5$)	44,65 kW e 14,68 kvar

Note in Fig. 4.1 that the MGCC is represented in the simulation, and the secondary control is implemented in the MGCC, note too that both BESS communicates with the MGCC, and the PV systems do not communicate with the MGCC. The communication system is represented as a delay in the simulation.

For the BESS and PVs controls, the grid-supporting control (V/f control mode) is employed for the BESS, and the grid-following control (PQ control mode) is adopted for the PV converters. In the grid-supporting control, two PI control loops are connected in series, a voltage loop and a current loop. The droop control with virtual impedance [26] is employed. The Fig. 4.2 illustrates the converter's control loops.

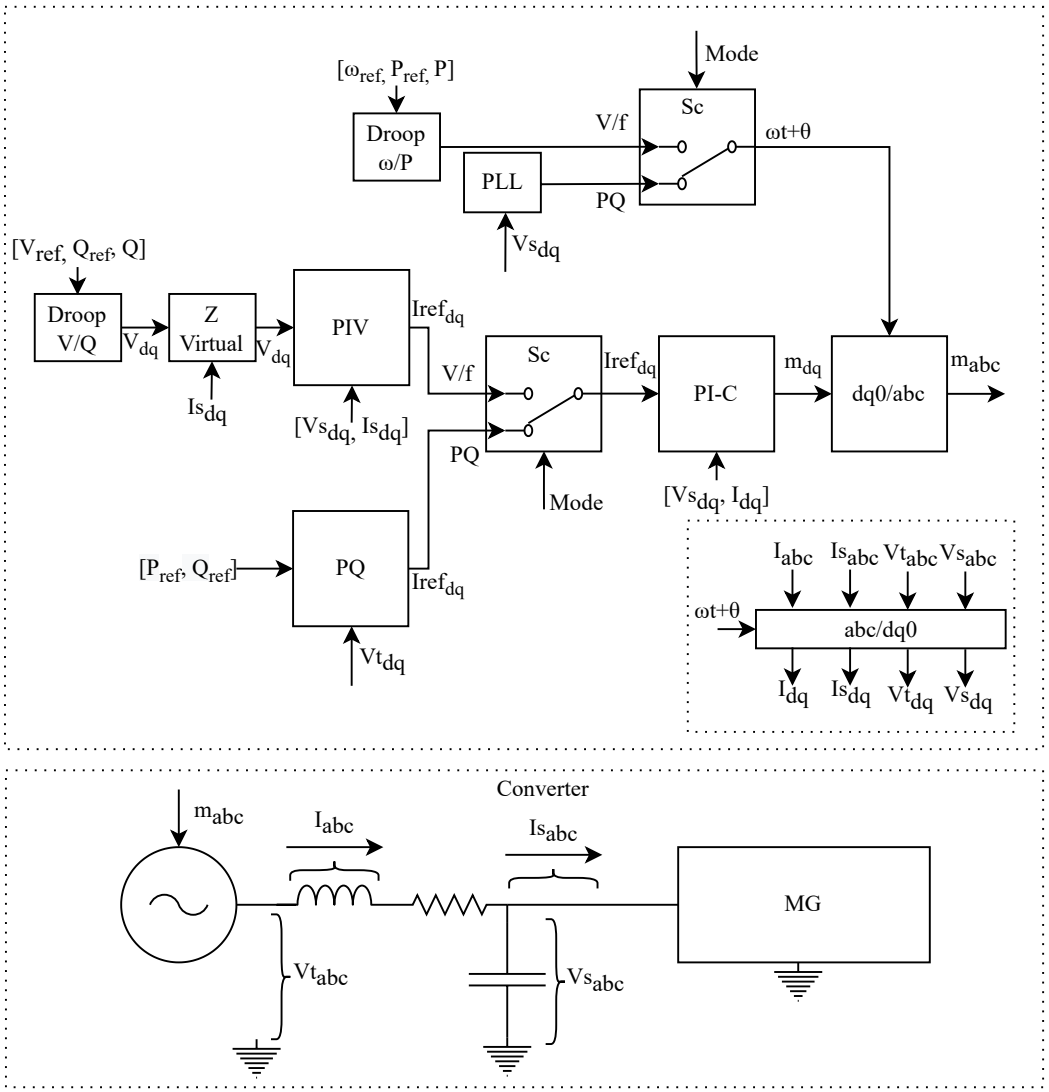

Figure 4.2: Converters control, [19].

The control of the PVs employed is also shown in Figure 4.2. The current PI loop references are generated through the power control loops. Unlike the BESS, the control of intermittent sources uses a Phase Lock Loop (PLL) to follow the angle and frequency reference of the grid. The control of the converters and their operating limits are presented in the Annex A.

4.3 Case 1: Decentralized Voltage Control Strategy

In order to evaluate the proposed decentralized voltage secondary control, simulations considering only decentralized control are carried out. The MG operation point considered is described in Table 4.2.

The following event sequence was considered in the simulations:

- In $t = 0$ s, the MG operates islanded without secondary control;

Table 4.2: MG operation Point.

Element	Value
Load R11 (kVA)	4,13 ∠18,18°
Load R15 (kVA)	14,30 ∠18,18°
Load R16 (kVA)	15,12 ∠18,18°
Load R17 (kVA)	9,63 ∠18,18°
Load R18 (kVA)	12,93 ∠18,18°
PV (kW)	0,00
Droop Pref (kW)	0,00
Droop Qref (kvar)	0,00

- In $t = 0,1$ s, the secondary control is activated;
- In $t = 2,2$ s, the Load R11 increases its values to 14,25 kW e 4,68 kvar.

The proportional control strategy with low pass filter [30] is applied as a decentralized strategy for frequency regulation. Thus, the proposed decentralized voltage control operates together with the decentralized frequency strategy. The strategy proposed by [30] can be described as following:

$$CD_{f_i} + \frac{d\,T_{2_i} \cdot CD_{f_i}}{dt} = \alpha_i(\omega_{s0} - \omega_i) \tag{4.1}$$

where, i is the index representing a DG, T_{2_i} is the low-pass filter time constant, α_i is the proportional gain, ω_i is the frequency measured locally.

The gains adopted for the simulations are presented in Table 4.3. It is noteworthy that the gains were selected following the algorithm proposed in B, thus the control is adjusted in order to maintain the MG stability for the possibles control structure and operation points. With the exception of parameters Z_{EQ}, which were taken from the Zbus matrix of the MG, that is, Z_{EQ} is equal to the Thévenin impedance between the bus where the DG is connected and the MG PCC.

Table 4.3: Decentralized Controls Gains.

Gain	Value [p.u.]
a	5
T_2	10
k_1	6
k_2	12
ϕ	0.3284
Z_{EQ_1}	0.0067
Z_{EQ_2}	0.2553

The Figs. 4.3(a) and 4.3(b) present the frequency and voltage at the MG PCC when the decentralized control strategies are employed. Note that the PCC MG frequency and voltage are not regulated to the desired reference value (1 p.u.), and the system remains stable during

its operation and load increase.

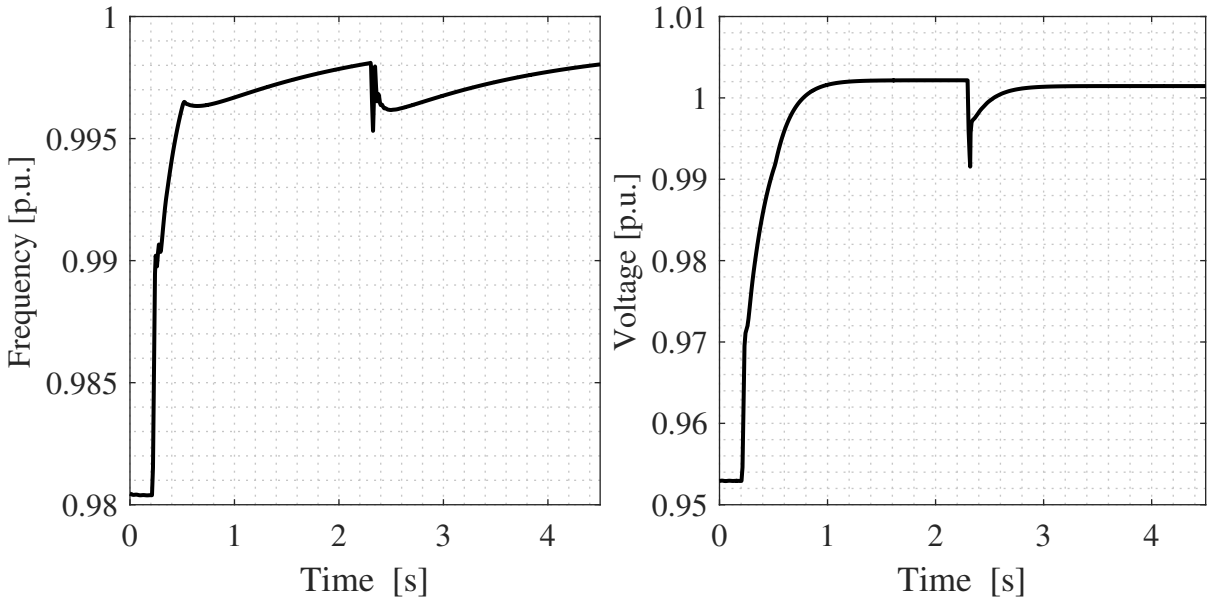

(a) (b)

Figure 4.3: MG dynamics when operating with the DSC only. (a) Frequency. (b) Voltage.

The active and reactive powers for each BESS are shown in Figs. 4.4(a) and 4.4(b). One can see that the active power has perfect sharing when observing both BESS, however, the reactive power presents some deviations in the power sharing. This behavior occurs due to the adjustment of the control gains and mostly due to the tangent of the power factor. Changing the value of the control gains k_2, it is possible to achieve better reactive power sharing, however, the voltage regulation will be affected.

Considering the control actions of both BESS, the Figs. 4.5(a) and 4.5(b) present the generated control actions of the decentralized secondary control. One can see that the generated frequency control actions in both BESS present the same values. However, for the voltage control action, the control actions start being generated with the same values, and after 1 second of simulation, the control actions start to present different values. This behavior is due to the voltage and reactive power in each BESS being different. For the frequency regulation case, the frequency is a global variable of the system, however, the voltage is a local variable, thus, the voltage value in each bus BESS is expected.

The Figs. 4.6(a) and 4.6(b) present the increment portions of VV (3.15) and VQ (3.16). Note that the module portion of the decentralized voltage control is larger for BESS 2, however, for the sharing portion BESS 1 presents a larger value. This occurs due to the voltage and reactive power generated in each BESS being different, thus different control actions are generated for each BESS.

It is important to observe that the proposed control can achieve voltage regulation and maintain the system's stability during its operation. Still, it is important to know that the pro-

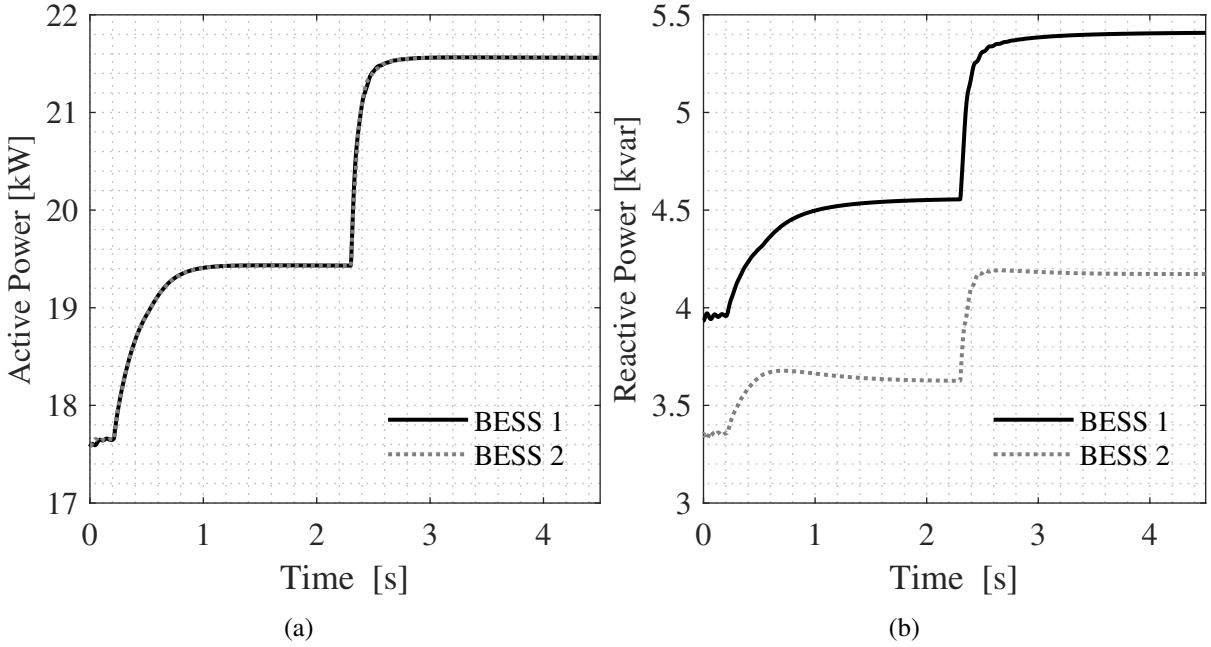

(a) (b)

Figure 4.4: MG dynamics when operating with the DSC only. (a) Active Power. (b) Reactive Power.

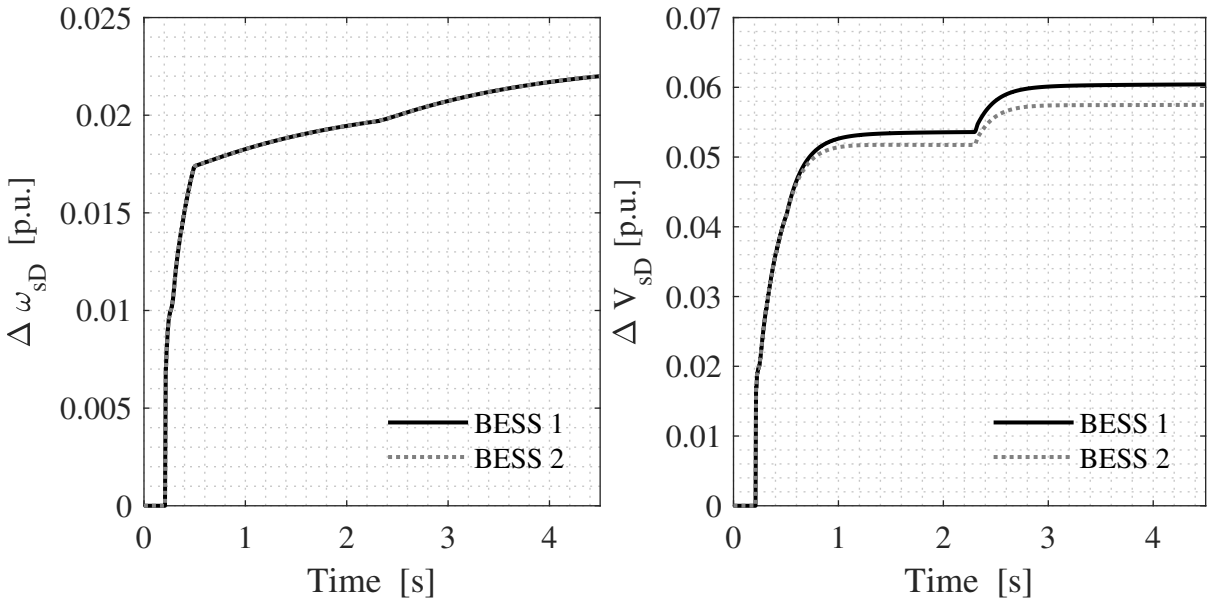

(a) (b)

Figure 4.5: MG dynamics when operating with the DSC only. (a) Frequency control action. (b) Voltage control action.

posed decentralized voltage strategy is proposed to operate with the USCS, thus the tangent of the power factor does not need to be estimated for each DG. However, to operate the MG only with the decentralized strategies, an estimation method for the tangent of the power factor must be employed.

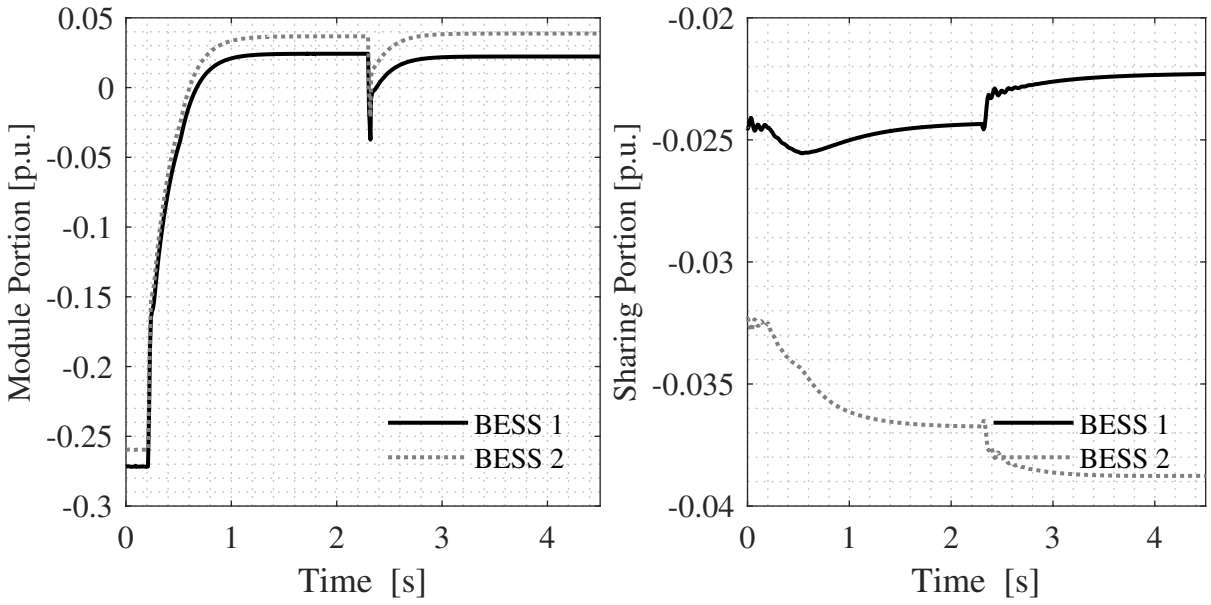

(a) (b)

Figure 4.6: MG dynamics when operating with the DSC only. (a) VV. (b) VQ.

4.4 Case 2: USCS with PI Strategies

In order to test the proposed USCS with the proposed decentralized voltage control, the PI control with fixed gains [4] is adopted as a centralized control strategy for both voltage and frequency regulation. Additionally, the proportional control strategy with low pass filter [30] is employed over again.

The PI control with fixed gain can be described using the following equations:

$$CC_f = Kp_\omega \cdot (\omega_{s0} - \omega_{PCC}) + Ki_\omega \cdot \int (\omega_{s0} - \omega_{PCC}) \tag{4.2}$$

$$CC_V = Kp_V \cdot (V_{s0} - V_{PCC}) + Ki_V \cdot \int (V_{s0} - V_{PCC}) \tag{4.3}$$

where Kp_ω and Kp_V are the proportional gains for frequency and voltage, Ki_ω and Ki_V are the integrative gains for frequency and voltage, Ω_{s0} and V_{s0} are the centralized secondary references for frequency and voltage, ω_{PCC} and V_{PCC} are the PCC frequency and voltage measured.

The gains adopted for the simulations for the decentralized controls are presented in Table 4.3, and the gains for the centralized control are presented in Table 4.4. The algorithm presented in B is employed for the control gain adjustment. Additionally, the same operating point for the decentralized control simulations is applied. Four cases are evaluated:

- Complete failure of the communication channel without communication delay;
- Complete failure of the communication channel with 150 ms of communication delay;

- Failure of the communication channel between BESS 1 and the MGCC, without communication delay;
- Failure of the communication channel between BESS 1 and the MGCC, with 150 ms of communication delay;

Table 4.4: Centralized Controls Gains.

Gain	Value [p.u.]
Kp_ω	0.3
Ki_ω	6.0
Kp_V	0.3
Ki_V	6.0

The four cases simulated consider the following sequencing of events:

- At $t = 0$ s, the MG is operating in islanded mode, without the presence of the secondary control;
- At $t = 0.1$ s, the secondary control is activated;
- At $t = 0.5$ s, the system failure occurs;
- In $t = 2.2$ s, load R11 increases its load to 14.25 kW and 4.68 kvar;
- In $t = 3$ s, the failure is removed and the system returns to normal operation.

4.4.1 Case 1: Total Failure

A total failure can occur for several reasons: failure of the communication equipment, making it impossible for the MGCC to send or receive information; the MGCC fails due to an internal or external failure; the MGCC is unable to measure the frequency or voltage. For the simulated condition, a failure in the central communication channel is considered, i.e. a failure in communication equipment. The MG frequency and voltage for this fault are presented in Figs. 4.7(a) and 4.7(b).

It is observed that before the secondary control is active, the frequency and voltage are maintained by the droop control. Thus, the voltage and frequency present deviations from the nominal values, wherein the voltage and frequency present a value in p.u. of 0.95 and 0.98, respectively. When the secondary control is activated, in $t = 0.1$ s of simulation, the voltage and frequency are quickly regulated for the nominal values.

However, due to the communication failure in $t = 0.5$ s of simulation, the MGCC cannot send its secondary control actions to the DCUs, thus, the DCUs identify the failure and change their operation mode to DSC. Therefore, the voltage and frequency are regulated by the decentralized strategies. Note that when the decentralized control takes action, the dynamics of

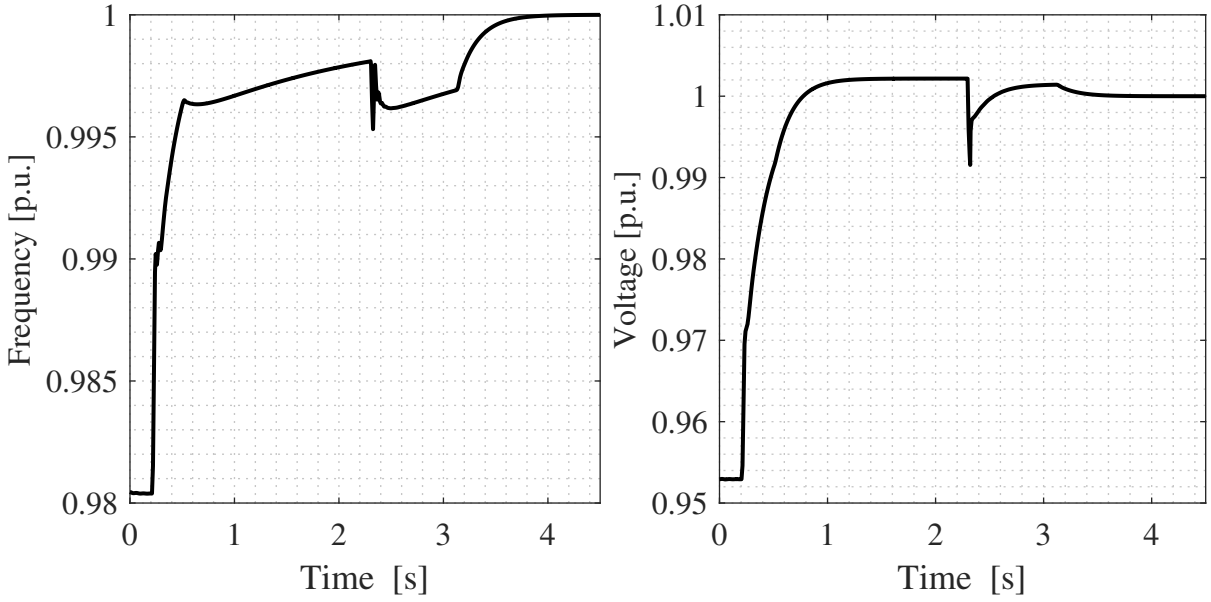

(a) (b)

Figure 4.7: MG dynamics with USCS - Total Failure (a) Frequency. (b) Voltage.

frequency and voltage change. However, abrupt variations are not observed when the control changes from centralized to decentralized mode. Observe too, that when the load R11 changes its values, in $t = 2.5$ s, the secondary controls take actions, maintaining the regulation and the system stability.

When the failure ends in $t = 3$ s, the system returns to operate in CSC mode, note that the frequency and voltage do not present abrupt variations in its values. Still, it is possible to observe the dynamic changes in the frequency and voltage regulation, when the system changes its operation mode.

The active and reactive powers of each BESS are illustrated in Figs. 4.8(a) and 4.8(b). It is observed that both the active and reactive power do not present sudden changes when the control modes occur in $t = 0.5$ s and $t = 3$ s. Note too that the active power presents the same values for both BESSs during both CSC and DSC mode. However, the reactive power presents different values during the simulation, and these differences are observed in both CSC and DSC modes.

The voltage and frequency control actions sent from the DCUs to the DGs are shown in Figs. 4.9(a) and 4.9(b). In both control actions, there were no abrupt variations when the control changed its operation mode from CSC to DSC or DSC to CSC, showing that the proposed strategy guarantees a smooth transition when there is a change of control mode.

The internal variables of the MGCC are illustrated in Fig. 4.10. It is observed that, when there is a failure in the communication channel, the MGCC stops receiving information from the DCUs, so all information received from the DCUs is null. Upon receiving the failure information, the MGCC changes the state of the internal variables $CmT1$ and $CmT2$ to logical level 1. The internal variables of the DCUs are shown in Figs. 4.11 and 4.12. When a total

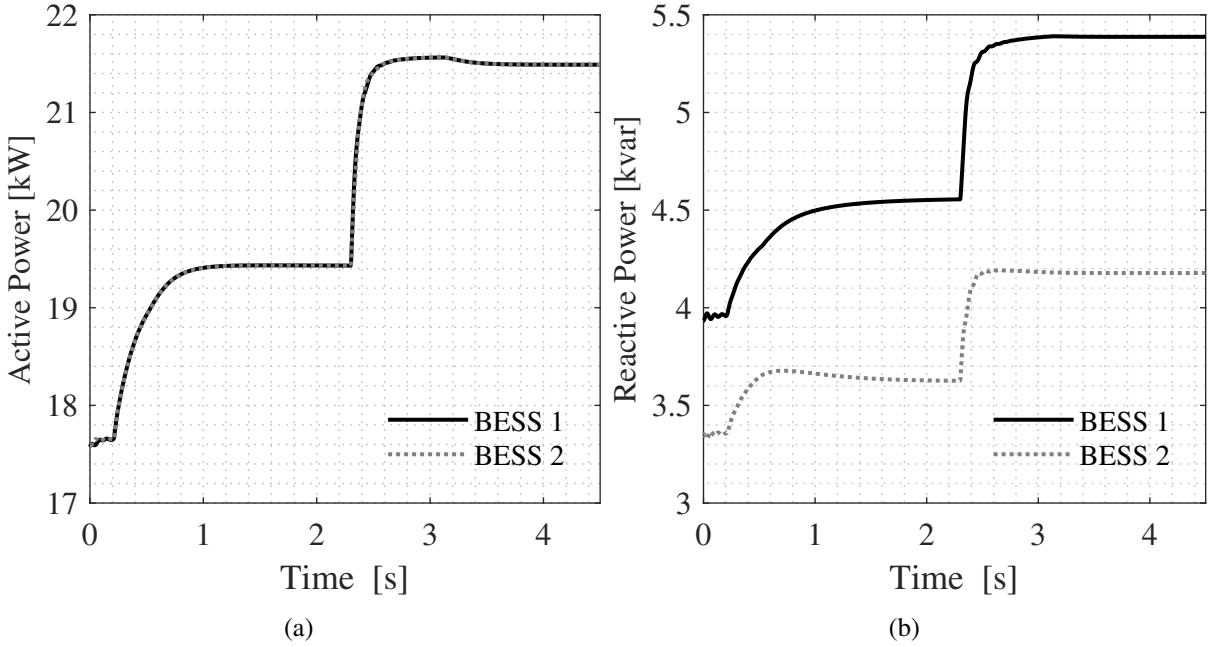

(a) (b)

Figure 4.8: MG dynamics with USCS - Total Failure (a) Active Power. (b) Reactive Power.

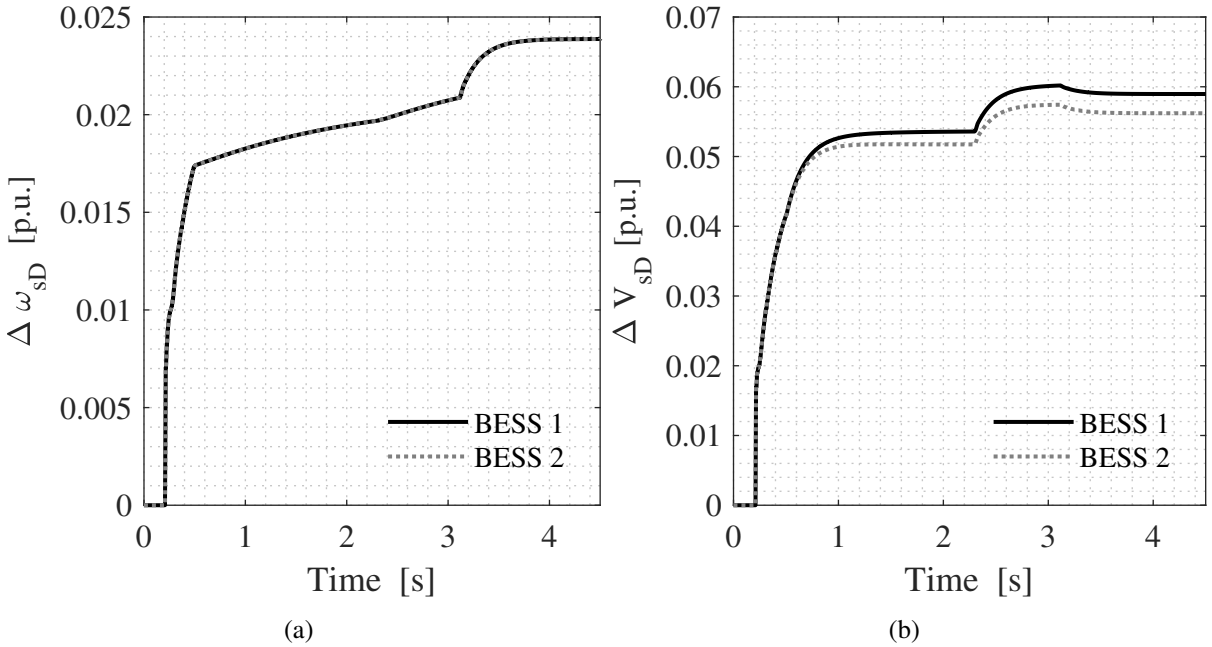

(a) (b)

Figure 4.9: MG dynamics with USCS - Total Failure (a) Frequency control action. (b) Voltage control action.

failure occurs, as soon as the UCDs stop receiving messages from the MGCC, they change control mode to decentralized, changing the variable CmK to logical level 1.

During the failure, the DCUs maintained their operation mode in DSC. Note that the variables received from MGCC during the failure receive null values.

After the failure ends ($t = 3$ s), the MGCC is able to receive the information from the DCUs, and the DCUs are able to receive the information from the MGCC. The MGCC, seeing that the communication returns maintains the variables CmT and RsT in logical level 1. And,

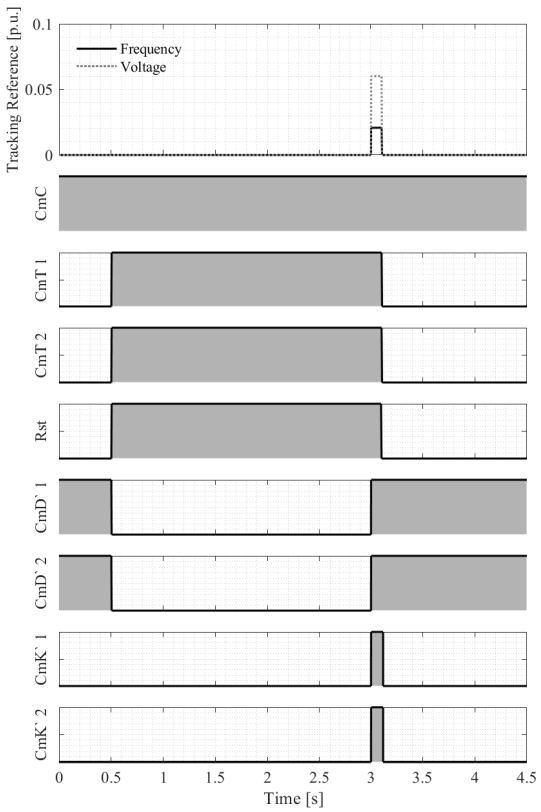

Figure 4.10: MG dynamics with USCS - Total Failure - MGCC.

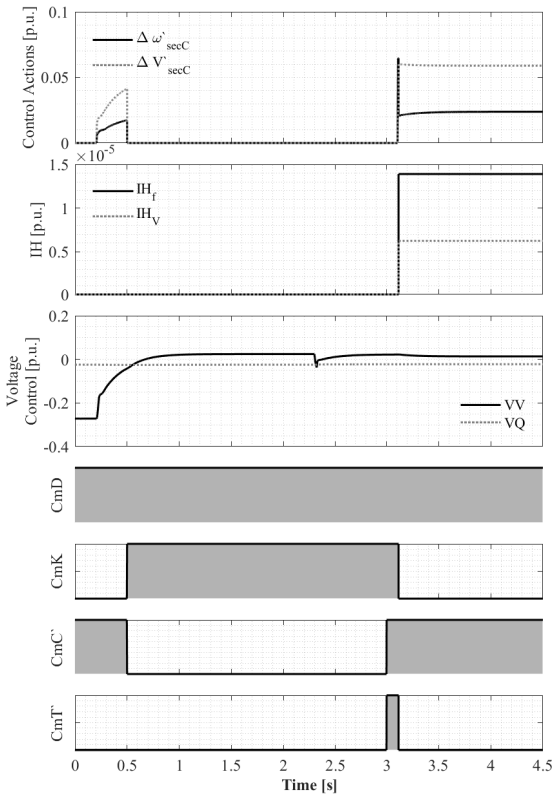

Figure 4.11: MG dynamics with USCS - Total Failure - DCU 1.

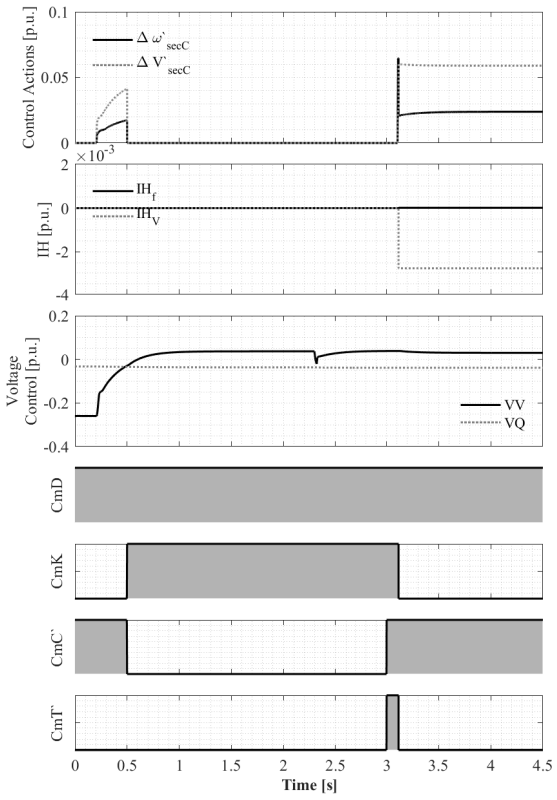

Figure 4.12: MG dynamics with USCS - Total Failure - DCU 2.

the DCUs maintain their operation in decentralized mode, due to the CmT variable sent by the MGCC.

The Rst variable operates at logic level 1 right after the failure, however, the MGCC only starts the tracking process after the communication channel returns. The BESS 1 is selected as a reference for the tracking process. It is possible to verify that the tracking references are only selected after the return of the communication channel.

The tracking process for this situation takes 0.1 s to be performed, and after that time the MGCC sends the signal to the DCUs to change operation mode. The DCUs after receiving the signal from the MGCC, calculate the new initialization variable and switch to the centralized control mode.

Note that the initialization variable of the DCU 1 receives values near zero, due to being selected as the reference for the tracking process. However, the DCU 2 presents different values for IH_V, due to the control actions generated by the decentralized voltage strategy during the DSC mode. Still, the initialization variable IH_f presents values near zero too, since the decentralized frequency strategy generates control actions similar in both DCUs.

4.4.2 Case 2: Total Failure with communication delay

In order to evaluate the performance of the new proposed structure considering communication delays, a simulation considering a fixed communication delay of 150 ms in the communication channels was performed. Additionally, the same events as in the case of total failure are considered. The frequency, voltage, active and reactive power are illustrated in Figs. 4.13(a), 4.13(b), 4.14(a) and 4.14(b), respectively.

For the states observed in the Figs. 4.13(a), 4.13(b), 4.14(a) and 4.14(b), one can see that the system maintains its stability and voltage regulation even during the communication failure. Additionally, when the DCUs change its operation modes, the system does not present abrupt variations.

The frequency and voltage control actions from the DCUs sent to the primary control are illustrated in Figs. 4.15(a) and 4.15(b), it is observed that there were no abrupt variations in the control actions when the DCUs changed their operating mode. It is important to comment that the dynamics when considering the communication delay are different from the case without delay due to the centralized control strategy, which is largely affected by the communication system.

The internal variables of MGCC and DCUs 1 and 2 are shown in Figs. 4.16, 4.17 and 4.18.

It is observed that the DCU and MGCC events sequence are similar to the events sequence

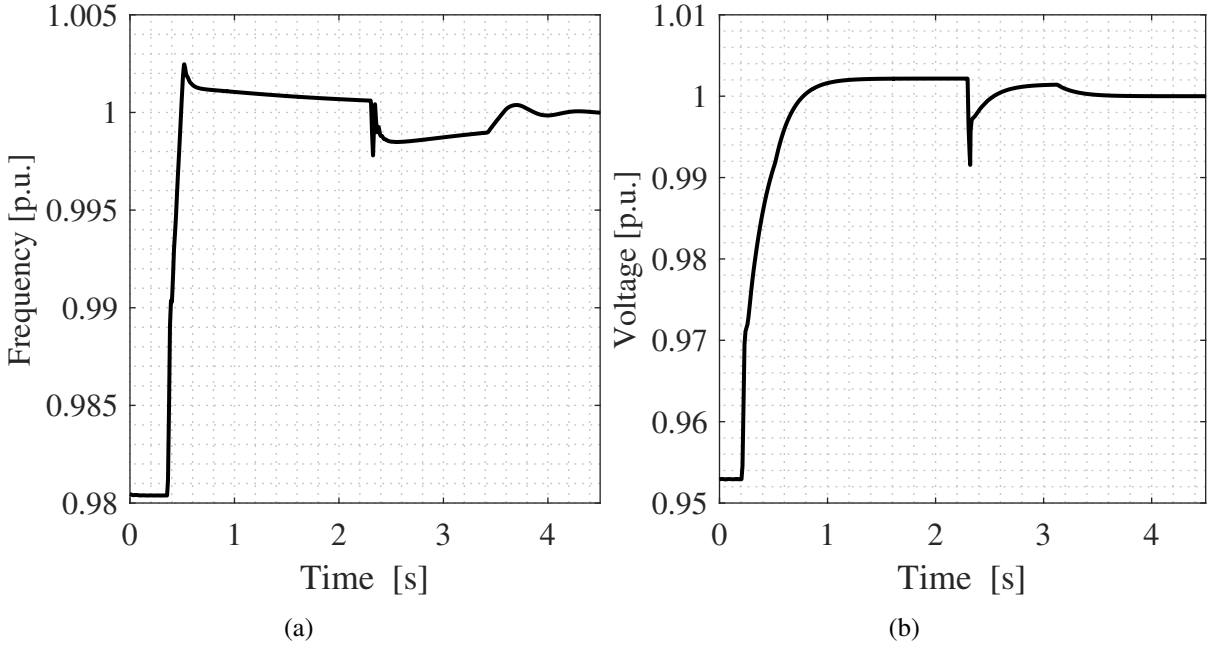

(a) (b)

Figure 4.13: MG dynamics with USCS and communication delay - Total Failure. (a) Frequency. (b) Voltage.

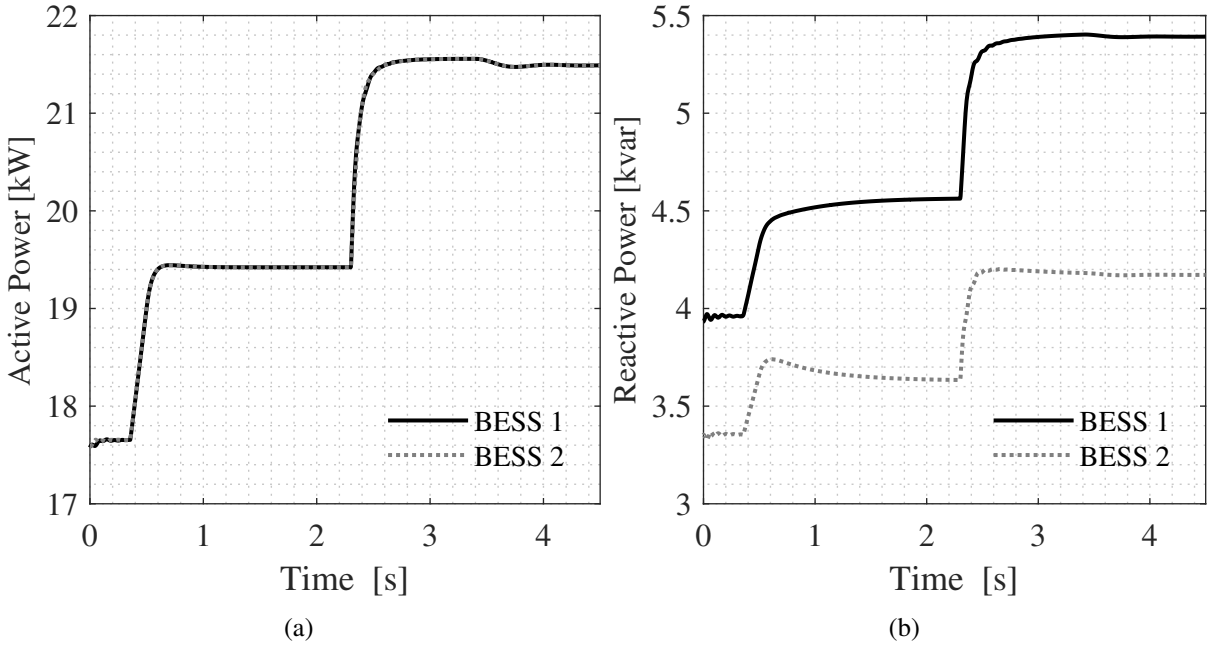

(a) (b)

Figure 4.14: MG dynamics with USCS and communication delay - Total Failure. (a) Active Power. (b) Reactive Power.

of the case without communication delay. However, due to the communication delay, the DCUs take a longer time to change operation mode. This phenomenon can be explained because the MGCC takes 150ms to receive information from the DCUs, and the DCUs take 150ms to receive information from the MGCC. Note that the variable CmT' received in the DCUs presents a duration time of 400 ms when with logic level 1, equivalent to the tracking process time plus twice the communication delay time.

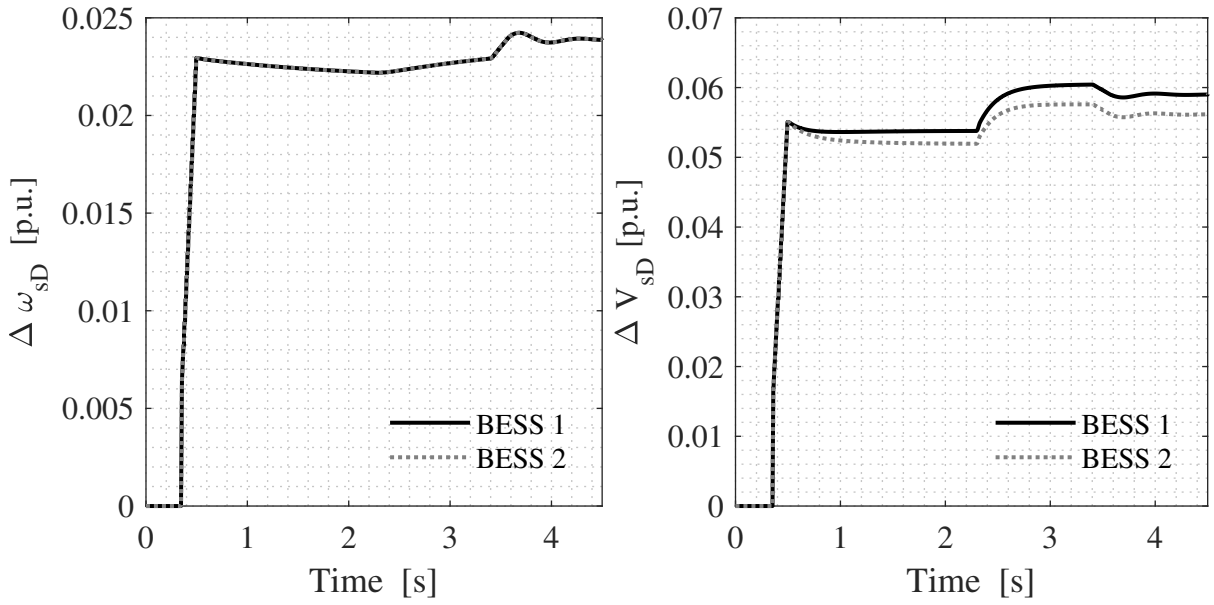

Figure 4.15: MG dynamics with USCS and communication delay - Total Failure. (a) Frequency control action. (b) Voltage control action.

4.4.3 Case 3: Partial Failure without communication delay

A partial failure only occurs when the communication channel between some DCUs and the MGCC goes out of operation. Internal failures in the DCUs cause the loss of the generating unit, since the DCU is part of the internal control of the unit, so a failure in this component is a failure in the DG control itself, which affects not only the frequency and voltage regulation but the unit control itself.

For the simulated condition, a partial failure in the communication channel between BESS 1 and the MGCC was considered. Figs. 4.19(a) and 4.19(b) illustrate the dynamics of PCC frequency and voltage.

For this scenario, the frequency and voltage are regulated to the nominal value (1 p.u.) since the BESS 2 continues to operate in CSC mode. It is observed that, during the control transition period, there were no abrupt variations in the frequency and voltage values.

The Figs. 4.20(a) and 4.20(b) illustrate the dynamics of active and reactive power of both BESS. It is observed that after DCU 1 changes to connected mode, the active power of BESS 1 decreases in value, while the power of BESS 2 increases. However, a similar dynamic cannot be observed for reactive power. Since the reactive power of BESS 2 decreases and the reactive power of BESS 1 increases when the DCU switches to decentralized mode. These dynamics can be explained through the control actions generated in each BESS.

The frequency and voltage control actions from the DCUs sent to the primary control are illustrated in Figs. 4.21(a) and 4.21(b). The frequency control action tends to remain constant after DCU 1 changes to DSC mode. Since the decentralized frequency strategy uses a propor-

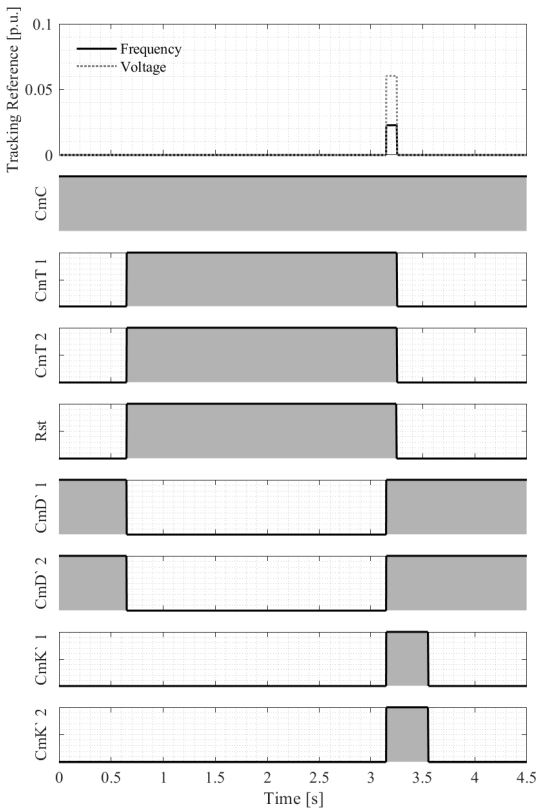

Figure 4.16: MG dynamics with USCS and communication delay - Total Failure - MGCC.

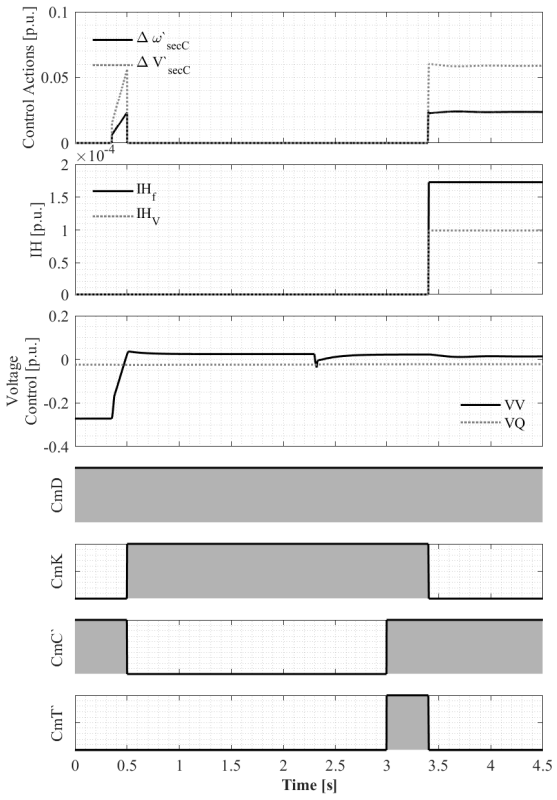

Figure 4.17: MG dynamics with USCS and communication delay - Total Failure - DCU 1.

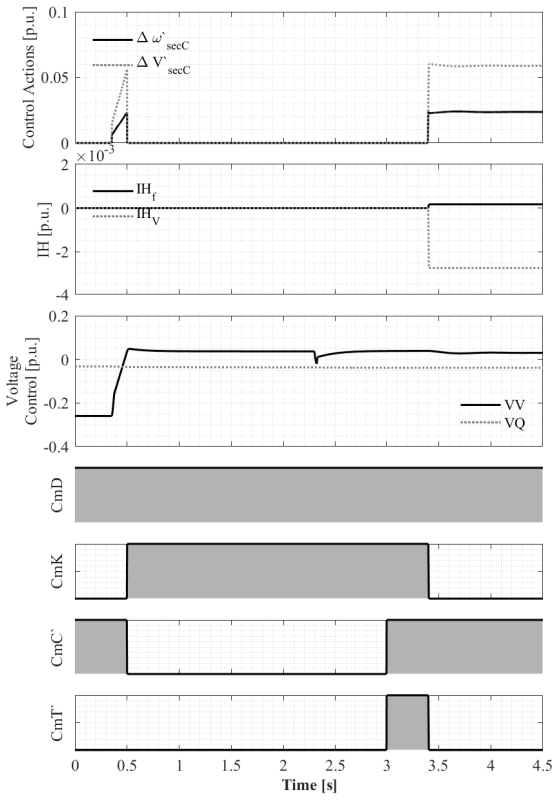

Figure 4.18: MG dynamics with USCS and communication delay - Total Failure - DCU 2.

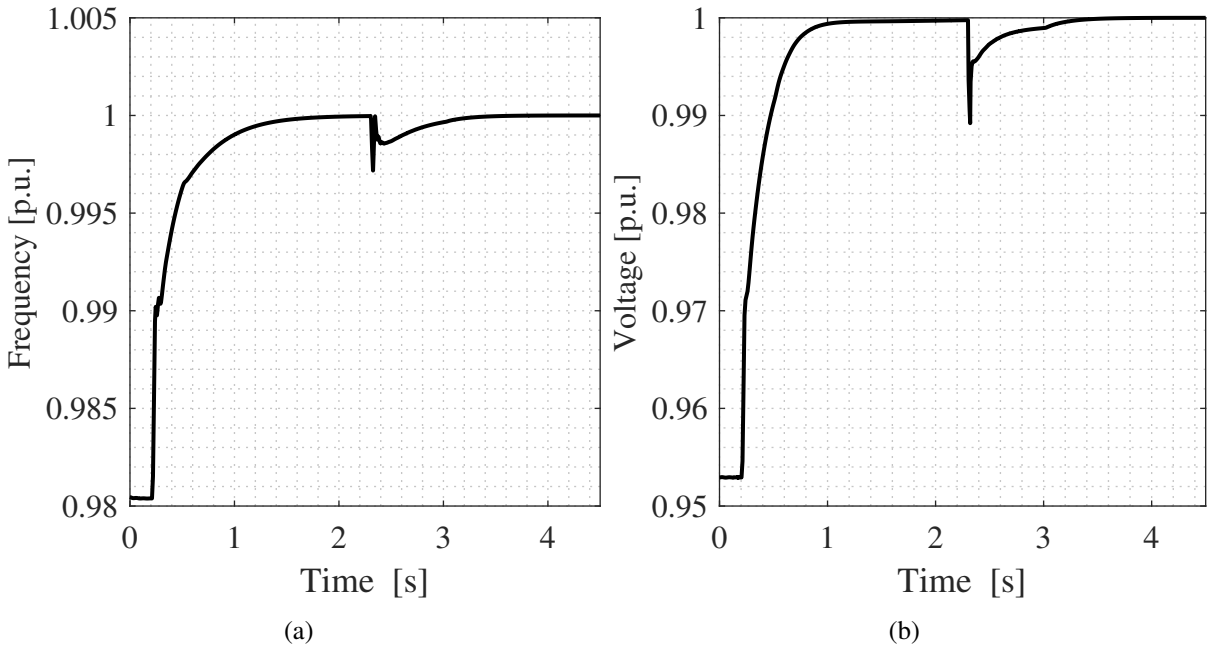

Figure 4.19: MG dynamics with USCS - Partial Failure. (a) Frequency. (b) Voltage.

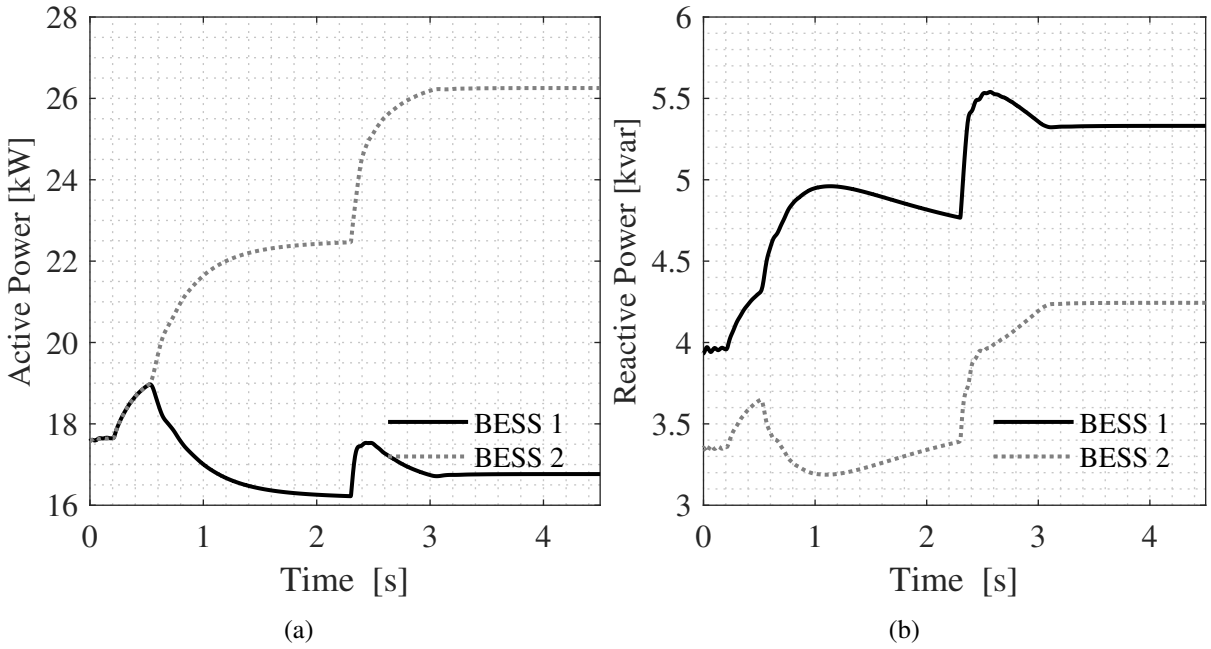

Figure 4.20: MG dynamics with USCS - Partial Failure. (a) Active Power. (b) Reactive Power.

tional control and the centralized strategy a PI that seeks null error, the decentralized frequency control strategy tends not to generate steady-state control actions when operating together with the centralized control strategy.

In steady state, only the DGs operating in CSC mode take action for frequency regulation. This may be a drawback of the structure, as it limits the frequency regulation capability to those DGs in CSC mode. However, if the DGs under CSC reach their maximum capacity, the DGs operating in DSC mode can step in to regulate the frequency. In such scenarios, the remaining DGs in DSC mode dispatch their power to maintain the power balance within the MG. This

coordination ensures that even when some DGs are unable to respond due to capacity constraints or communication failures, the overall system stability and power balance are preserved.

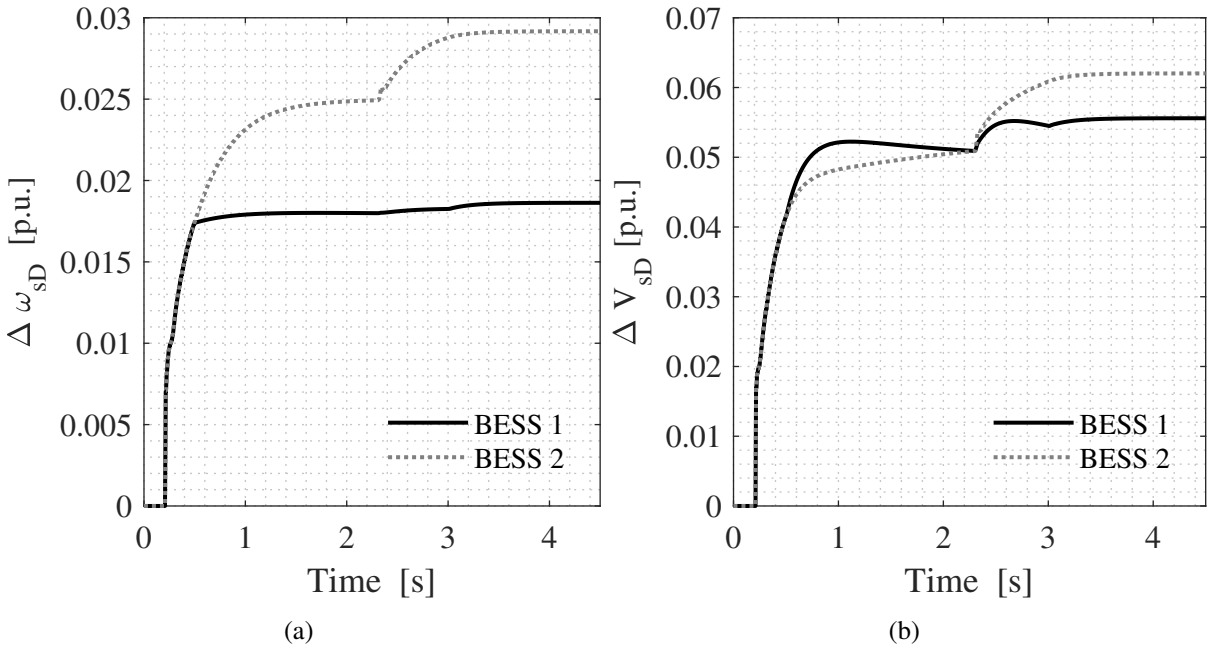

Figure 4.21: MG dynamics with USCS - Partial Failure. (a) Frequency control action. (b) Voltage control action.

However, for the proposed decentralized voltage control strategy, an integrative control with two inputs is applied, wherein one input is related to voltage control and another is related to reactive power sharing. The actions of the decentralized strategy after the failure tend to increase and then begin to decrease. This phenomenon can be explained through the increment portions of the DCU 1 decentralized strategy illustrated in Figs. 4.22(a) and 4.22(b).

Both increment portions of the decentralized strategy start with negative values, the modulus portion increases quickly and becomes a positive value after a few seconds of failure. The sharing portion also increases rapidly, however after approximately one second the sharing portion starts to decrease. The sudden increase in both portions occurs because both portions present negative values. As the integrator starts to generate the control action for the primary control, the DG voltage rises rapidly, also causing the reactive power to increase. With this increase, both control portions rise rapidly.

Additionally, the drop in reactive power after a few seconds of failure is due to the active power of the unit, and as the active power is used to estimate the reactive power of the equivalent unit, the share of power also decreases, causing a decrease in reactive power. The behavior of the control actions of secondary controls affects directly the behavior of the active and reactive power, thus, during a partial failure the power sharing is lost.

With the increase of the load R11, both BESSs respond through the primary control, then the active and reactive power increases, and the voltage is reduced, causing the action of the decentralized control strategy. However, the control actions generated by the decentralized

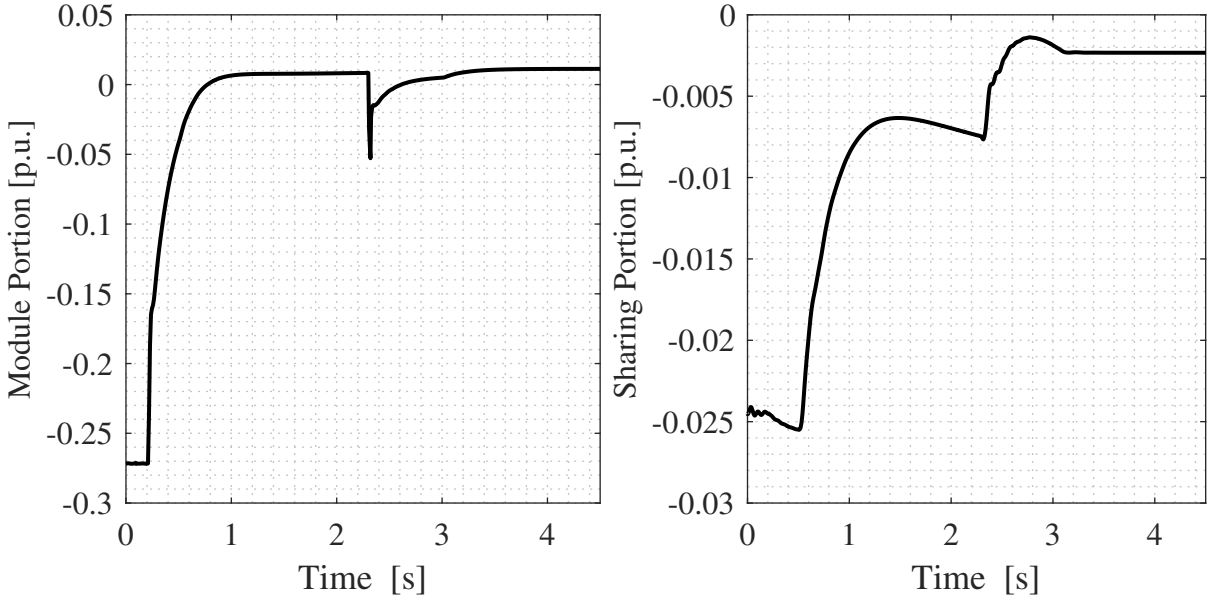

Figure 4.22: MG dynamics with USCS - Partial Failure. (a) VV. (b) VQ.

strategy tend to decrease over time. With the return of the communication channel at 3 s, the UCDs return to operating in centralized mode and maintain the MG voltage at 1 p.u. Note that, when the communication returns, the DCU employs its last decentralized control actions as initialization variables.

The MGCC and DCUs' internal variables are shown in Figs. 4.23, 4.24 and 4.25. When the failure occurs, the MGCC and DCU 1 are unable to communicate with each other, so the observed variables of each controller become zero. The MGCC, observing the output of UCD 1, sets the variable $CmT1$ to logic level 1. The DCU 1 understands that it is no longer able to communicate with the MGCC switches to the decentralized mode of control, and sets its variable CmK for logic level 1. Note that the states of the DCU 2 variables do not change during the simulation.

With the end of the failure in the communication channel, the DCU 1 and the MGCC returned to communicate with each other. The MGCC quickly sends the information to the DCU to switch to the centralized operating mode. The DCU 1 receiving this information changes its mode and sends its magnitudes to the MGCC. Unlike the previous case of total failure, in this scenario, the tracking process does not occur, since the DCU 2 continues to operate in CSC mode.

4.4.4 Case 4: Partial Failure with communication delay

In order to evaluate the performance of the proposed USCS considering communication delays for partial failures, a delay of 150 ms was considered. The same events as the previous

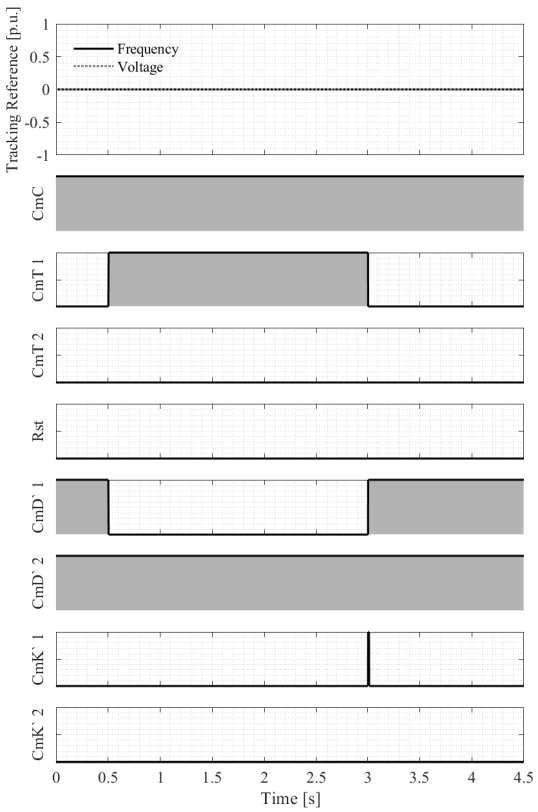

Figure 4.23: MG dynamics with USCS and communication delay - Partial Failure - MGCC.

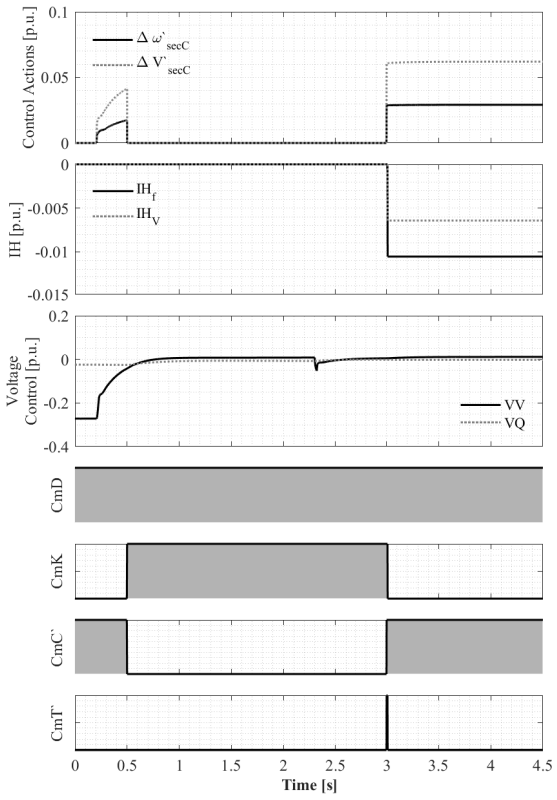

Figure 4.24: MG dynamics with USCS and communication delay - Partial Failure - DCU 1.

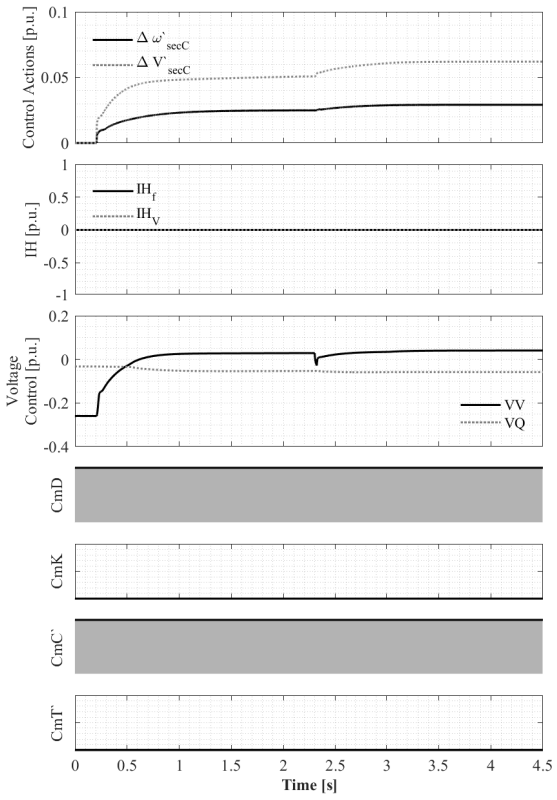

Figure 4.25: MG dynamics with USCS and communication delay - Partial Failure - DCU 2.

cases were employed in this case.

The Figs. 4.26(a), 4.26(b), 4.27(a), 4.27(b), 4.28(a), 4.28(b) and 4.29 illustrate the behavior of the frequency, voltage in the PCC, active and reactive power of the BESS, the voltage control action from DCU sent to the primary control and the DCU 1 variables, respectively.

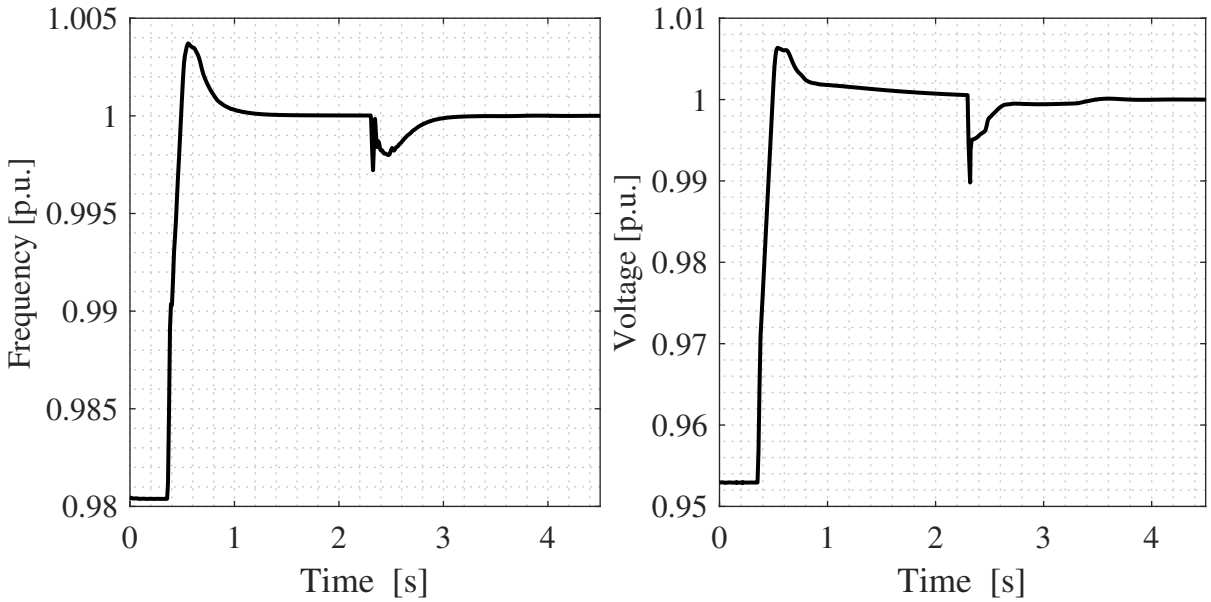

(a) (b)

Figure 4.26: MG dynamics with USCS and communication delay - Partial Failure. (a) Frequency. (b) Voltage.

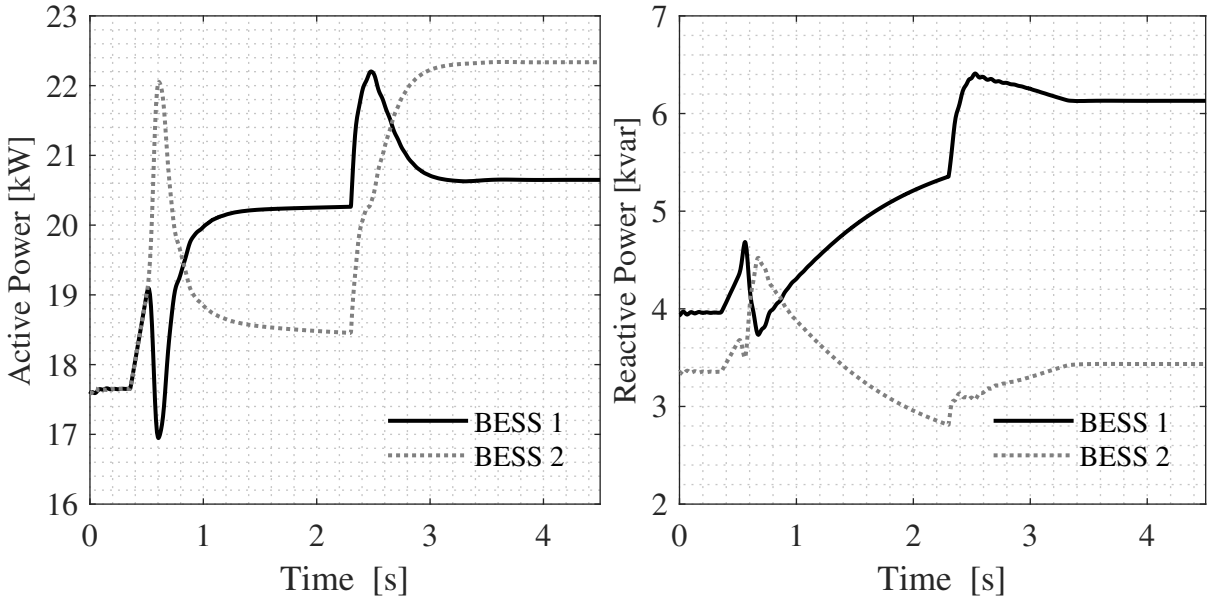

(a) (b)

Figure 4.27: MG dynamics with USCS and communication delay - Partial Failure. (a) Active Power. (b) Reactive Power.

From the results presented, one can see that the dynamics of the frequency, voltage, reac-

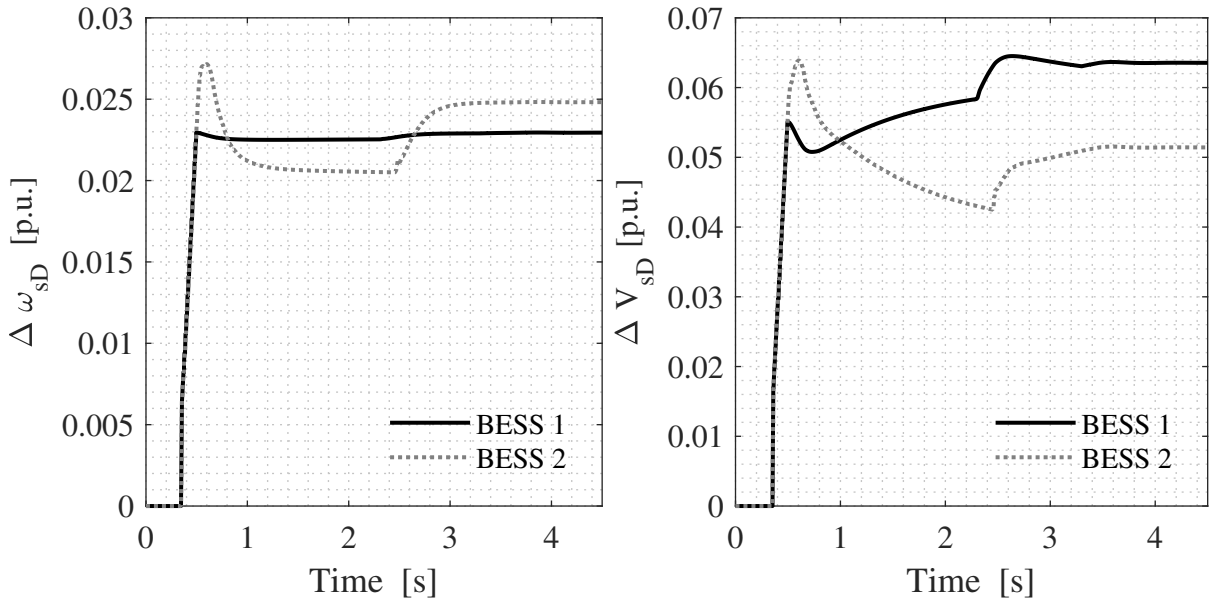

Figure 4.28: MG dynamics with USCS and communication delay - Partial Failure. (a) Frequency control action. (b) Voltage control action.

tive and active power are different from the case without communication delay. Since the communication delay directly affects the centralized control, which operates with UCD 2 throughout the simulation. As presented above, the behavior of the secondary control actions directly affects the MG dynamics. However, there were no abrupt variations in voltage or frequency when the DCUs changed their operating mode.

With the dynamics more oscillatory due to the communication delay, the control actions used as an initial condition by the DCU 1 after the communication failure were oscillatory values, which made the control actions value of the decentralized strategy much higher than the centralized strategy, causing both the active and reactive power of BESS 1 larger than the BESS 2.

Still, the frequency and voltage are controlled at the nominal values even while operating in the decentralized mode of DCU 1. Additionally, the tracking process is not carried out at this stage, however, it is observed that DCU 1 takes approximately 300 ms to switch from decentralized to centralized mode.

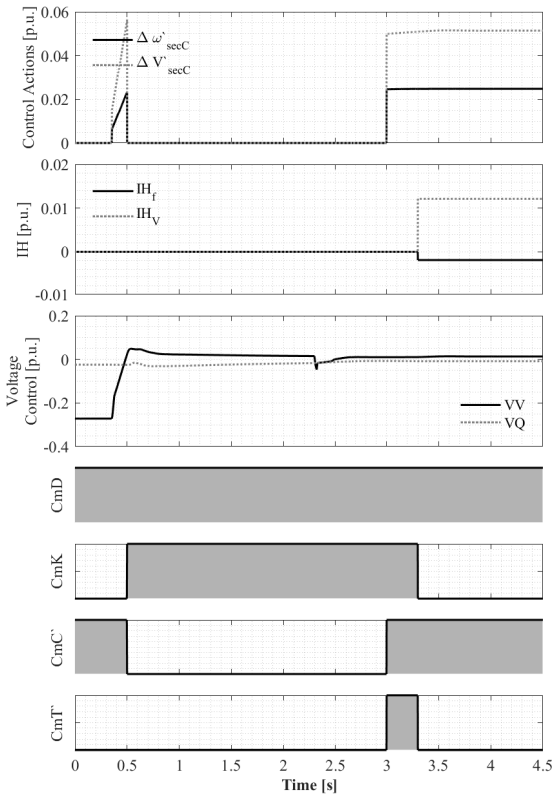

Figure 4.29: MG dynamics with USCS and communication delay - Partial Failure - DCU 1.

4.5 Case 3: Frequency control Comparison between USCS and UCDFCS

In order to compare both the proposed USCS and the UCDFCS, a case with partial failure is considered. As presented in [18], the UCDFCS is influenced by the communication delay. These influences can be better observed in a partial failure. Fig. 4.30 shows the MG frequency for both strategies.

In this scenario, the MG presents a total load of 50%, and all the PV systems are disconnected. At the beginning of the simulation, the MG operates islanded with BESS 1 in decentralized secondary control mode and BESS 2 in centralized secondary control mode. At 0.6 s of simulation, the MG load increases to 55%. At 1.3 s, the communication link returns to normal operation. Additionally, a communication delay of 150 ms is considered.

One can see in Fig. 4.30 that both strategies present a similar behavior during the load increases. However, the behavior when the communication channels return is different. For the UCDFCS, the frequency suffers oscillations due to the initialization variable being calculated in the MGCC, and with the presence of the communication delay, the reference value received by the DCU is different from the actual value. This difference in the reference value occurs due to the oscillations of load variation.

For the proposed USCS, the initialization variable is calculated in the DCU. Thus, the communication delay does not influence the initialization variable value because the initialization variable is calculated locally, without being influenced by the communication delay. The initialization variable and the decentralized control reference are shown in Fig. 4.31.

One can observe in the frequency plot that the decentralized secondary control reference of the UCDFCS exhibits oscillations when the DCUs change to centralized mode. Notably, the initialization variable of the UCDFCS demonstrates a dynamic behavior that converges to its value, which differs from the USCS, exhibiting a step-like behavior. The behavior of the UCDFCS is attributed to the communication delay, as the MGCC continues to perceive the DCUs operating in DSC mode.

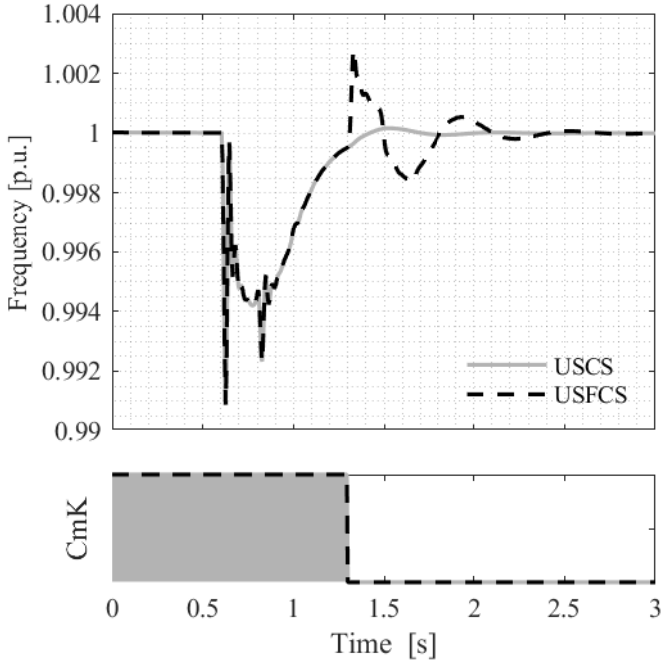

Figure 4.30: Frequency comparison between the USCS and UCDFCS.

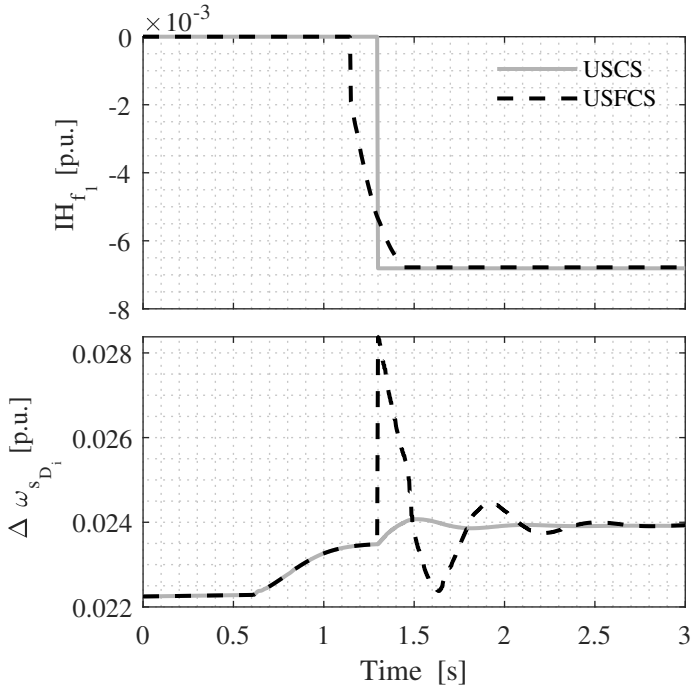

Figure 4.31: Variables comparison between the USCS and UCDFCS.

Chapter 5

Control Hardware in the Loop Results

5.1 Initial considerations

In Chapter 4 the proposed decentralized secondary voltage control and the novel USCS were tested in a simulation environment, where the Matlab/Simulink software was employed. Thus, in order to achieve more reliable results when employing the proposed controls in a real MG, a HIL simulation is carried out.

Thus, in this Chapter, the MG model and control and the simulation results are presented for HIL simulations. The simulation considers two cases, the first shows the results of a total failure, and the second case presents the results of a partial failure.

5.2 Laboratory Framework and Test System

In order to test the proposed system in the HIL environment, the RTDS computer is employed. The same MG presented in Chapter 4 is applied for the test system. In the HIL environment, the MGCC is built in a real-time controller, while the MG system, converter controls, and the DCUs are implemented in the simulation environment.

The same laboratory framework presented in [73] is employed in this thesis, as illustrated in Fig. 5.1. The MGCC with the frequency and voltage centralized secondary strategy is built in the RTAC-SEL controller. The DCUs, MG topology, DGs, and DGs controllers are implemented in the RTDS platform. The amplifier Double F6350e serves as an interface between the RTDS and the RTAC-SEL.

The RTDS solves the MG equations and controls. The PCC three-phase voltage is externalized through the Giga-Transceiver Analogue Output (GTAO) card. The GTAO card's maximum voltage output is ±10 V, which is too low for the RTAC-SEL to measure. Thus, the amplifier Double F6350e is employed to amplify the voltages from the GTAO and send them to the RTAC-SEL.

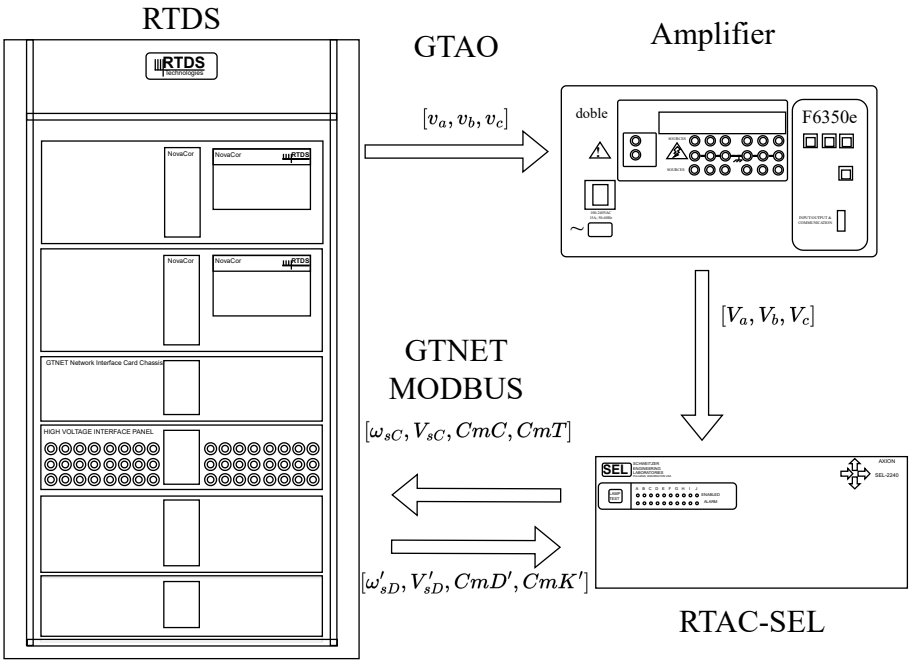

Figure 5.1: Laboratory Setup, [73].

The RTAC-SEL communicates with the RTDS through the MODBUS protocol, with a latency of approximately 200 ms for both the controller and communication. In the RTDS, each BESS has its own DCU, and each DCU has its own MODBUS server. The RTAC-SEL can identify if the network is offline through the MODBUS function's "Offline" variable. However, the DCU servers cannot determine if the communication system is operating. Therefore, the heartbeat strategy [76] is employed in each DCU. In this strategy, the MGCC sends pulses to the DCUs. If the DCUs do not receive several pulses within a determined time, they consider the system to be under failure.

The MGCC sends a message containing three variables (CmC, CmT, and $\Delta\omega_{sC}$) and the heartbeat (HB). The DCUs implement logic to detect communication failure. If a failure is detected, the variables CmC' and CmT' in the DCU are set to zero, maintaining the DCUs logic as proposed.

For the simulations, the loads in the MG are considered to consume only 10 kW and 1 kvar each. The decentralized control gains are the same as presented in Table 4.3. For the decentralized controls, the gains are presented in Table 5.1. Note that these gains are different from the gains presented in Table 4.4. Different control gains are selected in order to observe different behaviors in centralized control.

Table 5.1: Centralized Controls Gains HIL.

Gain	Value [pu]
Kp_ω	1
Ki_ω	1
Kp_V	0.1
Ki_V	0.1

5.2.1 Case CHIL: Total Failure

In this case, the simulation is divided into two stages. The first one presents the results when the failure occurs, and the second stage when the failure ends.

Figs. 5.2, 5.3, 5.4, 5.4 and 5.6 show the results for PCC, MGCC and DCUs states for the first stage. In this stage, the simulation starts with the MG in island mode. At 4 s, the centralized secondary control is enabled, and at 8.3 s, the total failure occurs, where the communication channel between the DCUs and MGCC is out of operation.

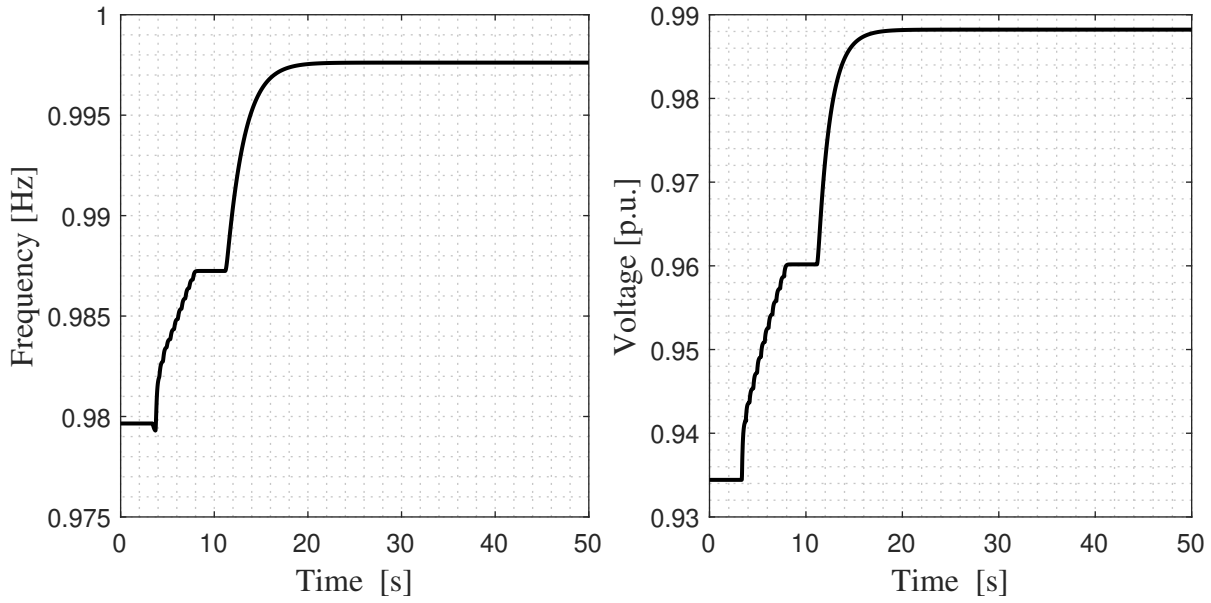

Figure 5.2: MG dynamics with USCS - First Stage of Case 1 (a) Frequency. (b) Voltage.

Fig. 5.2 shows the MG frequency and voltage for stage 1. Without the secondary control, only the primary control is operating. In this case, the frequency is 0.978 p.u., and the voltage is 0.935 p.u. When the controller turns on, the frequency and the voltage are regulated to the reference value (1 p.u.). One can see that the variables have been regulated in step changes; this behavior occurs due to the control and communication latency. However, the failure occurs before the variables reach steady-state, around 0.996 p.u. for frequency and 0.988 p.u. for voltage.

Note that the active and reactive power increase their values when the secondary control is acting. This behavior occurs due to the load being modeled as constant impedance, thus the load consumption is related to the square of the voltage.

When a failure occurs, the control actions of the MGCC cannot be sent to the DCUs. Thus, the DCUs will not receive new variables. After the failure, the frequency and voltage stay constant for around 1 second. This behavior occurs due to the heartbeat strategy since the DCUs need time to identify the communication failure. When the DCU determines the communication

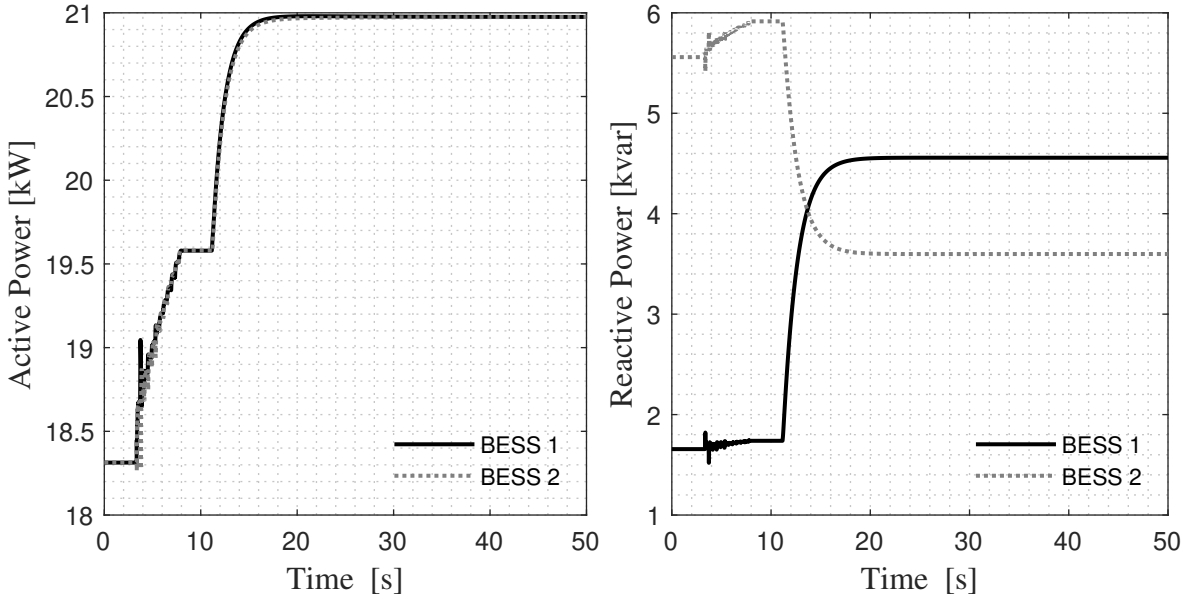

(a) (b)

Figure 5.3: MG dynamics with USCS - First Stage of Case 1 (a) Active Power. (b) Reactive Power.

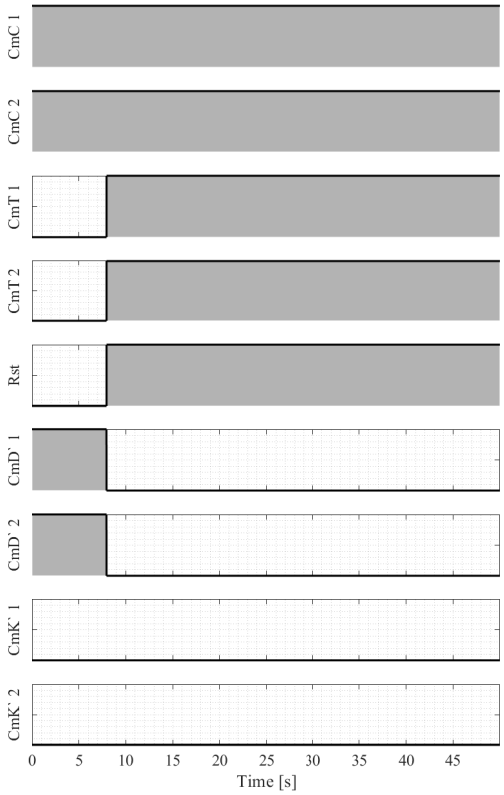

Figure 5.4: MG dynamics with USCS - First Stage of Case 1 - MGCC.

failure, the control mode changes to decentralized, and the frequency and voltage return to be regulated. This behavior can be better seen in the MGCC's and DCU's internal variables.

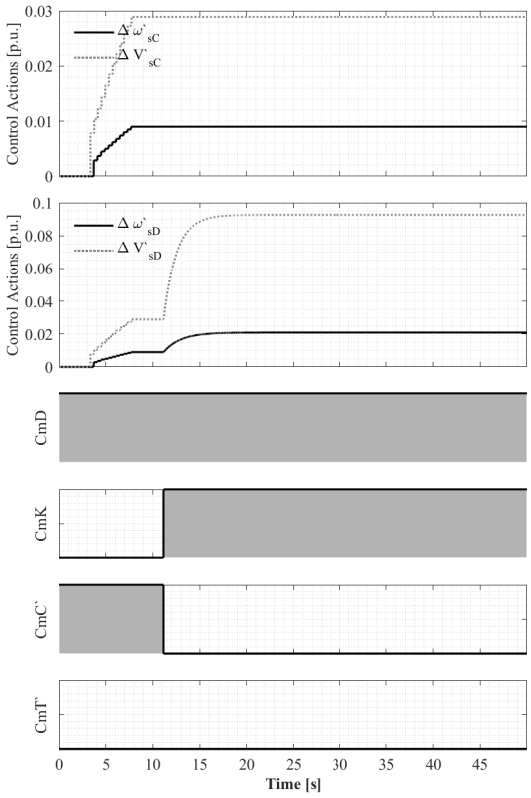

Figure 5.5: MG dynamics with USCS - First Stage of Case 1 - DCU 1.

Before the failure, the MGCC operates with the variables $CmC1 = CmC2 = 1$ and $CmT1 = CmT2 = 0$ as shown in Fig. 5.4. And the DCUs operate with the variables $CmD1 = CmD2 = 1$ and $CmK1 = CmK2 = 0$, as shown in Figs. 5.5 and 5.6. When the secondary control starts, the MGCC sends the same value of the secondary control increment to the DCUs.

When a failure occurs, both MGCC $CmD'1$ and $CmD'2$ variables are set to zero, and the variables $CmT1$, $CmT2$, and Rst are set to one. One can see that, in the DCUs, the values of $CmC'1$ and $CmC'2$ only receive zero when the DCU detects the failure. It is important to note that the DCUs cannot receive the values of the variables from the MGCC due to communication failure.

When the DCUs detect the failure, around 10 s of simulation, the $CmK1$ and $CmK2$ variables are set to one, and the DCUs change to the decentralized secondary control mode. One can see that the decentralized control strategy applies the last value received from the MGCC as an initialization variable. Thus, the generated increment stays the same. The initialization value used for both DCUs is 0.009 p.u. for frequency and 0.009 p.u. for voltage.

The frequency and voltage are regulated when the decentralized control starts operating. Note that active power sharing maintains its behavior during the decentralized operation, as shown in Fig. 5.3. However, it is possible to observe that reactive power sharing improves after decentralized control. For example, before the decentralized strategy, the difference in reactive

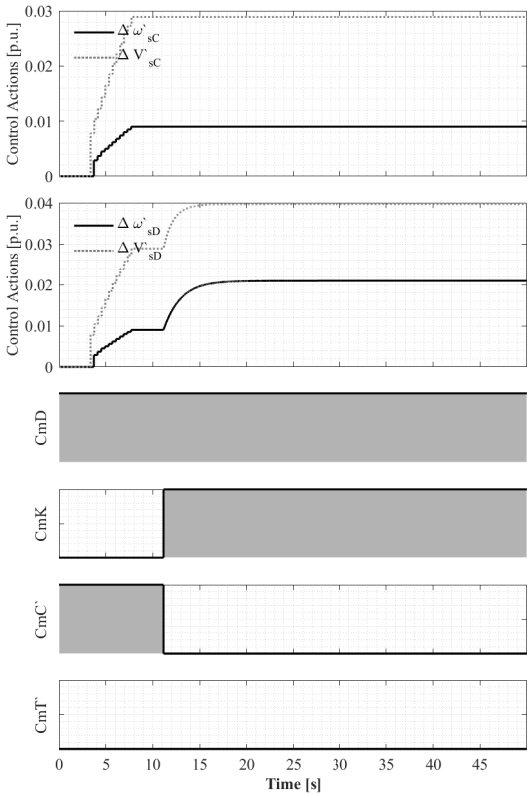

Figure 5.6: MG dynamics with USCS - First Stage of Case 1 - DCU 2.

power between the batteries was 4.190 kvar. After the decentralized control, the differences were reduced to 0.958 kvar.

The improvement of the reactive power sharing is due to the proposed decentralized secondary voltage control. As explained before, the proposed voltage control acts over the voltage through two portions, one responsible for the voltage magnitude correction and the other for reactive power sharing. With the presented results, it is possible to observe that the proposed voltage control can achieve good reactive power sharing by regulating the voltage, different from the centralized control, where only voltage regulation is considered.

For the decentralized voltage and frequency controls, steady-state values of frequency and voltage are 0.997 p.u. and 0.988 p.u., respectively. These values are close to the reference. However, these decentralized strategies cannot achieve null errors due to their operation.

Figs. 5.7, 5.8, 5.9, 5.10 and 5.11 show the results for PCC, MGCC and DCUs states for the second stage. In the second stage, the simulation starts with the MG in islanded mode where all DCUs operate in decentralized mode. At 7 s, the communication link returns to operation.

The control behavior can be explained through the MGCC's and DCU's internal variables. Before the communication link returns, the MGCC and the DCUs operate with the last states of the First Stage. However, when the communication link returns, the MGCC can read the states of the DCUs. The MGCC receives the states of the DCU 2 first, at 8.01 s, and starts the tracking

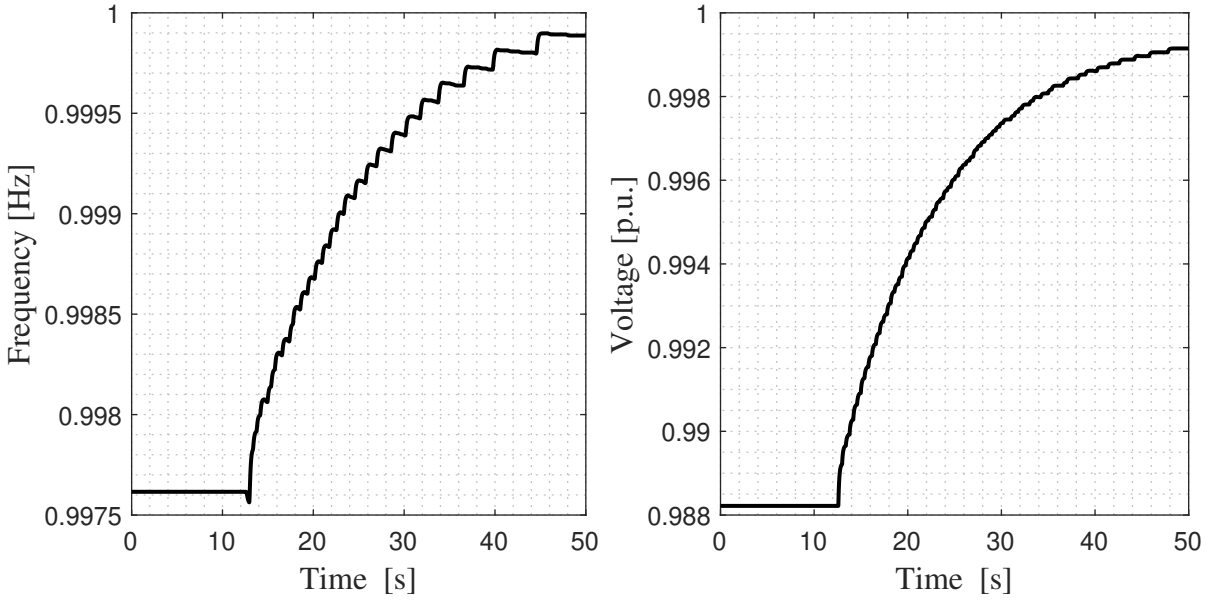

(a) (b)

Figure 5.7: MG dynamics with USCS - Second Stage of Case 1 (a) Frequency. (b) Voltage.

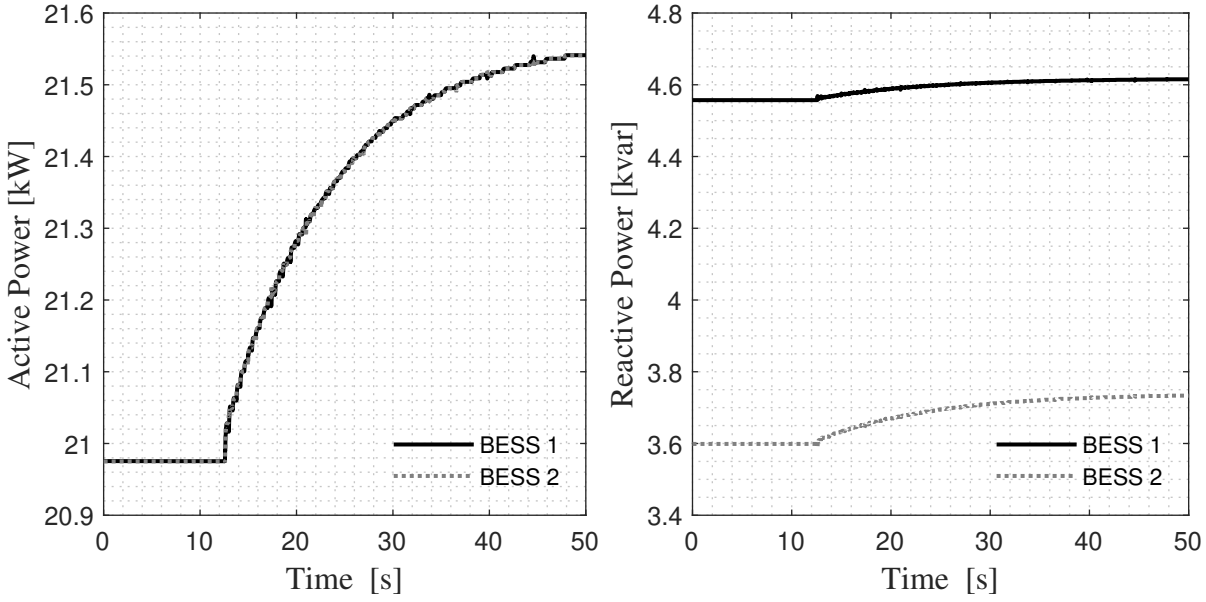

(a) (b)

Figure 5.8: MG dynamics with USCS - Second Stage of Case 1 (a) Active Power. (b) Reactive Power.

process using the DCU 2 as a reference. Then the MGCC receives the message from DCU 1 at 8.41 s. Note that the DCUs only identify that the communication link returns at 8.18 s for DCU 2 and 8.91 s for DCU 1. This behavior is due to the heartbeat strategy and communication delay.

During the tracking process, the values of $CmT1$ and $CmT2$ are kept to one. Thus, the DCUs still operate in the decentralized mode. The tracking process lasts for 4 s. The MGCC changes the state CmT to zero at 12.6 s to inform the DCUs to change their mode. At the same

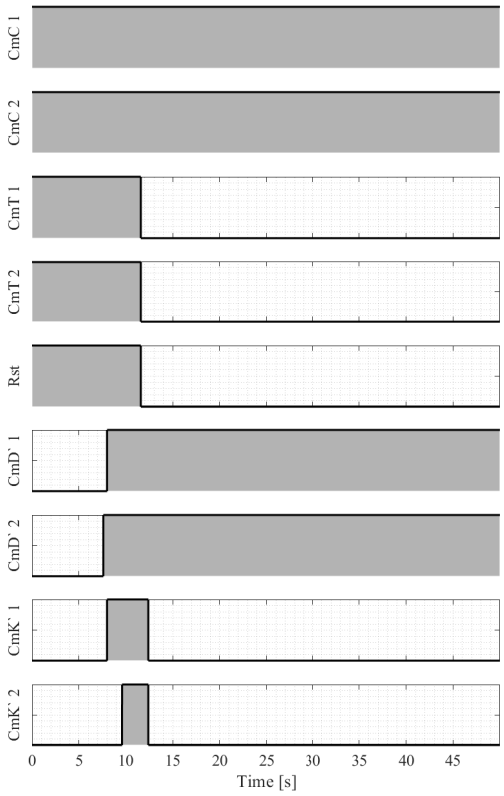

Figure 5.9: MG dynamics with USCS - Second Stage of Case 1 - MGCC.

time, the variable Rst changes its values to zero too.

Both DCUs receive the message $CmT = 0$ at 10.36 s of simulation and change their control mode to centralized. Thus, the variables CmK change their values to zero. However, only at 12.80 s of simulation that the MGCC receives the state CmK from the DCUs.

When the DCUs change to centralized control mode, the secondary voltage and frequency control actions stay the same. Only at 13.32 s the DCUs start to receive the MGCC centralized control actions. Thus, the voltage and frequency are regulated to their nominal values. As mentioned in Stage 1, the smooth transition between the decentralized and centralized modes is due to the initialization variable being calculated in the DCUs.

Also, reactive power sharing is maintained when the control mode changes. This behavior occurs due to the DCUs maintaining their secondary voltage control actions. As shown in Figs. 5.10 and 5.11, the centralized secondary control actions sent by the MGCC are the same for both DCUs. However, the decentralized secondary voltage control action generated is different in each DCU. Thus, when the DCU changes its control, it calculates a new initialization variable. For the DCU 1, the initialization variable receives the value $IH_{V_1} = 0.053$ p.u. and the DCU 2 receives $IH_{V_2} = 2E - 5$ p.u.

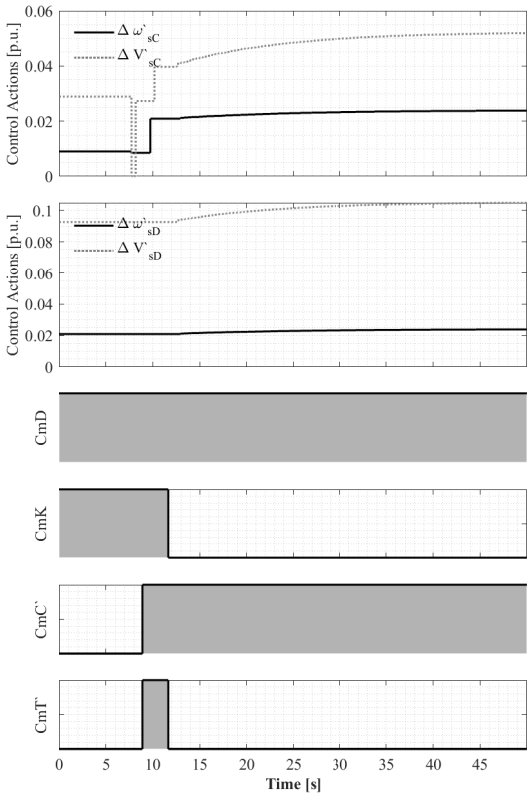

Figure 5.10: MG dynamics with USCS - Second Stage of Case 1 - DCU 1.

5.2.2 Case CHIL: Partial Failure

As in Case 1, the simulation is divided into two stages for this case. The first one presents the results when the failure occurs, and the second stage shows the results when the failure ends. The Figs. 5.12, 5.13, 5.14, 5.15 and 5.16 show the results for PCC, MGCC and DCUs states for the first stage. In this stage, the simulation starts with the MG in islanded mode. At 4.21 s, the centralized secondary control is enabled, and at 8.19 s, the partial failure occurs, where the communication channel between the DCU 2 and MGCC gets out of operation.

When the failure occurs, the MGCC does not receive messages from the DCU 1, thus its variable CmD'_1 receives values zero, and the variable CmK_1 in the MGCC is set to value one, as shown in Fig 5.14. DCU 2 stops receiving the values of the MGCC. However, due to the heartbeat strategy, DCU 2 only detects the failure at 12.84 s of simulation.

Unlike Case 1, where all DCUs change to decentralized mode, only the DCU with failure changes to decentralized mode. In Fig. 5.12 one can see that the frequency and voltage are regulated to the nominal values because the centralized secondary control still acts over the DCU 1. Due to the objective of the centralized secondary control being to regulate the voltage and the frequency in the PCC to its nominal values, the actions of the decentralized secondary control in DCU 1 are influenced.

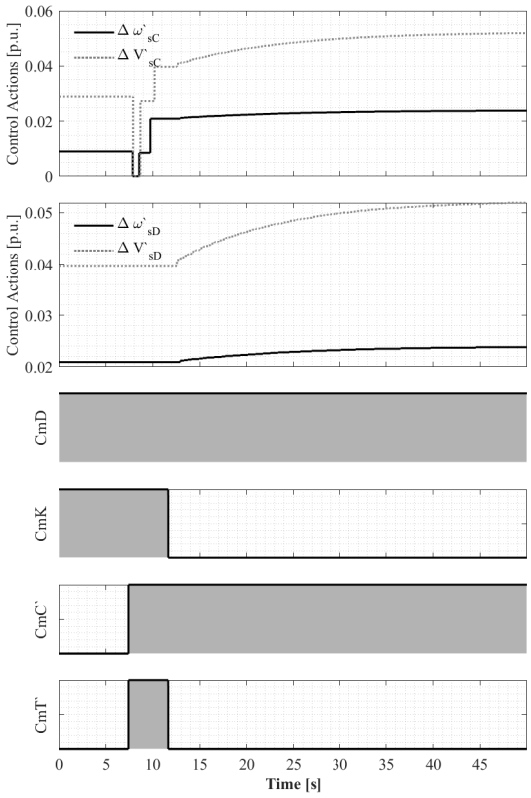

Figure 5.11: MG dynamics with USCS - Second Stage of Case 1 - DCU 2.

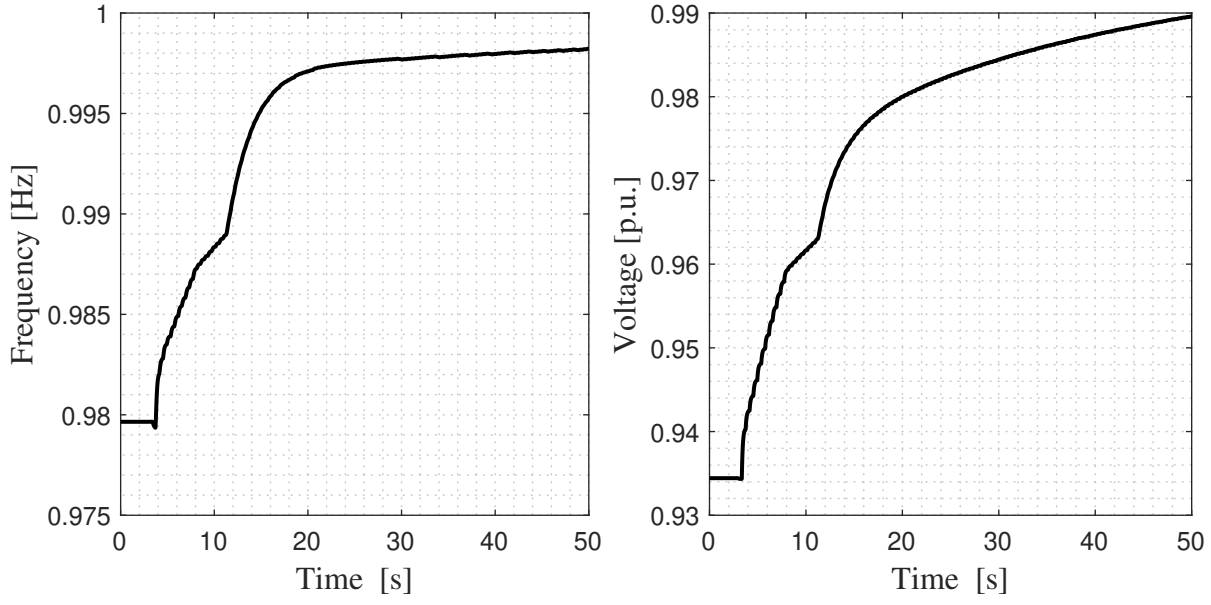

(a) (b)

Figure 5.12: MG dynamics with USCS - First Stage of Case 1 (a) Frequency. (b) Voltage.

With the frequency being regulated to the nominal value, the decentralized frequency strategy [30], which only takes control actions if the frequency presents a deviation, will not participate in the steady state, only in the transitory state. On the other hand, the proposed

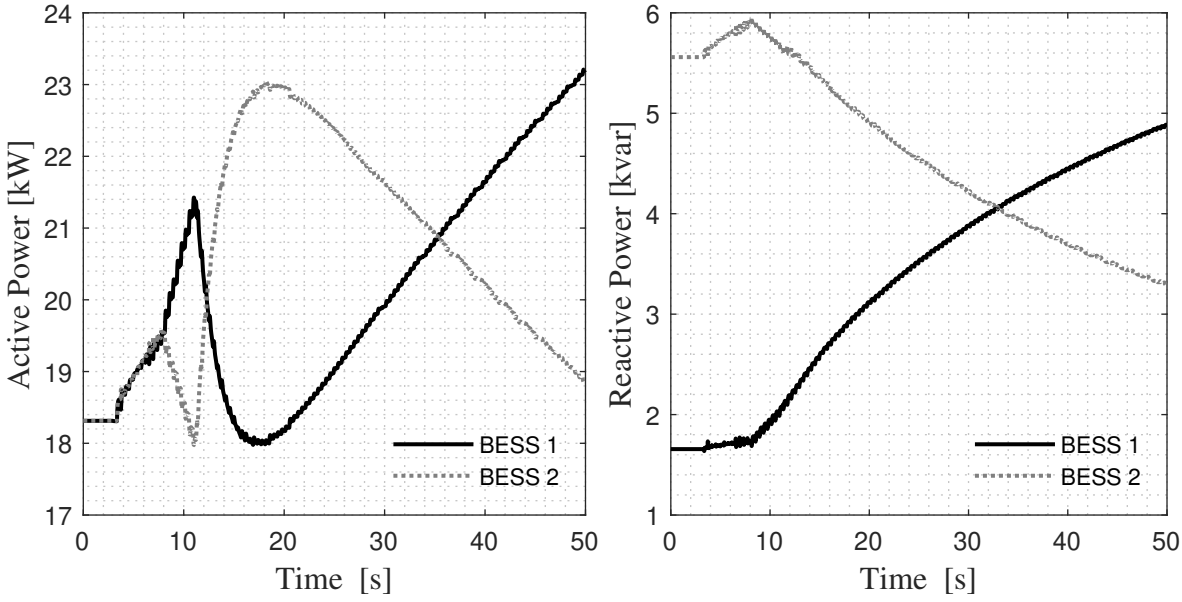

(a) (b)

Figure 5.13: MG dynamics with USCS - First Stage of Case 2 (a) Active Power. (b) Reactive Power.

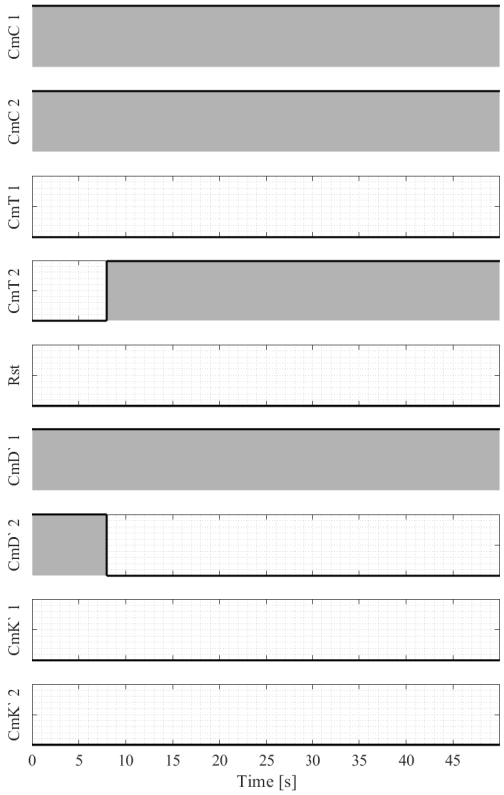

Figure 5.14: MG dynamics with USCS - First Stage of Case 2 - MGCC.

decentralized voltage regulation strategy presents a different behavior. It regulates the voltage based on a local measurement and estimates the PCC voltage through the current. Errors in the

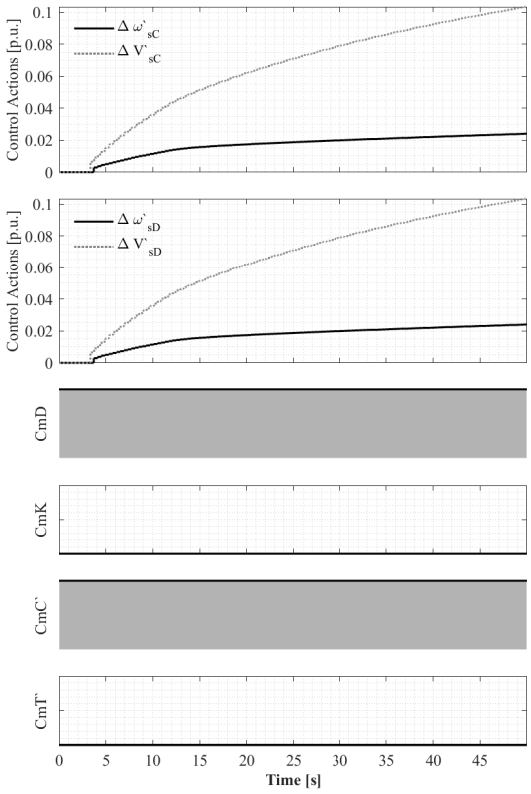

Figure 5.15: MG dynamics with USCS - First Stage of Case 2 - DCU 1.

voltage regulation may be present as the voltage estimation is not completely accurate. However, the decentralized voltage strategy action presents the power-sharing portion that depends on the active power. Thus, in a steady state, the voltage strategy tends to follow the behavior of the decentralized control.

After DCU 2 changes its control mode, the values of active and reactive powers of BESS 2 are increased faster than BESS 1. This behavior occurs because the decentralized controls act faster than the centralized control, as shown in Figs. 5.15 and 5.16 where the DCU 2 control actions are bigger than the DCU 1. However, as the centralized strategy takes action, the control actions sent to decentralized control are lowered.

Figs. 5.17, 5.18, 5.19, 5.20 and 5.21 show the results for PCC, MGCC and DCUs states for the second stage. In the second stage, the simulation starts with the MG in islanded mode where DCU 2 operates in decentralized mode and DCU 1 operates in the centralized mode. Around 6 s of simulation, the communication link of DCU 2 returns.

From the simulation, it is possible to observe three points in the MGCC: first, when the communication channel of the DCU returns, the tracking process is not active (see Fig. 5.19 RsT variable); secondly, when the MGCC detects the return of communication, the state $CmT1$ is set to zero. Thus the MGCC sends the signal to DCU 2 to change its operation mode. Thirdly, the MGGC detects that the DCU changed to centralized mode at 7.26 s of simulation.

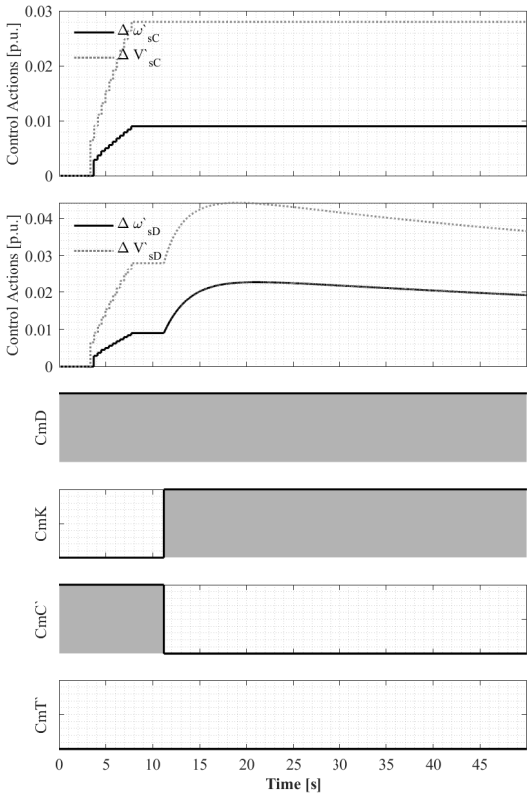

Figure 5.16: MG dynamics with USCS - First Stage of Case 2 - DCU 2.

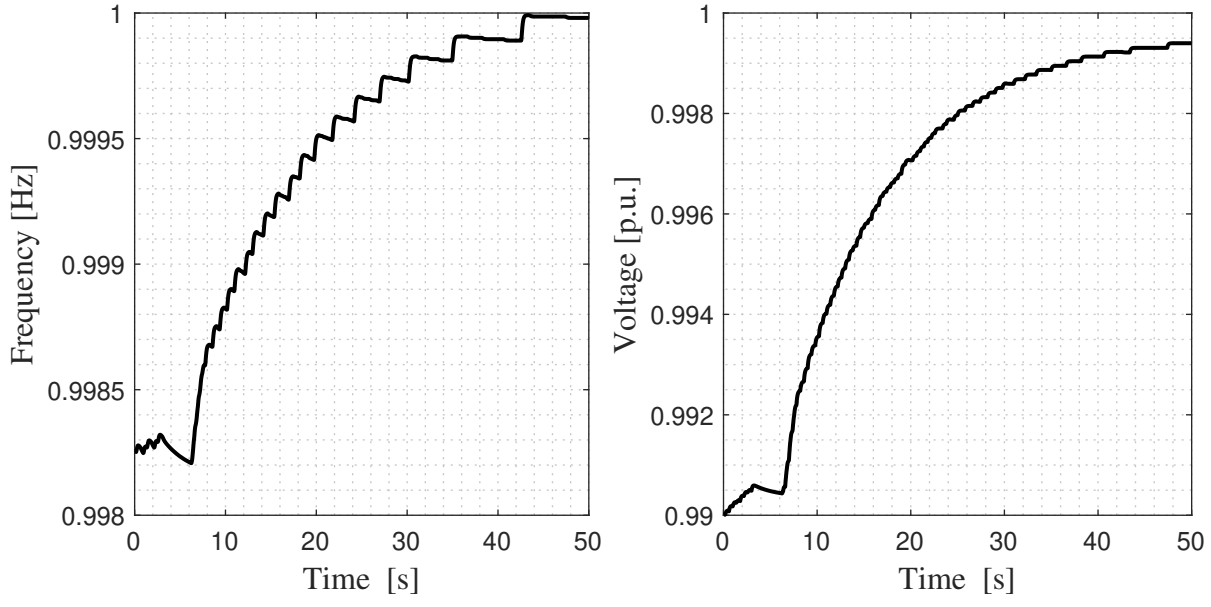

(a) (b)

Figure 5.17: MG dynamics with USCS - Second Stage of Case 1 (a) Frequency. (b) Voltage.

For the DCUs, the frequency and voltage control actions in DCU 2 maintain their values when changed to centralized mode. Additionally, note that the difference between the control actions is maintained in the centralized operation. As explained above, the decentralized

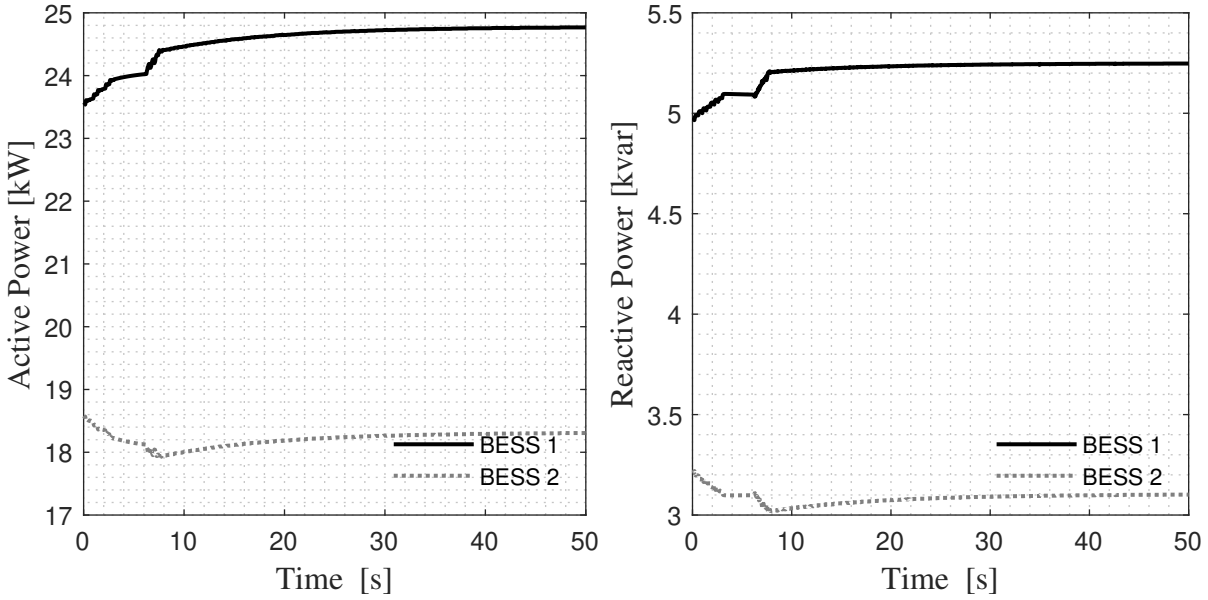

(a) (b)

Figure 5.18: MG dynamics with USCS - Second Stage of Case 2 (a) Active Power. (b) Reactive Power.

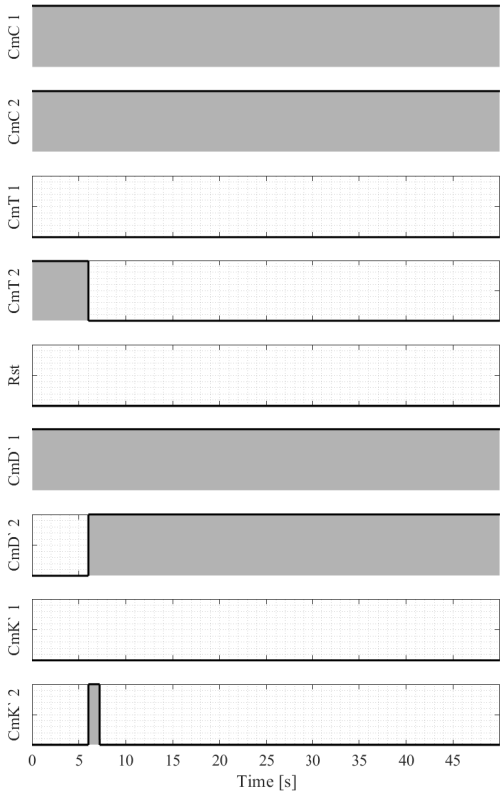

Figure 5.19: MG dynamics with USCS - Second Stage of Case 2 - MGCC.

strategies present control action values distinct from the centralized strategy. Thus when the control changes, the DCU calculates its new initialization variable and maintains the last values

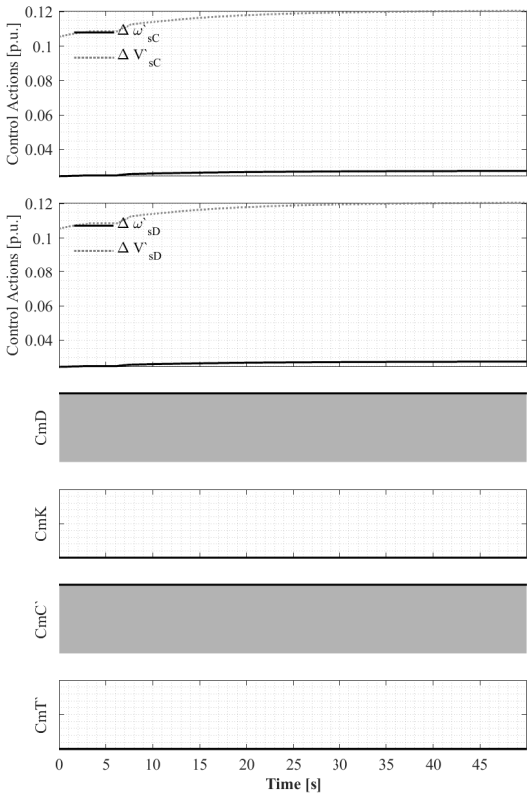

Figure 5.20: MG dynamics with USCS - Second Stage of Case 2 - DCU 1.

of control actions.

Also, note that the active power presents different values for both batteries and when the DCU returns to centralized operation, this difference is preserved. This behavior occurs due to the last increment sent by the decentralized strategy being employed as an initialization variable. Thus, the differences between the secondary control actions are maintained in the centralized operation.

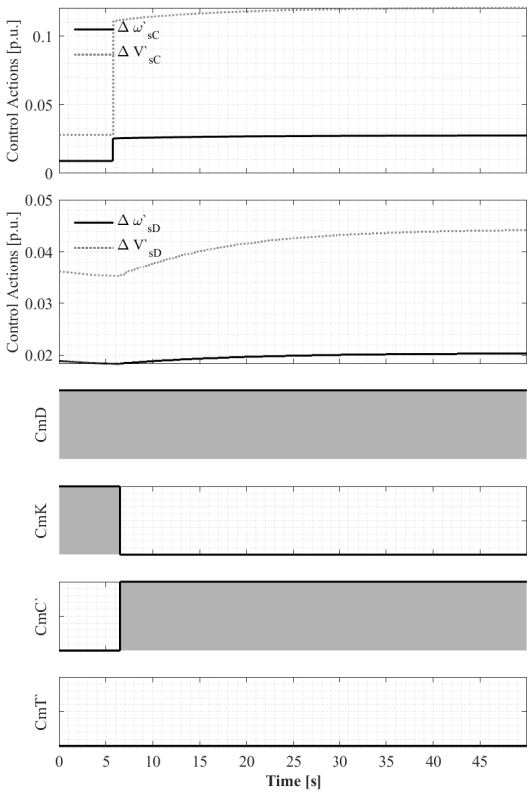

Figure 5.21: MG dynamics with USCS - Second Stage of Case 2 - DCU 2.

Chapter 6

Conclusion

6.1 Initial considerations

This work presented a proposal for a secondary control strategy, with the main objective of maintaining MG frequency and voltage regulation even after communication failures and/or MGCC failures. This strategy unifies centralized and decentralized control through a communication structure, where decentralized strategies act as backups for the centralized strategies. Thus, during a failure where the centralized strategies cannot regulate frequency and voltage, the decentralized strategy is activated to maintain MG operation.

Initially, the USFCS was proposed to ensure frequency regulation reliability. However, due to some issues highlighted in this work, this strategy presents oscillations during control mode changes. Therefore, a novel USCS is proposed not only for frequency regulation but also for voltage regulation. In the USCS strategy, DCUs are inserted as interfaces between the MGCC and the DGs. In normal operation, the DCUs and the MGCC can exchange information, so the MGCC generates secondary control actions and sends them to each of the DCUs, which pass this information on to their respective DGs. If there is a failure in the MGCC or communication channel, the DCUs stop receiving information from the MGCC and switch to DSC mode. In DSC mode, the DCUs regulate MG frequency and voltage only through local variables, without communication. If the failure is corrected and the system returns to normal operation, the MGCC receives information from the DCUs and can automatically resume MG frequency and voltage regulation and generate new control actions.

Additionally, a novel decentralized secondary control strategy is proposed to achieve decentralized voltage regulation in the USCS. This decentralized voltage strategy is based on equivalent system representation and local measurement, leveraging the concept that reactive power in the system varies similarly to active power. Therefore, knowing that active power presents good power sharing, the decentralized strategy calculates new reactive power based on active power.

The European low voltage MR CIGRE [17] was proposed and implemented in Matlab/Simulink to serve as the test platform for the proposed USCS. Additionally, RTDS was

employed for HIL tests, with centralized control built in an RTAC-SEL. In Matlab/Simulink, four cases were tested: total failure, total failure with communication delay, partial failure, and partial failure with communication delay. For the HIL tests, two cases were performed: total failure and partial failure.

Through the simulations, it was possible to compare the USFCS with the proposed USCS. A smooth transition between control modes when a communication delay is present was observed in the USCS. Additionally, the proposed USCS was tested in a HIL environment, with two cases performed: partial failure and total failure. In both cases, the results demonstrated a smooth transition between control modes, and the system maintained its stability.

The proposed USCS proved to be effective in regulating frequency and voltage in MGs, demonstrating superiority over the USFCS in some aspects, according to the results presented. However, this strategy can still be improved, allowing other centralized and decentralized secondary control strategies to be applied in conjunction with the proposed USCS. Additionally, the proposed strategy may be adapted for other areas of research.

6.2 Future Works

As suggestions for future work, the following items are proposed:

- Analyses of the operation of the USCS when a partial failure occurs and the DGs in centralized controls achieves its maximum capacity, thus the remains DG in decentralized controls dispatch its power to maintains the power balance;
- Application of different centralized and decentralized control techniques in the proposed USCS;
- Analyses of the effect of the clock-drift in the proposed USCS;
- Stability analysis of the MG operating in DSC and CSC modes through the Lyapunov direct and indirect methods;
- The proposed decentralized voltage control could be studied for stand-alone operation;
- A meta-heuristic algorithm to find control gains for the strategies employed in the USCS;
- Application of the proposed USCS in a real or laboratory MG system;
- Adaptation of the proposed USCS for distributed strategies, where the decentralized strategies are employed as backup for the distributed strategies;
- Adaptation of the proposed structure for tertiary control, maintain the MG autonomy even during control or communication failure.

Bibliography

[1] R. Lasseter, "MicroGrids," in *2002 IEEE Power Engineering Society Winter Meeting. Conference Proceedings (Cat. No.02CH37309)*, vol. 1. IEEE, 2002, pp. 305–308. [Online]. Available: http://ieeexplore.ieee.org/document/985003/ Cited 3 times on the pages 1, 8 e 9.

[2] CERTS, "The CERTS MicroGrid Concept," *Integration of Distributed Energy Resources – The CERTS MicroGrid Concept*, p. 32, 2002. [Online]. Available: http://certs.lbl.gov/pdf/50829.pdf Cited 3 times on the pages 1, 8 e 9.

[3] J. Lopes, C. Moreira, and A. Madureira, "Defining Control Strategies for MicroGrids Islanded Operation," *IEEE Transactions on Power Systems*, vol. 21, no. 2, pp. 916–924, 2006. [Online]. Available: http://ieeexplore.ieee.org/document/1626398/ Cited 2 times on the pages 1 e 9.

[4] J. M. Guerrero, J. C. Vasquez, J. Matas, L. G. de Vicuna, and M. Castilla, "Hierarchical Control of Droop-Controlled AC and DC Microgrids—A General Approach Toward Standardization," *IEEE Transactions on Industrial Electronics*, vol. 58, no. 1, pp. 158–172, jan 2011. [Online]. Available: http://ieeexplore.ieee.org/document/5546958/ Cited 6 times on the pages 2, 3, 9, 10, 11 e 40.

[5] A. Bidram and A. Davoudi, "Hierarchical structure of mmicrogrid control system," *IEEE Trans. on Smart Grid*, vol. 3, no. 4, pp. 1963–1976, 2012. Cited 4 times on the pages 2, 3, 9 e 11.

[6] D. E. Olivares, A. Mehrizi-Sani, A. H. Etemadi, C. A. Cañizares, R. Iravani, M. Kazerani, A. H. Hajimiragha, O. Gomis-Bellmunt, M. Saeedifard, R. Palma-Behnke, G. A. Jiménez-Estévez, and N. D. Hatziargyriou, "Trends in microgrid control," *IEEE Transactions on Smart Grid*, vol. 5, no. 4, pp. 1905–1919, 2014. Cited 2 times on the pages 2 e 13.

[7] F. Dorfler, J. W. Simpson-Porco, and F. Bullo, "Breaking the hierarchy: Distributed control and economic optimality in Microgrids," *IEEE Transactions on Control of Network Systems*, vol. 3, no. 3, pp. 241–253, 2016. Cited on page 2.

[8] Y. Xu, H. Sun, W. Gu, Y. Xu, and Z. Li, "Optimal Distributed Control for Secondary Frequency and Voltage Regulation in an Islanded Microgrid," *IEEE Transactions on Industrial Informatics*, vol. 3203, no. c, 2018. Cited 3 times on the pages 2, 11 e 15.

[9] G. Lou, W. Gu, W. Sheng, X. Song, and F. Gao, "Distributed Model Predictive Secondary Voltage Control of Islanded Microgrids With Feedback Linearization," *IEEE Access*, vol. 6, pp. 50 169–50 178, 2018. [Online]. Available: https://ieeexplore.ieee.org/document/8457078/ Cited on page 2.

[10] Y. Khayat, Q. Shafiee, R. Heydari, M. Naderi, T. Dragičević, J. W. Simpson-Porco, F. Dörfler, M. Fathi, F. Blaabjerg, J. M. Guerrero, and H. Bevrani, "On the secondary control

architectures of ac microgrids: An overview," *IEEE Transactions on Power Electronics*, vol. 35, no. 6, pp. 6482–6500, 2020. Cited 2 times on the pages 2 e 15.

[11] R. Zamora and A. K. Srivastava, "Controls for microgrids with storage: Review, challenges, and research needs," *Renewable and Sustainable Energy Reviews*, vol. 14, no. 7, pp. 2009–2018, sep 2010. [Online]. Available: http://dx.doi.org/10.1016/j.rser.2010.03.019https://linkinghub.elsevier.com/retrieve/pii/S1364032110000742 Cited on page 2.

[12] E. Planas, A. Gil-de Muro, J. Andreu, I. Kortabarria, and I. Martínez de Alegría, "General aspects, hierarchical controls and droop methods in microgrids: A review," *Renewable and Sustainable Energy Reviews*, vol. 17, pp. 147–159, jan 2013. [Online]. Available: https://linkinghub.elsevier.com/retrieve/pii/S1364032112005333 Cited 4 times on the pages 2, 3, 9 e 11.

[13] A. Dimeas and N. Hatziargyriou, "A multiagent system for microgrids," *IEEE Power Engineering Society General Meeting, 2004.*, pp. 55–58, 2005. Cited 2 times on the pages 2 e 13.

[14] G. Mokhtari, G. Nourbakhsh, and A. Ghosh, "Smart coordination of energy storage units (ESUs) for voltage and loading management in distribution networks," *IEEE Transactions on Power Systems*, vol. 28, no. 4, pp. 4812–4820, 2013. Cited on page 2.

[15] G. Lou, W. Gu, Y. Xu, M. Cheng, and W. Liu, "Distributed MPC-Based Secondary Voltage Control Scheme for Autonomous Droop-Controlled Microgrids," *IEEE Transactions on Sustainable Energy*, vol. 8, no. 2, pp. 792–804, 2017. Cited on page 2.

[16] Q. Hui and W. M. Haddad, "Distributed nonlinear control algorithms for network consensus," *Automatica*, vol. 44, no. 9, pp. 2375–2381, 2008. Cited on page 2.

[17] D. Ioris, P. T. de Godoy, K. D. R. Felisberto, P. Poloni, A. B. de Almeida, and D. Marujo, *Microgrid Operation and Control: From Grid-Connected to Islanded Mode*. Cham: Springer International Publishing, 2022, pp. 233–256. [Online]. Available: https://doi.org/10.1007/978-3-030-90812-6_9 Cited 5 times on the pages 3, 13, 14, 34 e 80.

[18] P. T. Godoy, A. B. Almeida, and D. Marujo, "Unified centralised/decentralised frequency control structure for microgrids," *IET Renewable Power Generation*, p. rpg2.12041, jan 2021. [Online]. Available: https://onlinelibrary.wiley.com/doi/10.1049/rpg2.12041 Cited 8 times on the pages 3, 4, 17, 18, 19, 22, 25 e 62.

[19] D. Ioris, P. T. de Godoy, K. D. R. Felisberto, P. Poloni, A. B. de Almeida, and D. Marujo, "A power electronic converter-based microgrid model for simulation studies," *Energy Systems*, may 2021. [Online]. Available: https://link.springer.com/10.1007/s12667-021-00440-0 Cited 8 times on the pages 4, 5, 12, 34, 35, 36, 92 e 93.

[20] B. Tavassoli, A. Fereidunian, and S. Mehdi, "Communication system effects on the secondary control performance in microgrids," *IET Renewable Power Generation*, vol. 14, no. 12, pp. 2047–2057, sep 2020. Cited on page 4.

[21] M. C. Chandorkar, D. M. Divan, and R. Adapa, "Control of parallel connected inverters in standalone ac supply systems," *IEEE Transactions on Industry Applications*, vol. 29, no. 1, pp. 136–143, 1993. [Online]. Available: http://ieeexplore.ieee.org/document/195899/ Cited on page 9.

[22] J. M. Guerrero, J. Matas, L. García De Vicuña, M. Castilla, and J. Miret, "Decentralized control for parallel operation of distributed generation inverters using resistive output impedance," *Industrial Electronics, IEEE Transactions on*, vol. 54, no. 2, pp. 994–1004, 2007. Cited on page 11.

[23] C. K. Sao and P. W. Lehn, "Control and power management of converter fed microgrids," *IEEE Transactions on Power Systems*, vol. 23, no. 3, pp. 1088–1098, 2008. Cited on page 11.

[24] K. De Brabandere, B. Bolsens, J. Van den Keybus, A. Woyte, J. Driesen, and R. Belmans, "A Voltage and Frequency Droop Control Method for Parallel Inverters," *IEEE Transactions on Power Electronics*, vol. 22, no. 4, pp. 1107–1115, jul 2007. [Online]. Available: http://ieeexplore.ieee.org/document/1355222/http://ieeexplore.ieee.org/document/4267747/ Cited on page 11.

[25] J. C. Vasquez, J. M. Guerrero, A. Luna, P. Rodríguez, and R. Teodorescu, "Adaptive droop control applied to voltage-source inverters operating in grid-connected and islanded modes," *IEEE Transactions on Industrial Electronics*, vol. 56, no. 10, pp. 4088–4096, 2009. Cited on page 11.

[26] J. Guerrero, L. GarciadeVicuna, J. Matas, M. Castilla, and J. Miret, "Output Impedance Design of Parallel-Connected UPS Inverters With Wireless Load-Sharing Control," *IEEE Transactions on Industrial Electronics*, vol. 52, no. 4, pp. 1126–1135, aug 2005. [Online]. Available: http://ieeexplore.ieee.org/document/1490703/ Cited 2 times on the pages 11 e 35.

[27] J. M. Guerrero, M. Chandorkar, T.-L. Lee, and P. C. Loh, "Advanced Control Architectures for Intelligent Microgrids—Part I: Decentralized and Hierarchical Control," *IEEE Transactions on Industrial Electronics*, vol. 60, no. 4, pp. 1254–1262, apr 2013. [Online]. Available: http://ieeexplore.ieee.org/document/6184305/ Cited on page 11.

[28] F. Katiraei, M. Iravani, and P. Lehn, "Micro-Grid Autonomous Operation During and Subsequent to Islanding Process," *IEEE Transactions on Power Delivery*, vol. 20, no. 1, pp. 248–257, jan 2005. [Online]. Available: http://ieeexplore.ieee.org/document/1375102/ Cited on page 13.

[29] N. Ainsworth and S. Grijalva, "Design and quasi-equilibrium analysis of a distributed frequency-restoration controller for inverter-based microgrids," *45th North American Power Symposium, NAPS 2013*, pp. 1–6, 2013. Cited on page 14.

[30] H. Xin, L. Zhang, Z. Wang, D. Gan, and K. P. Wong, "Control of island AC microgrids using a fully distributed approach," *IEEE Transactions on Smart Grid*, vol. 6, no. 2, pp. 943–945, 2015. Cited 4 times on the pages 14, 37, 40 e 73.

[31] Y. Han, K. Zhang, H. Li, E. A. A. Coelho, and J. M. Guerrero, "MAS-Based Distributed Coordinated Control and Optimization in Microgrid and Microgrid Clusters: A Comprehensive Overview," *IEEE Transactions on Power Electronics*, vol. 33, no. 8, pp. 6488–6508, 2018. Cited on page 14.

[32] E. Weitenberg, Y. Jiang, C. Zhao, E. Mallada, C. De Persis, and F. Dorfler, "Robust Decentralized Secondary Frequency Control in Power Systems: Merits and Trade-Offs," *IEEE Transactions on Automatic Control*, vol. PP, no. c, p. 1, 2018. Cited on page 14.

[33] Y. Wang, Z. Chen, X. Wang, Y. Tian, Y. Tan, and C. Yang, "An estimator-based distributed voltage-predictive control strategy for AC islanded microgrids," *IEEE Transactions on Power Electronics*, vol. 30, no. 7, pp. 3934–3951, 2015. Cited 2 times on the pages 14 e 31.

[34] W. Gu, G. Lou, W. Tan, and X. Yuan, "A Nonlinear State Estimator-Based Decentralized Secondary Voltage Control Scheme for Autonomous Microgrids," *IEEE Transactions on Power Systems*, vol. 32, no. 6, pp. 4794–4804, 2017. Cited 2 times on the pages 14 e 31.

[35] G. Lou, W. Gu, L. Wang, B. Xu, M. Wu, and W. Sheng, "Decentralised secondary voltage and frequency control scheme for islanded microgrid based on adaptive state estimator," *IET Generation, Transmission & Distribution*, vol. 11, no. 15, pp. 3683–3693, 2017. Cited 2 times on the pages 14 e 31.

[36] M. Castilla, A. Camacho, J. Miret, M. Velasco, and P. Martí, "Local secondary control for inverter-based islanded microgrids with accurate active power sharing under high-load conditions," *IEEE Transactions on Industrial Electronics*, vol. 66, no. 4, pp. 2529–2539, 2019. Cited on page 14.

[37] J. Schiffer, C. A. Hans, T. Kral, R. Ortega, and J. Raisch, "Modeling, analysis, and experimental validation of clock drift effects in low-inertia power systems," *IEEE Transactions on Industrial Electronics*, vol. 64, no. 7, pp. 5942–5951, 2017. Cited on page 14.

[38] M. Velasco, P. Martí, A. Camacho, J. Miret, and M. Castilla, "Synchronization of local integral controllers for frequency restoration in islanded microgrids," in *IECON 2016 - 42nd Annual Conference of the IEEE Industrial Electronics Society*, 2016, pp. 3906–3911. Cited on page 15.

[39] J. Torres-Martínez, M. Castilla, J. Miret, M. Moradi-Ghahderijani, and J. M. Rey, "Experimental study of clock drift impact over droop-free distributed control for industrial microgrids," in *IECON 2017 - 43rd Annual Conference of the IEEE Industrial Electronics Society*, 2017, pp. 2479–2484. Cited on page 15.

[40] P. Marti, J. Torres, C. Rosero, M. Velasco, J. Miret, and M. Castilla, "Analysis of the effect of clock drifts on frequency regulation and power sharing in inverter-based islanded microgrids," *IEEE transactions on power electronics*, vol. 33, no. 12, pp. 10 363–10 379, 02 2018. [Online]. Available: https://ieeexplore.ieee.org/document/8290685/ Cited on page 15.

[41] C. Alfaro, M. Castilla, A. Camacho, P. Marti, and M. Velasco, "A distributed control for accurate active-power sharing in islanded microgrids subject to clock drifts," *IET power electronics*, vol. 14, no. 3, pp. 1–13, 01 2021. [Online]. Available: https://ietresearch.onlinelibrary.wiley.com/doi/10.1049/pel2.12010 Cited on page 15.

[42] C. Rosero, P. Marti, M. Velasco, M. Castilla, J. Miret, and A. Camacho, "Consensus for active power sharing and frequency restoration in islanded microgrids subject to drifting clocks," in *IEEE International Symposium on Industrial Electronics*. Institute

of Electrical and Electronics Engineers (IEEE), 06 2017, p. 70. [Online]. Available: https://ieeexplore.ieee.org/document/8001225 Cited on page 15.

[43] M. Castilla, A. Camacho, P. Marti, M. Velasco, and G. Mohammad, "Impact of clock drifts on communication-free secondary control schemes for inverter-based islanded microgrids," *IEEE transactions on industrial electronics*, vol. PP, no. 9, pp. 1–11, 11 2017. [Online]. Available: http://ieeexplore.ieee.org/document/8106668/ Cited on page 15.

[44] Q. Shafiee, S. Member, J. M. Guerrero, S. Member, and J. C. Vasquez, "Distributed Secondary Control for Islanded MicroGrids - A Novel Approach - Research - Aalborg University," *IEEE Transactions on Power Electronics*, vol. 29, no. 2, pp. 1018–1031, 2014. Cited on page 15.

[45] J. W. Simpson-Porco, Q. Shafiee, F. Dorfler, J. C. Vasquez, J. M. Guerrero, and F. Bullo, "Secondary Frequency and Voltage Control of Islanded Microgrids via Distributed Averaging," *IEEE Transactions on Industrial Electronics*, vol. 62, no. 11, pp. 7025–7038, nov 2015. [Online]. Available: http://ieeexplore.ieee.org/document/7112129/ Cited on page 15.

[46] F. Guo, C. Wen, J. Mao, and Y. D. Song, "Distributed Secondary Voltage and Frequency Restoration Control of Droop-Controlled Inverter-Based Microgrids," *IEEE Transactions on Industrial Electronics*, vol. 62, no. 7, pp. 4355–4364, 2015. Cited on page 15.

[47] P. Marti, M. Velasco, E. Martin, M. Castilla, J. Miret, and A. Camacho, "Communication-aware consensus for frequency restoration in islanded microgrids," in *IEEE International Symposium on Industrial Electronics*. Institute of Electrical and Electronics Engineers (IEEE), 06 2016, p. 690. [Online]. Available: http://ieeexplore.ieee.org/document/7744973/ Cited on page 15.

[48] C. Rosero, M. Velasco, P. Marti, A. Camacho, J. Miret, and M. Castilla, "Analysis of consensus-based islanded microgrids subject to unexpected electrical and communication partitions," *IEEE transactions on smart grid*, vol. 10, no. 5, pp. 5125–5135, 01 2019. [Online]. Available: https://ieeexplore.ieee.org/document/8501583 Cited on page 15.

[49] C. X. Rosero, M. Velasco, P. Martí, A. Camacho, J. Miret, and M. Castilla, "Active power sharing and frequency regulation in droop-free control for islanded microgrids under electrical and communication failures," *IEEE Transactions on Industrial Electronics*, vol. 67, no. 8, pp. 6461–6472, 2020. Cited on page 15.

[50] J. Rey, P. Vergara, M. Castilla, A. Camacho, M. Velasco, and P. Marti, "Droop-free hierarchical control strategy for inverter-based ac microgrids," *IET power electronics*, vol. 13, no. 7, pp. 1403–1415, 05 2020. [Online]. Available: https://ieeexplore.ieee.org/document/9110282 Cited on page 15.

[51] J. Duarte, M. Velasco, P. Marti, A. Camacho, J. Miret, and C. Alfaro, "Decoupled simultaneous complex power sharing and voltage regulation in islanded ac microgrids," *IEEE transactions on industrial electronics*, vol. 70, no. 4, pp. 3888–3898, 04 2023. [Online]. Available: https://ieeexplore.ieee.org/document/9789995 Cited on page 15.

[52] C. Alfaro, R. Guzman, J. Garcia de Vicuña, H. Komurcugil, and H. Martín, "Distributed direct power sliding-mode control for islanded ac microgrids," *IEEE transactions on industrial electronics*, vol. 69, no. 10, pp. 9700–9710, 10 2022. [Online]. Available: https://ieeexplore.ieee.org/abstract/document/9658265 Cited on page 15.

[53] G. de Doile, P. Balestrassi, M. Castilla, A. Zambroni, and J. Miret, "An experimental approach for secondary consensus control tuning for inverter-based islanded microgrids," *Energies*, vol. 16, no. article 517, 01 2023. [Online]. Available: https://www.mdpi.com/1996-1073/16/1/517 Cited on page 16.

[54] T. Qian, Y. Liu, W. Zhang, W. Tang, and M. Shahidehpour, "Event-Triggered Updating Method in Centralized and Distributed Secondary Controls for Islanded Microgrid Restoration," *IEEE Transactions on Smart Grid*, vol. 11, no. 2, pp. 1387–1395, 2020. Cited on page 16.

[55] Z. Li, Z. Cheng, J. Liang, J. Si, L. Dong, and S. Li, "Distributed Event-Triggered Secondary Control for Economic Dispatch and Frequency Restoration Control of Droop-Controlled AC Microgrids," *IEEE Transactions on Sustainable Energy*, vol. 11, no. 3, pp. 1938–1950, jul 2020. Cited on page 16.

[56] J. Lai, X. Lu, X. Yu, and A. Monti, "Stochastic Distributed Secondary Control for AC Microgrids via Event-Triggered Communication," *IEEE Transactions on Smart Grid*, vol. 11, no. 4, pp. 2746–2759, 2020. Cited on page 16.

[57] J. M. Rey, P. Marti, M. Velasco, J. Miret, and M. Castilla, "Secondary Switched Control with no Communications for Islanded Microgrids," *IEEE Transactions on Industrial Electronics*, vol. 64, no. 11, pp. 8534–8545, 2017. Cited on page 16.

[58] J. Rey, P. Vergara, M. Castilla, A. Camacho, and J. Miret, "Local hierarchical control for industrial microgrids with improved frequency regulation," in *IEEE International Conference on Industrial Technology*, 02 2018, p. 1019. [Online]. Available: https://ieeexplore.ieee.org/document/8352318 Cited on page 16.

[59] J. Rey, C. Rosero, M. Velasco, P. Marti, J. Miret, and M. Castilla, "Local frequency restoration for droop-controlled parallel inverters in islanded microgrids," *IEEE transactions on energy conversion*, vol. 34, no. 3, pp. 1232–1241, 01 2019. [Online]. Available: https://ieeexplore.ieee.org/document/8572796 Cited on page 16.

[60] S. C, C. Yammani, and S. Maheswarapu, "Load Frequency Control of Multi-microgrid System considering Renewable Energy Sources Using Grey Wolf Optimization," *Smart Science*, vol. 7, no. 3, pp. 198–217, 2019. Cited on page 16.

[61] M. Gheisarnejad and M. H. Khooban, "Secondary load frequency control for multi-microgrids: HiL real-time simulation," *Soft Computing*, vol. 23, no. 14, pp. 5785–5798, 2019. [Online]. Available: https://doi.org/10.1007/s00500-018-3243-5 Cited on page 16.

[62] H. Bevrani, F. Habibi, P. Babahajyani, M. Watanabe, and Y. Mitani, "Intelligent frequency control in an AC microgrid: Online PSO-based fuzzy tuning approach," *IEEE Transactions on Smart Grid*, vol. 3, no. 4, pp. 1935–1944, 2012. Cited on page 16.

[63] S. Ahmadi, S. Shokoohi, and H. Bevrani, "Electrical Power and Energy Systems A fuzzy logic-based droop control for simultaneous voltage and frequency regulation in an AC microgrid," *International Journal of Electrical Power and Energy Systems*, vol. 64, pp. 148–155, 2015. [Online]. Available: http://dx.doi.org/10.1016/j.ijepes.2014.07.024 Cited on page 16.

[64] S. Shokoohi, S. Golshannavaz, R. Khezri, and H. Bevrani, "Intelligent secondary control in smart microgrids: an on-line approach for islanded operations," *Optimization and Engineering*, vol. 19, no. 4, pp. 917–936, 2018. [Online]. Available: https://doi.org/10.1007/s11081-018-9382-9 Cited on page 16.

[65] A. Abazari, M. G. Dozein, and H. Monsef, "A New Load Frequency Control Strategy for an AC Micro-grid: PSO-based Fuzzy Logic Controlling Approach," *Proceedings - 2018 Smart Grid Conference, SGC 2018*, pp. 1–7, 2018. Cited on page 16.

[66] A. Abazari, M. G. Dozein, H. Monsef, and B. Wu, "Wind turbine participation in micro-grid frequency control through self-tuning, adaptive fuzzy droop in de-loaded area," *IET Smart Grid*, vol. 2, no. 2, pp. 301–308, 2019. Cited on page 16.

[67] S. Liu, X. Wang, S. Member, P. X. Liu, and S. Member, "Impact of Communication Delays on Secondary Frequency Control in an Islanded Microgrid," *IEEE Transactions on Industrial Electronics*, vol. 62, no. 4, pp. 2021–2031, 2015. Cited 2 times on the pages 16 e 101.

[68] G. Lou, W. Gu, Y. Xu, W. Jin, and X. Du, "Stability Robustness for Secondary Voltage Control in Autonomous Microgrids with Consideration of Communication Delays," *IEEE Transactions on Power Systems*, vol. 33, no. 4, pp. 4164–4178, 2018. Cited on page 17.

[69] C. Ahumada, R. Cárdenas, D. Sáez, and J. M. Guerrero, "Secondary Control Strategies for Frequency Restoration in Islanded Microgrids With Consideration of Communication Delays," *IEEE Transactions on Smart Grid*, vol. 7, no. 3, pp. 1430–1441, 2016. Cited 2 times on the pages 17 e 101.

[70] K. D. R. Felisberto, P. T. de Godoy, D. Marujo, A. B. de Almeida, and R. de Barros Iscuissati, "Trends in Microgrid Droop Control and the Power Sharing Problem," *Journal of Control, Automation and Electrical Systems*, jan 2022. [Online]. Available: https://link.springer.com/10.1007/s40313-021-00856-0 Cited 2 times on the pages 32 e 34.

[71] F. de Andrade, M. Castilla, and B. D. Bonatto, *Basic Tutorial on Simulation of Microgrids Control Using MATLAB & Simulink Software*, ser. SpringerBriefs in Energy. Cham: Springer International Publishing, 2020. [Online]. Available: http://link.springer.com/10.1007/978-3-030-43013-9 Cited on page 34.

[72] P. T. D. Godoy, P. Poloni, A. B. D. Almeida, and D. Marujo, "Centralized Secondary Control Assessment of Microgrids with Battery and Diesel Generator," in *2019 IEEE PES Innovative Smart Grid Technologies Latin America (ISGT LATAM)*. Godoy2019: IEEE, 2019. Cited 2 times on the pages 34 e 100.

[73] P. T. D. Godoy, A. B. D. Almeida, A. C. Z. D. Souza, B. Venkatesh, F. C. D. Santos, and J. V. D. Souza, "Analysis and implementation of the unified centralized/decentralized frequency control structure in hardware in the loop environment with rtds," *2022 IEEE*

Power & Energy Society General Meeting (PESGM), pp. 1–5, 7 2022. Cited 3 times on the pages 34, 64 e 65.

[74] P. T. D. Godoy, P. Poloni, A. B. D. Almeida, and D. Marujo, "Modelo Matemático de Conversores para Aplicação em Estudos de Microrredes," in *XVIII ENCONTRO REGIONAL IBERO-AMERICANO DO CIGRE*. CIGRE, 2019. Cited 3 times on the pages 34, 92 e 94.

[75] A. Yazdani and R. Iravani, *Voltage-Sourced Converters in Power Systems*. Hoboken, NJ, USA: John Wiley & Sons, Inc., jan 2010. [Online]. Available: http://doi.wiley.com/10.1002/9780470551578 Cited 6 times on the pages 34, 90, 91, 92, 94 e 95.

[76] G. Ashokkumar and A. Gould, "Detecting a Loss of Communication Between an RTAC and a Relay," Schweitzer Engineering Laboratories - SEL, Tech. Rep., 2020. Cited on page 65.

[77] A. Gkountaras, S. Dieckerhoff, and T. Sezi, "Evaluation of current limiting methods for grid forming inverters in medium voltage microgrids," *2015 IEEE Energy Conversion Congress and Exposition, ECCE 2015*, pp. 1223–1230, 2015. Cited on page 95.

[78] P. Kundur, N. J. Balu, and M. G. Lauby, *Power system stability and control*. McGraw-hill New York, 1994, vol. 7. Cited on page 98.

[79] R. Majumder, "Some Aspects of Stability in Microgrids," *IEEE Transactions on Power Systems*, vol. 28, no. 3, pp. 3243–3252, aug 2013. [Online]. Available: http://ieeexplore.ieee.org/document/6412768/ Cited on page 98.

[80] Z. Shuai, Y. Sun, Z. J. Shen, W. Tian, C. Tu, Y. Li, and X. Yin, "Microgrid stability: Classification and a review," *Renewable and Sustainable Energy Reviews*, vol. 58, pp. 167–179, may 2016. [Online]. Available: https://linkinghub.elsevier.com/retrieve/pii/S1364032115015841 Cited 2 times on the pages 98 e 99.

[81] M. Farrokhabadi, C. A. Canizares, J. W. Simpson-Porco, E. Nasr, L. Fan, P. A. Mendoza-Araya, R. Tonkoski, U. Tamrakar, N. Hatziargyriou, D. Lagos, R. W. Wies, M. Paolone, M. Liserre, L. Meegahapola, M. Kabalan, A. H. Hajimiragha, D. Peralta, M. A. Elizondo, K. P. Schneider, F. K. Tuffner, and J. Reilly, "Microgrid Stability Definitions, Analysis, and Examples," *IEEE Transactions on Power Systems*, vol. 35, no. 1, pp. 13–29, jan 2020. [Online]. Available: https://ieeexplore.ieee.org/document/8750828/ Cited 3 times on the pages 98, 99 e 100.

Appendix A

Converters: Models and Controls

A.1 Initial Considerations

To carry out the simulations of the proposed control strategy in Matlab/Simulink and in the RTDS environment, it is necessary to study the modeling and control of the converters applied in MGs. The main objective of this Appendix is to present the model of average values adopted for the converters, the control loops for the different operating modes, and, finally, how the reactive power limit works in a converter.

A.2 Converters Model

A converter is responsible for facilitating the exchange of energy between two subsystems. These devices are composed of switching cells formed by semiconductor elements, which are controlled using Pulse-Width Modulation (PWM) techniques [75].

Fig. A.1 shows the basic diagram of a single-phase DC/AC half-bridge converter, composed of two semiconductor elements represented by switches S1 and S4 and a filter. Switches S1 and S4 are controlled alternately, when switch S1 is conducting, switch S4 is blocked. The filter, formed by passive elements (inductance and capacitance), aims to reduce the harmonic content generated by the switching processes.

A converter can be represented in two models: the switched model, which represents the switching actions coming from the semiconductor elements; or the Average values model, which represents the converter as being an ideal controlled source, that is, the switching dynamics are not considered.

Considering the single-phase half-bridge converter, shown in Fig. A.1, the output voltage V_t can be mathematically represented by:

$$V_t(t) = \frac{V_{DC}}{2}(S_1(t) - S_4(t)) \tag{A.1}$$

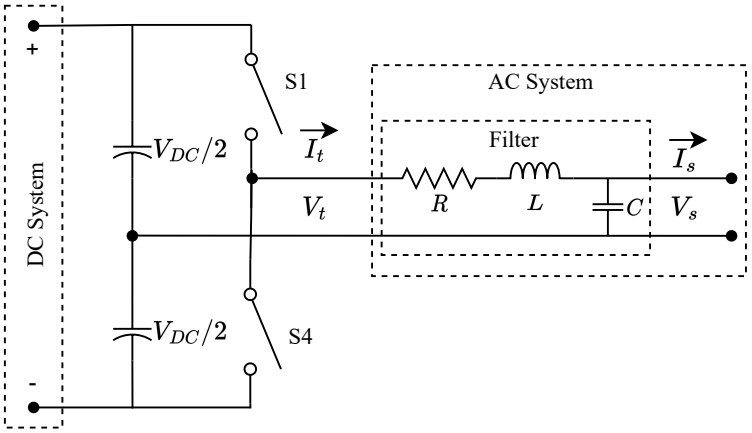

Figure A.1: Single phase converter.

$$S_1(t) + S_4(t) \equiv 1 \tag{A.2}$$

where V_{DC} represents the DC link voltage. $S_1(t)$ and $S_4(t)$ represent the switching function of switch S1 and S4, respectively.

However, for some studies of the control and operation of systems or the converter, it is not interesting to consider the switching dynamics. The use of the switched model considerably increases the simulation time. For an MG with several converters, computational cost and simulation time are significantly increased.

In contrast to the switched model, the average values model describes the converter dynamics through the modulated signal, that is, the high-frequency dynamics resulting from the switching of semiconductor devices are disregarded [75].

Considering the single-phase converter illustrated in Fig. A.1, the alternating current from the switching process is:

$$L\frac{d}{dt}i_t(t) + R \cdot i_t(t) = V_t(t) - V_s(t) \tag{A.3}$$

where, L and R are respectively the inductance and resistance of the filter, $i_t(t)$ the output current of the switching process, $V_t(t)$ the voltage before the filter, $V_s(t)$ the voltage after the filter.

The voltage $V_t(t)$ is a periodic function with period T_s, which depends on the semiconductor control function. Describing $V_t(t)$ through the Fourier series, and substituting in the equation (A.3):

$$L\frac{d}{dt}i_t(t) + R \cdot i_t(t) = \frac{1}{T_s}\int_0^{T_s} V_t(\tau)d\tau + \sum_{h=1}^{h=\infty}[a_h cos(h\omega_s t) + b_h sen(h\omega_s t)] - V_s \tag{A.4}$$

where h is the harmonic order. ω_s is the angular frequency. T_s is the period. a_h and b_h are the

Fourier constants.

If the frequency ω_s is much higher than the cutoff frequency of the filter, then the harmonic plots in the equation (A.4) can be disregarded [75]. Then the dynamics of the converter can be described by:

$$L\frac{d}{dt}i_t(t) + R \cdot i_t(t) = \int_0^{T_s} V_t(\tau)d\tau - V_s(t) \tag{A.5}$$

Thus, in order to extend this method to other variables, is defined the average operator:

$$\overline{W}(t) = \int_0^{T_s} W(\tau)d\tau \tag{A.6}$$

where W is a oscillatory variable and $\overline{W}$ represents the moving average of the variable W.

Applying the average operator, for the switching functions S1 and S4 we have:

$$\overline{S1}(t) = \overline{d} \tag{A.7}$$

$$\overline{S4}(t) = 1 - \overline{d} \tag{A.8}$$

where $\overline{d}$ represents the ratio between the time switch S1 is conducting and the switching time.

The relationship between the modulating signal M and the time relationship $\overline{d}$ can be described as $\overline{d} = (M + 1)/2$. Thus, the output voltage of the converter can be represented through the modulating signal:

$$\overline{V_t}(t) = M \cdot \frac{V_{DC}}{2} \tag{A.9}$$

A.3 Converters Control

The converters can present two types of controls: Grid-Forming, called V/f mode; or Grid-Following, called PQ mode. When an MG is in islanded mode, the converters present their control loops depending on whether they are intermittent or dispatchable generation sources. Intermittent sources (photovoltaic system and wind generator) operate in PQ mode, that is, their control loops follow an active and reactive power reference. The dispatchable sources (battery banks) operate in V/f mode, in which the loops follow a voltage and frequency reference [19, 74].

The control structure for the converters was shown in Fig. 4.2, which is shown again in Fig. A.2. This structure is composed of three main control loops:

- The current control loop: present in both control modes (PQ or V/f), it is responsible for controlling the converter current;
- The power control loop: employed only in PQ mode. Is responsible for generating the current references for the current control, where the objective is to follow a determined reactive and active power;
- Voltage control loop: applied only in V/f mode. This control generates the current references for the current control too, however, the objective is to follow a determined voltage and frequency value;
- Droop control: employed only in V/f mode. This control is applied when various converters in V/f mode are employed in the MG. This control generates the voltage to the voltage control and the frequency reference for the dq0 transformer.

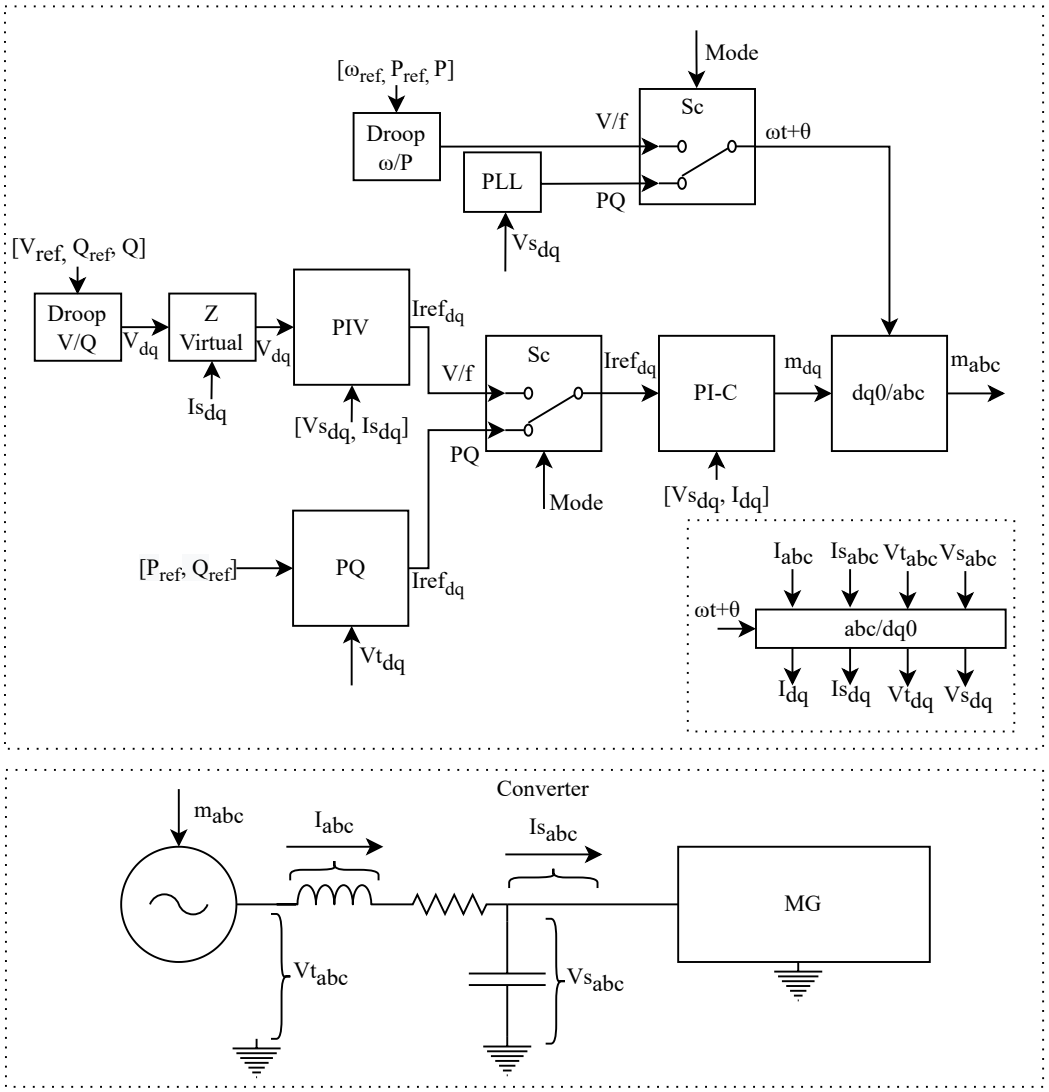

Figure A.2: Converter control mesh, [19].

The converters' controls are usually carried out in the dq0 axes, since the dq0 transform (Clarke and Park transform) transforms the sinusoidal voltage and current variables into vari-

ables in the direct and quadrature axis, facilitating the application of the control in three-phase converters [75]. The transform dq0 is presented in the equation A.10.

$$Y_{dq0}(t,\omega,\theta) = T \cdot Y_{abc} = \sqrt{\frac{2}{3}} \begin{bmatrix} \cos\omega \cdot t + \theta & \cos\omega \cdot t + \theta - \frac{2\pi}{3} & \cos\omega \cdot t + \theta + \frac{2\pi}{3} \\ \sin\omega \cdot t + \theta & \sin\omega \cdot t + \theta - \frac{2\pi}{3} & \sin\omega \cdot t + \theta + \frac{2\pi}{3} \\ \frac{1}{\sqrt{2}} & \frac{1}{\sqrt{2}} & \frac{1}{\sqrt{2}} \end{bmatrix} \cdot Y_{abc} \tag{A.10}$$

where Y_{abc} is a three-phase sinusoidal quantity, $Y_{dq0}(t,\omega,\theta)$ is a three-phase quantity transformed into dq0, T is the transformation matrix and θ is the transform angular reference.

The voltage (Vt_{abc} and Vs_{abc}) and current (I_{abc} and Is_{abc}) variables in the RLC filter are measured and converted for dq0 (see Fig. A.2). As expressed in (A.10), the dq0 transform needs an angle and frequency references ($\omega \cdot t + \theta$). For the PQ mode, the converter employs a PLL to follow the angular reference of the network, using the voltage Vs_{abc} as reference. However, in V/f mode, the converter uses the angular reference generated by the droop control [74].

As illustrated in Fig. A.2, the current control loop is present in both operating modes: PQ and V/f. This mesh is responsible for generating the modulating signals mo_d and mo_q. These signals, in dq coordinates, are converted to sinusoidal variables through the inverse transform dq0 ($Y_{abc} = T^{-1} \cdot Y_{dq0}$). The current control loop is illustrated in Fig. A.3, where Lf is the inductance of the RLC filter. PIC is a PI controller with proportional (Kc_p) and integrative (Kc_i) gains [75].

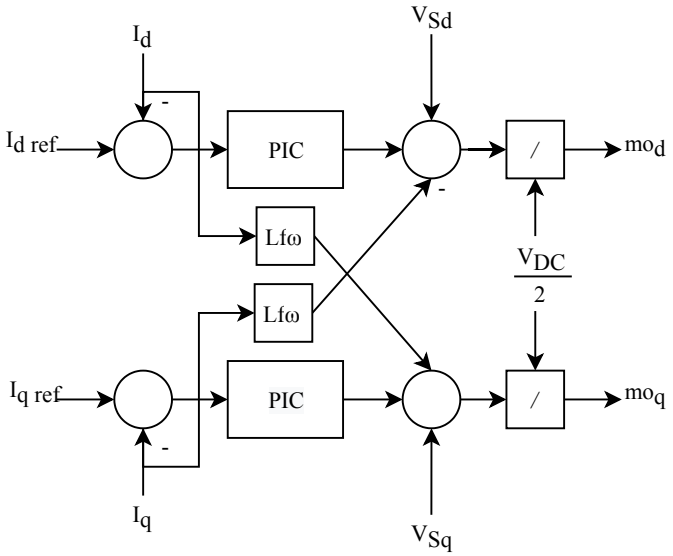

Figure A.3: Converters current control, [75].

The power control loop, when the converter operates in PQ mode, is responsible for generating the current references ($Iref_{dq0}$) for the current control loop (see Fig. A.2). The power control loop operates in an open loop, however, it uses the converter output voltage values

(Vt_{dq0}) to calculate the instantaneous reference power. This mesh can be expressed by:

$$Iref_d = \frac{Vt_d \cdot Pref + Vt_q \cdot Qref}{Vt_d^2 + Vt_q^2} \tag{A.11}$$

$$Iref_q = \frac{Vt_q \cdot Pref - Vt_d \cdot Qref}{Vt_d^2 - Vt_q^2} \tag{A.12}$$

where $Pref$ and $Qref$ are the active and reactive reference powers for the control loop.

The voltage control loop is responsible for generating the current references ($Iref_{dq}$) for the current control loop, however, only when the converter operates in V/f mode (see Fig. A.2). The voltage control is shown in Fig. A.4, where Cf is the capacitance of the RLC filter and PIV is a PI controller with proportional gain Kv_p and integrative Kv_i [75]. The voltages reference ($VS_{dq_{ref}}$) are generated by the droop control loop with virtual impedance.

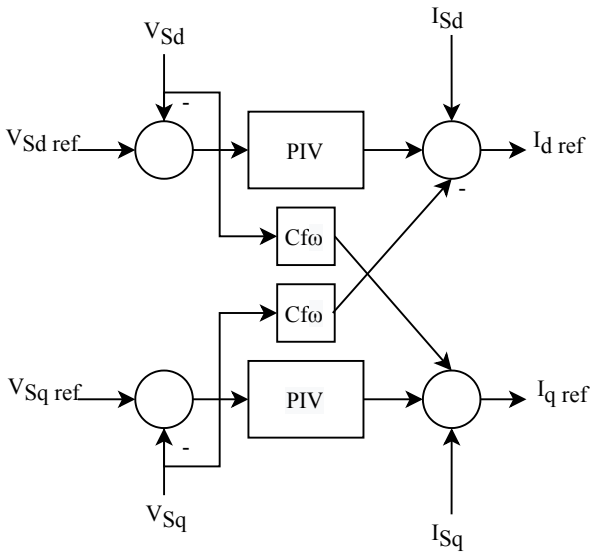

Figure A.4: Converters voltage control, [75].

A.4 Converter Reactive Power Limits

The reactive power limit for a Converter is similar to the reactive power limit in a synchronous machine [77], thus a capability curve can be obtained. Consider a converter connected to a bus, as illustrated in Fig A.5. To facilitate the calculations, the resistance effects of the filter are ignored, and the capacitor is not considered, since the voltage at the bus is considered constant.

The reactive power limit in a converter can be described as:

$$S^2 = P^2 + Q^2 \tag{A.13}$$

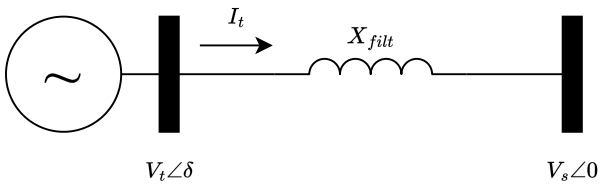

Figure A.5: Converter connected in a bus, with constant voltage.

where S is the power delivered by the converter to the infinite bus, P is the active power delivered, Q is the reactive power delivered.

However, in electrical equipment, the power limits are related to the equipment current, so it is possible to rewrite (A.13) through the voltage and current delivered to the infinite bus:

$$(I_t V_s)^2 = P^2 + Q^2 \tag{A.14}$$

where, I_t is the converter current, V_s is the voltage at the infinite bus.

The active and reactive power can be rewritten as:

$$P = V_s I_t \cos(\theta_p) = \frac{V_s V_c}{X_{filt}} \sin(\delta) \tag{A.15}$$

$$Q = V_g I_g \sin(\theta_p) = \frac{V_s V_t}{X_{filt}} \cos(\delta) - \frac{{V_s}^2}{X_{filt}} \tag{A.16}$$

where θ_p is the power factor angle, V_t is the internal voltage of the converter.

Thus, rearranging the equations (A.14), (A.15) and (A.16) we have an equation similar to the capability curve equations for a synchronous machine:

$$\frac{V_s {V_t}^2}{X_{filt}} = P + (Q + \frac{{V_s}^2}{X_{filt}})^2 \tag{A.17}$$

However, unlike synchronous machines, the internal voltage of the converter is defined by the value of the DC voltage and not by a field current. The maximum internal voltage for a converter can be defined by:

$$\sqrt{2} V_{t_{max}} = \frac{V_{DC}}{2} \tag{A.18}$$

where, V_{DC} is the DC voltage.

Thus, two reactive power limits are present, one limited by the maximum current of the converter Q_{max_C} and another limit defined by the maximum DC voltage of the converter Q_{max_V}. These limits can be calculated using the following equations:

$$Q_{max_C} = \sqrt{(I_{t_{max}} V_s)^2 - P^2} \tag{A.19}$$

$$Q_{max_V} = \sqrt{\frac{V_{t_{max}} {V_s}^2}{X_{filt}} - P^2} - \frac{{V_g}^2}{X_{filt}} \tag{A.20}$$

The general reactive power limit of a converter is given by the minimum between the two calculated values.

Appendix B

Control Adjustment and System Stability

B.1 Initial Considerations

Power system stability can be defined as the property of the system to remain in an equilibrium state during normal operations and reach an acceptable equilibrium state after being subjected to a disturbance [78].

Stability is evaluated according to the behavior of the system under a disturbance. The disturbances can be classified as [78]:

- Small: load increment disturbances that occur continuously in the system. The system has the ability to self-adjust to these disturbances;
- Large: disturbances from loss of generators, short circuits, and other contingencies. System response is involved with the actions of equipment such as protective devices.

Classifying stability into various categories helps to understand and study stability problems in a system. In the conventional power system, we can classify the stability in [78]:

- Rotor angular stability: It is the ability of the synchronous machines in the system to stay in sync. The fundamental factor of this problem is how the output power of the machines varies with the oscillation of the rotor;
- Voltage stability: It is the ability of the system to maintain an acceptable voltage level on all buses in the system during normal conditions and after being subjected to a disturbance. Voltage instability can occur when the system is unable to meet demand;
- Medium and long-term stability: They are related to problems of the dynamic response of the system under different conditions, which invoke slow processes, controls, and protection, which are not normally modeled in a transient regime study.

For MG applications, the authors present different concepts [79, 80, 81]. In [79] the stability problems in MG are considered similar to stability problems in power systems, where they are divided into:

- Small signals: problems related to controls with feedback, continuous load change, power limit in MR, and small disturbances;
- Transient: problems that cause major disturbances such as islanding, faults, loss of DG, and large load excursions;
- Voltage: problems related to the reactive limit, load dynamics, and transformer tap changes.

However, for [80], the stability studies in MG differ from studies in power systems due to the nature of the inverter-based generation sources, and due to the other operating characteristics, like the operation modes, low inertia, and the MG time responses. For the author, the dynamic processes of MG are more complex than those of a conventional power system. The stability of an MG is classified into four categories: small disturbances for islanded mode; transient stability (large disturbances) for islanded mode; small disturbances for connected mode; and, transient stability for connected mode;

In [81], the MG stability is classified differently from the conventional power system, due to its operation characteristics and size. Thus, for the authors in [81] the MG stability can be classified in two:

- Control system stability: is the phenomena related to equipment control. The instability arises due to inadequate control schemes, or poor tuning of one or more pieces of equipment controllers;
- Power supply and balance stability: is the phenomena related to the power-sharing and load balance. This stability is related to the ability of the system to maintain power balance, and effectively share the demand power among DGs, satisfying operational requirements.

Additionally, in [81], both stability classes can present small and large disturbances, wherein both disturbances can be classified as short or long-term phenomena. The Fig. B.1 presents the concept of MG stability.

In order to assess the MG stability, some analyses are possible:

- System linearization: the system is linearized and using the indirect method of Lyapunov (can be used eigenvalue analysis too) the system stability is verified;
- Lyapunov direct method: using the nonlinear system state space the Lyapunov direct method can be employed to determine the system stability;
- Time-Domain Simulations: using time-domain simulations, based on accurate models of the system components and loads is possible to verify the MG stability for different operations conditions.

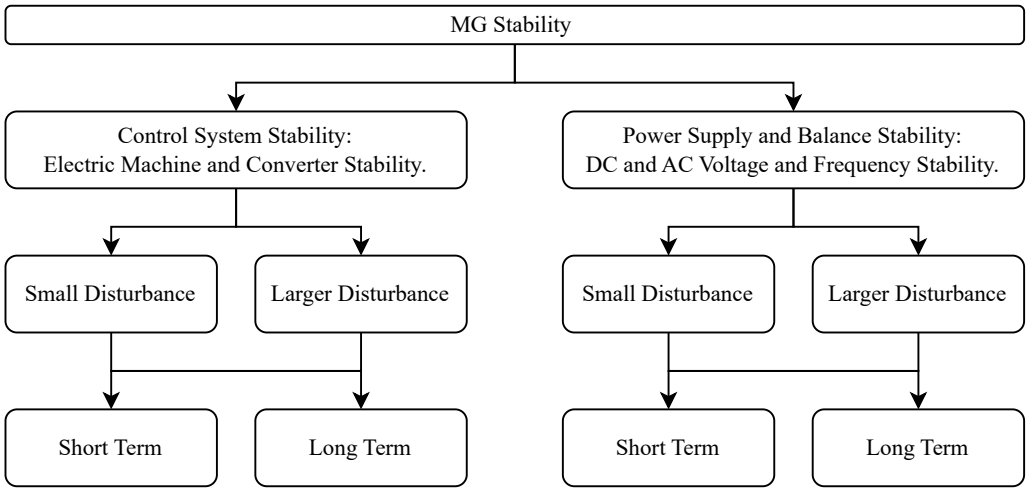

Figure B.1: Classification of stability in MGs, [81].

The analysis methods can be employed to assess the MG stability. However, the System linearization method can only verify small perturbations and small-perturbation stability might not give an accurate representation of stability in MGs.

In the Lyapunov direct method, the nonlinear differential equations associated with the system do not need to be solved analytically for transient stability analysis, however, finding the proper Lyapunov function is a significant difficulty and requires many simplifying assumptions.

The Time-Domain Simulation is the most effective way to investigate stability issues in MGs [81]. This method presents advantages over Lyapunov-based techniques, including higher accuracy and validity. However, this method is computationally intensive, and typically many simulations are required to ensure system stability over a wide variety of initial conditions and disturbances. As observed, the Time-Domain Simulations method is employed in this thesis.

B.2 Control Adjustment Algorithm

As presented above the MG's stability is verified through simulations, however, in order to adjust the secondary control strategies in the USCS a method is proposed. The method is based on the following criteria:

- Simulations are carried out to verify the control gains
- The control gains of the strategies (centralized and decentralized), must be determined together. In other words, all operation cases possibles must be considered (DG operating in the DSC and/or in the CSC mode);
- The control must be adjusted so that the MG maintains stability when the generation sources and larger loads groups start or stop their operation [72];
- The control must be adjusted so that the MG maintains stability considering a maximum

communication delay value [67, 69];

- The control must be adjusted so that the actuation of the frequency and voltage control is fast enough in order to avoid the unnecessary actions of the protection system.

The Fig. B.2 presents the gain adjustment algorithm proposed for the USCS. Note that the algorithm presents 12 steps. Each step is commented on below:

1. MG System Model: in this step, the MG is modeled in an electromagnetic transient (EMT) software. The converter control, secondary control, communication delay, and loads must be modeled in order to ensure a good representation of the real MG system;

2. Define the Possible Control Scenarios for the USCS: in this step is necessary to define the control operations scenarios. For example, for an MG with two dispatchable DGs, both DGs can operate in CSC or in DSC, however, one DG can operate in DSC mode and the other in CSC mode, and vice versa. Thus, four scenarios are possible for an MG with two dispatchable DGs. For an MG with N dispatchable DGs, 2^N scenarios are possible. It is important for the simulations to contain their operation points;

3. Define the Operations Points and Perturbations (it = 1): For each scenario defined in step 2, it is important to define the initial operations points and the perturbations for the simulations. The conditions of maximum and minimum load are suggested for the operations points. For the perturbations, load variation, generation loss, and operation are suggested. Note that the counter (it) stars its value with 1 in this step;

4. Select New Initial Control Gains: In this step the initial secondary control gain must be defined, to start the algorithm it is suggested a low value;

5. Simulates all the Predefined Conditions: In this step, simulations are carried out to verify the control gains defined;

6. MG System Stable?: Verify if the proposed gains are stable for all the MG conditions and simulations;

7. Have control criteria been met?: Verify if the proposed gains ensure the defined criteria, like fast/slow enough in order to avoid the unnecessary actions of the protection system for all the MG conditions and simulations;

8. Save Control Gains Values: Save the values of the control gains that satisfy the criteria of step 7;

9. Increase Control Gain (it = it + 1): Increase the value of one gain or multiple gains of the secondary control (centralized and/or decentralized strategies) and return to step 5. The modification of the control gain in this step depends on the willingness of the user;

10. Evaluate the Reason, and change the control Gain: If the control criteria in step 7 are not met, the control gain can be changed differently from step 9. For example, if the frequency or the voltage regulation is too slow, the gains can increase with a greater value than step 7. Or, if the frequency or the voltage regulation is fast, the gains can be reduced;

11. it > 10?: If the counter number is superior to a value, the algorithm stops. This step is employed to ensure the algorithm stops when some gains are verified, and prevents the algorithm from entering a loop due to steps 9 and 10, if the criterion is not met the algorithm returns to step 5;

12. it > 10?: Same as step 11. However, it is employed to prevent a loop due to steps 4 and 9, if the criteria is not met the algorithm returns to step 4.

Note that the proposed gain adjustment method can be improved. Employing a meta-heuristic - like a Particle Swarm Optimization algorithm - in steps 4, 9, and 10 for defining the new control gains, is possible to achieve better control gains, ensuring the MG stability and achieving the control criteria defined.

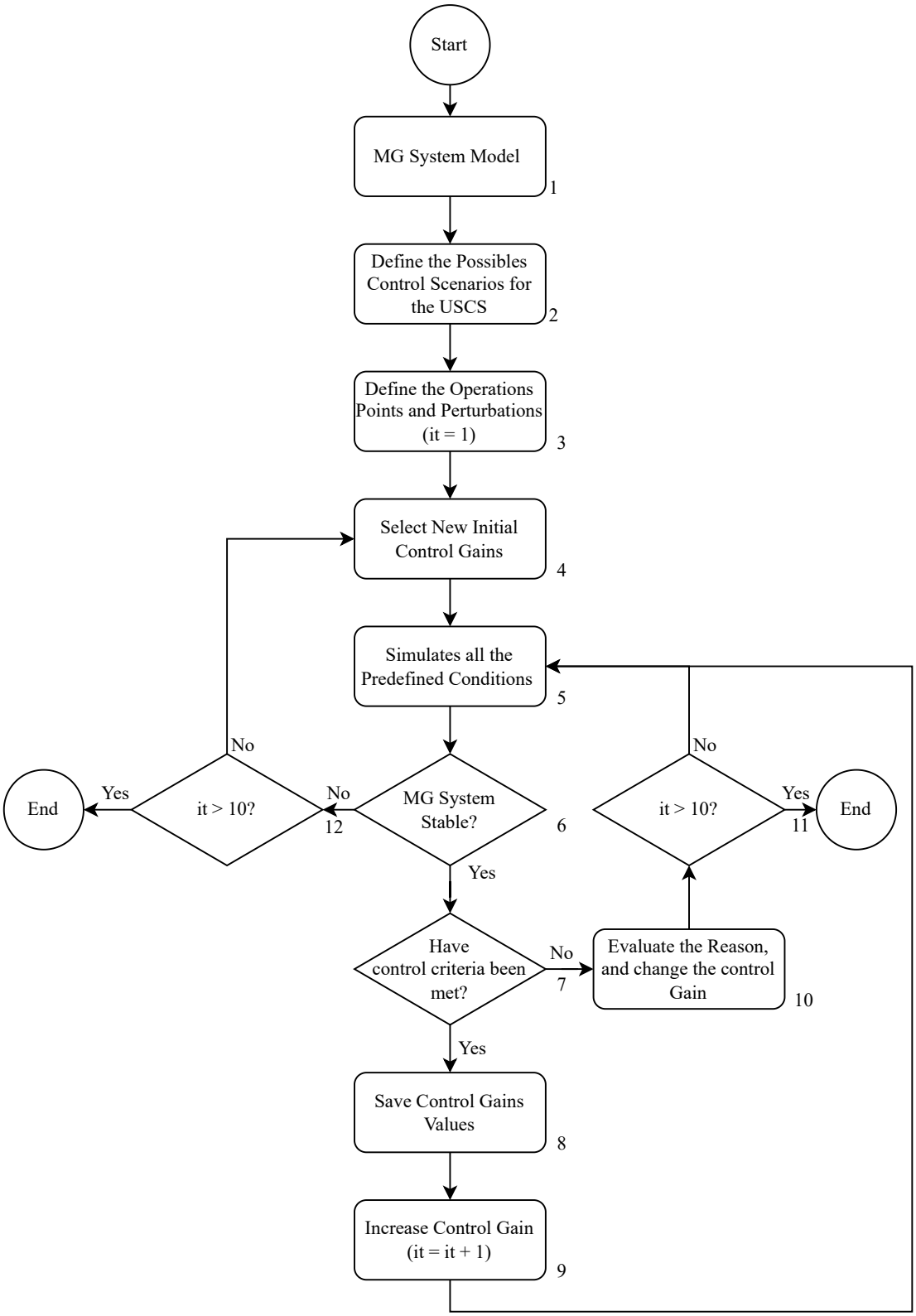

Figure B.2: Gain Adjustment Algorithm.